

POLITECNICO DI TORINO

Master of Science in Electronic Engineering

Master Thesis

Molecular Dynamics Simulations of Nanofabrication Processes



Supervisors

prof. Gianluca Piccinini
prof. Mariagrazia Graziano
M.Eng. Yuri Ardesi

Candidate

Daniele Volpintesta

July 2021

Abstract

Molecular dynamics (MD) is a computational technique that allows to simulate the motion of a set of atoms or molecules. The main advantage of MD is that it is possible to simulate complex molecular systems containing several thousands atoms in a relatively short time. Moreover, a system that is not accessible to experimental techniques can be studied.

This work is focused in using the MD to simulate nanofabrication processes with particular attention to the creation of a wire of MQCA cells. MQCA stands for Molecular Quantum Cellular Automata, which is emerging technique for computational logic that can overcome the current CMOS scaling limits.

In the first chapter of this thesis, an introduction of QCA technology and on its molecular implementation (MQCA) is given.

In the second chapter, is described the molecular dynamics algorithm which is fundamental for the understanding of the following chapters. Then, LAMMPS (Large-scale Atomic/Molecular Massively Parallel Simulator), the used simulator that implements the algorithm, is introduced.

In the third chapter, a simple explanation of the Density Functional Theory (DFT) is given. This is a technique able to obtain the ground state energy of a generic system constituted by an arbitrary number of nuclei and electrons. Subsequently, a method conceived in this work to evaluate force field parameters for bonds, angles and dihedrals within a molecule is proposed. This method uses the DFT technique which is implemented, in this thesis, by ORCA, an ab initio quantum chemistry program package.

The fourth chapter is mainly focused on a MD simulation regarding the formation of a Self-Assembled Monolayer (SAM) of alkanethiols on a perfect (111) gold surface.

In the fifth chapter, the growth of a gold thin film above a silicon substrate is simulated. A first simulation is performed interposing a copper thin film between silicon and gold that prevent reactions between them. A second simulation is carried out depositing gold atoms directly on the silicon substrate. In both simulations interfaces between the materials are quantitatively analyzed. Subsequently, the SAM simulation is proposed again above the non-ideal gold surface obtained.

In the sixth and last chapter, MD simulations with bisferrocenes, that are molecules specifically synthesized for MQCA, are performed. Since there is no scientific literature about a force field developed for bisferrocenes, in this thesis, one is arranged using parameters of other molecules, others obtained in chapter 3 and making approximations.

Sommario

La dinamica molecolare (MD) è una tecnica computazionale che permette di simulare il moto di un set di atomi o di molecole. Il vantaggio principale di questa tecnica è che è possibile simulare sistemi molecolari complessi contenenti migliaia di atomi in tempi relativamente veloci. Inoltre, è possibile studiare sistemi che non sono accessibili dal punto di vista delle tecniche sperimentali.

Questo lavoro è incentrato nell'uso della dinamica molecolare per simulare processi di nanofabbricazione con particolare attenzione alla creazione di un filo di celle MQCA. MQCA è l'acronimo di Molecular Quantum Cellular Automata che è un'emergente tecnica di logica computazionale che può superare i limiti dello scalamento della tradizionale logica CMOS.

Nel primo capitolo di questa tesi viene data un'introduzione della tecnologia QCA e della sua implementazione molecolare (MQCA).

Nel secondo capitolo viene descritto l'algoritmo di dinamica molecolare che è di fondamentale importanza per la comprensione dei capitoli successivi. Viene poi introdotto LAMMPS (Large-scale Atomic/Molecular Massively Parallel Simulator), che è il simulatore che implementa l'algoritmo usato in questa tesi.

Nel terzo capitolo viene data una semplice spiegazione della teoria del funzionale della densità (Density Functional Theory, DFT), che è una tecnica in grado di ottenere l'energia dello stato fondamentale di un generico sistema costituito da un numero arbitrario di nuclei ed elettroni. Successivamente, viene proposto un metodo pensato in questo lavoro per stimare i parametri del campo di forze di legami, angoli e torsioni all'interno di una molecola. Questo metodo usa la tecnica DFT che è implementata, in questa tesi, da ORCA, un ab initio programma di chimica quantistica.

Il quarto capitolo è principalmente incentrato su una simulazione di dinamica molecolare riguardante la formazione di un monostrato auto-assemblato (Self-Assembled Monolayer, SAM) di alcantioli sopra ad una perfetta superficie di oro di tipo (111).

Nel quinto capitolo viene simulata la crescita di un sottile strato di oro sopra ad un substrato di silicio. Una prima simulazione viene eseguita interponendo un sottile strato di rame fra silicio e oro per impedire che questi due reagiscano fra di loro. Una seconda simulazione viene condotta depositando direttamente di atomi di oro sopra al substrato di silicio. In entrambe le simulazioni vengono analizzate quantitativamente le interfacce fra i materiali. Successivamente, viene nuovamente proposta la simulazione del SAM al di sopra della superficie non ideale ottenuta.

Nel sesto e ultimo capitolo vengono eseguite simulazioni di dinamica molecolare con i bisferroceni che sono molecole sintetizzate appositamente per implementare celle MQCA. Poiché nella letteratura scientifica non esiste un campo di forze

sviluppato per i bisferroceni, in questa tesi, ne è stato arrangiato uno usando parametri di altre molecole, altri parametri ottenuti nel capitolo 3 e facendo approssimazioni.

Contents

1	Introduction	1
1.1	Quantum Cellular Automata	1
1.2	The Clock System	3
1.3	Molecular Quantum Cellular Automata	4
2	Molecular Dynamics Simulations	9
2.1	Molecular Dynamics Algorithm	9
2.2	LAMMPS Molecular Dynamics Simulator	15
2.2.1	Neighbor List	16
2.2.2	Boundary Conditions	18
2.2.3	Ensembles	18
2.3	LAMMPS Results & VMD	20
3	Force Field Computation with Density Functional Theory	23
3.1	Density Functional Theory	24
3.1.1	Many-body Schrödinger Equation	24
3.1.2	The Variational Principle	26
3.1.3	The Electron Density & Hohenberg-Kohn Theorems	27
3.1.4	The Kohn-Sham Approach	28
3.2	Force Field Evaluation	31
3.2.1	Butane-1-thiol	34
3.2.2	Carbazole	36
3.2.3	Isobutane	38
3.2.4	Alkylcarbazole	39
4	Self-Assembled Monolayer of Alkanethiols on Gold (111)	41
4.1	MD Simulation of One Alkanethiol above Au(111) Surface Using Reactive Force Field	44
4.2	MD Simulation of a Self-Assembled Monolayer above Au(111) Surface	46
5	Growth of an Au Thin Film above a Si Substrate	51
5.1	Growth of Au Thin Film on Si Substrate Interposing a Cu Buffer in the Middle	51
5.2	Growth of Au Thin Film Depositing Au Atoms Directly on the Si Substrate	58
5.3	Self-Assembled Monolayer of Alkanethiols on a Non-ideal Gold Surface	62

6	MD Simulations with Bisferrocene Molecules	69
6.1	Bisferrocenes without the Hydrocarbon Chain above a SAM . . .	69
6.2	Bisferrocenes above Au(111) Surface	72
6.3	Bisferrocenes above an Au Wire	74
6.4	Bisferrocenes Mixed with Thiols	78
	Conclusions	83
A	Definition of a Molecular Structure	85
A.1	Internal Coordinates	85
A.2	Z-matrix	87
	Bibliography	89

Chapter 1

Introduction

The semiconductor industry had a huge development in the last decades. MOS-FET dimensions have shrunk from a gate length of 5 μm in the early 1970s to 10 nm in 2020 [1] doing that the well-known Moore's law, which states that the number of transistor on a chip double every 18 months, continued unabated until now. To achieve this goal, technology had to overcome many challenges, such as the increasing interconnect power consumption and gate leakage currents, but now we are approaching the physical limits. Below a gate length of 10 nm, is not possible employing traditional lithographic processes to make a transistor, therefore a new technology of manufacturing, that involves huge costs, should need to continue scaling. Thus, even if the trend of the Moore's law will be kept for another time, the reduction of the cost per unit may not be guaranteed. In other words, it may happen that to continue packing more and more transistors in a chip, new technologies need to be developed which can be so expensive that reduction of the cost per unit is not insured.

Nowadays, in order to find solutions beyond CMOS conventional scaling, the research explores multiple fields such as emerging memory and logic devices or alternative architectures and computing paradigms. In particular future digital logic technologies that can overcome the current CMOS scaling limits are referred as "Beyond CMOS".

Among the various emerging technologies, in this thesis, we are interested in Quantum Cellular Automata (QCA) [2] which is a technique for computational logic that is expected to reach switching frequencies of the order of 1 THz, but, the most important advantage is that the power dissipation is significantly reduced with respect to the standard CMOS technology [3].

In the following of this chapter a simple introduction of QCA technology and on its molecular implementation will be given.

1.1 Quantum Cellular Automata

A Quantum Cellular Automata (QCA) is a new paradigm for computing which consists of an array of quantum device cells. Each cell must be bistable, which means that it has two stable states to encode the binary information, and must be also coupled with neighbor ones for propagating the information [2].

The considered cell is made of four quantum dots which host two electrons.

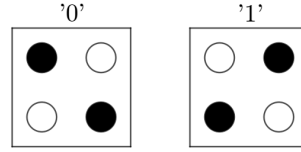


Figure 1.1: QCA cell. In each cell the four circles represent the quantum dots. Dots occupied by the electrons are depicted in black. Due to the Coulomb repulsion the two electrons organize in one of the two possible diagonals which are associated to two logical values.

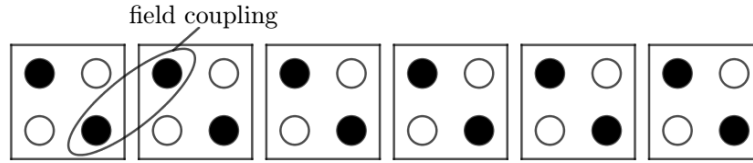


Figure 1.2: QCA wire implemented by a linear arrangement of QCA cells. The two electrons in each cell interact Coulombically with neighboring cells doing that the information propagates from the first cell to the last.

The two electrons tend to occupy antipodal sites due to the Coulombic repulsion leading to two possible arrangement which are associated to two logic values (figure 1.1).

Starting from the QCA cell it is possible to implement a simple wire or logic devices such as the inverter or AND and OR gates [4]. A wire has the function of propagating the information from a point to another and can be obtained by a linear arrangement of QCA cells as shown in figure 1.2. The polarization of each cell tends to align with that of its neighbors thanks to the Coulomb repulsion between the electrons of adjacent cells. If the first cell is forced to change polarization, for example with an external electric field, all other cells will change as well in a domino style (one after the other).

A logic function can be implemented arranging five cells as in figure 1.3. This structure is called majority voter gate because the state of the central cell is determined by which is the most frequent polarization in A, B and C inputs. Then, the output will follow the central cell, therefore, this basic device implements the following truth table

A	B	C	OUT
0	0	0	0
0	0	1	0
0	1	0	0
0	1	1	1
1	0	0	0
1	0	1	1
1	1	0	1
1	1	1	1

which can be expressed by the following boolean function

$$OUT = C(A + B) + \overline{C}(AB) \quad (1.1)$$

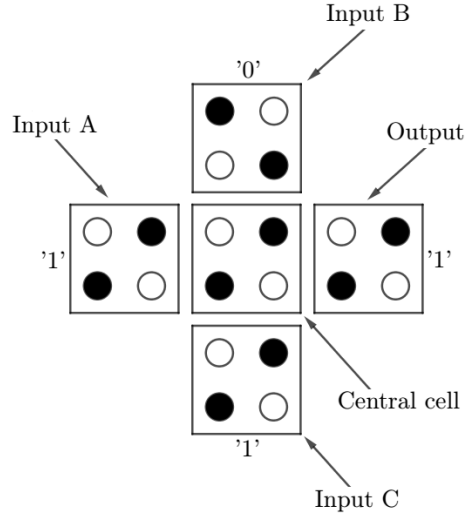


Figure 1.3: Majority voter gate.

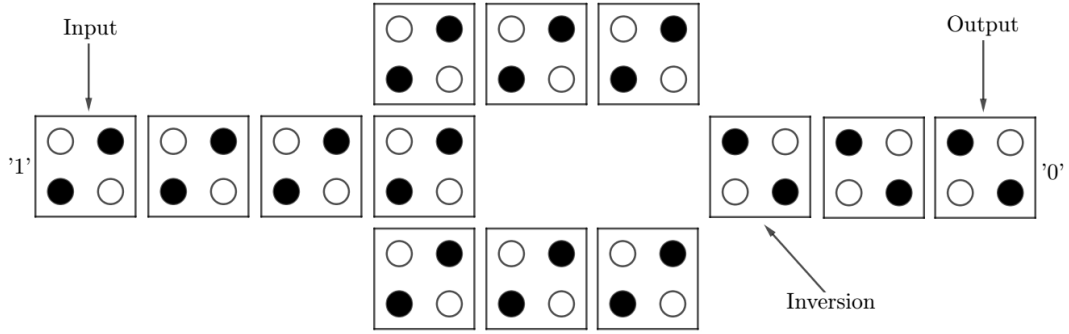


Figure 1.4: QCA inverter.

where C acts as a control input to select what is the logic function to implement between AND or OR, indeed it is simple to note that

$$OUT = \begin{cases} AB & \text{if } C = 0 \\ A + B & \text{if } C = 1 \end{cases} \quad (1.2)$$

In combination with the AND and OR gates, the inverter is needed to implement any boolean function. To build it, QCA cells can be arranged as shown in figure 1.4.

1.2 The Clock System

Due to thermodynamic effects there is a maximum number of QCA cells in a wire beyond which the information cannot propagate properly [5]. Moreover if a cell is switched suddenly, more power is dissipated with respect to the case

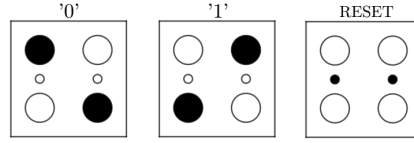


Figure 1.5: QCA cell with two more dots to implement the RESET state.

in which it is switched gradually (adiabatic switching) [6]. To solve these problems, two more dots are added in the QCA cell as shown in figure 1.5. When the two electrons are in the two new dots, the cell is in the RESET or NULL state. The RESET is an unstable state, that means that the electrons do not reach it spontaneously, but they have to be forced to move there by an external electric field. When the electric field is applied, the two electrons move in the RESET state, then, when the electric field is released, the electrons move spontaneously in one of the two possible stable states '0' or '1' depending on the input.

Figure 1.6 [6] shows this concept: for the moment consider in the picture to have only the input and the clock (ck) zone 1 columns. In each clock zone there is only one cell represented within a box, where the cell on the left represents the state of the cell at the beginning of the time step, while the cell on the right represents the state of the cell at the end of the time step. Considering only the ck zone 1, the cell is initially in the so-called *relaxed* phase that means that the electric field is applied to force the cell in the RESET state. In the second time step, the cell moves in the *switch* phase where the electric field is gradually removed. At the beginning of this phase the cell is in the RESET state, while at the end is switched to the stable state forced by the input cell. In the next time step, called *hold* phase, the cell does not change state because the electric field is absent for all the duration of this phase. Finally, in the fourth time step, the *release* phase, the electric field is gradually applied, therefore the cell moves to the RESET state. Subsequently the cycle is repeated.

This mechanism solves the problem mentioned above about abrupt switching, indeed during the switch and release phases, the electric field is gradually removed to make sure the cell changes state smoothly.

To solve the issue regarding the maximum number of cell beyond which the information is not propagated correctly, the wire is divided in clock zones as shown in figure 1.6. In the picture, each clock zone contains just a single cell, but in general you can have more cells that allows to propagate the information properly within the clock zone. Each clock zone has its own electric field that is called clock. Applying the clocks as shown in figure, the information advances in one clock zone at a time, like in a pipeline, reaching correctly the end of the wire.

1.3 Molecular Quantum Cellular Automata

There are four types of QCA implementations that are Metal-Island QCA, Semiconductor QCA, Molecular QCA and Magnetic QCA [7].

This thesis is focused on MQCA which has several advantages [8]:

- Can be made uniformly sized devices since molecules are all of the same size;

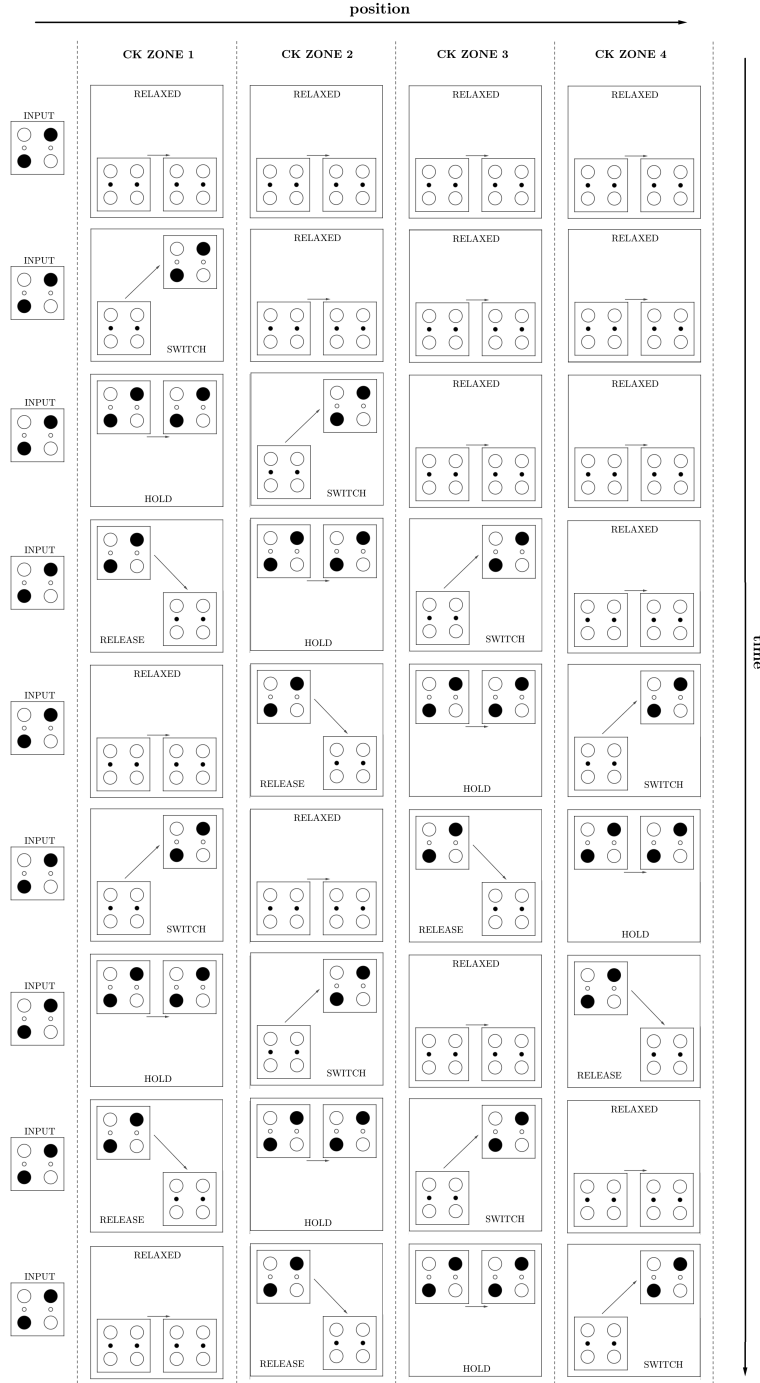


Figure 1.6: Pipeline in a QCA wire. The wire is divided into four segments called clock zones. In each clock zone there is just a single cell represented within a box, where the cell on the left represents the state of the cell at the beginning of the time step, while the cell on the right represents the state of the cell at the end of the time step. The information advances in one clock zone at a time like in a pipeline [6].

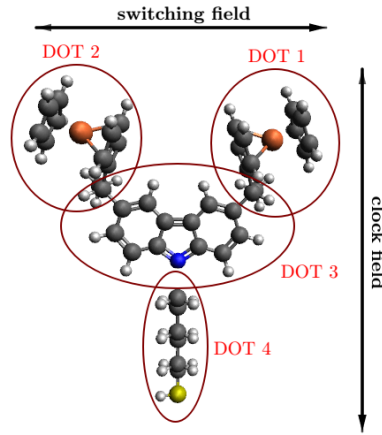


Figure 1.7: Bisferrocene molecule. Dark grey is carbon (C), light grey is hydrogen (H), yellow is sulphur (S), blue is nitrogen (N) and orange is iron (Fe).

- The small size of molecules allows high density;
- MQCA cells do not require cryogenic conditions and can be used at ambient temperature;
- Ultra-low power consumption;
- Switch speed of the order of 1 THz is expected to be reached.

A MQCA cell can be made with two molecules arranged next to each other. Each molecule has to have at least two redox centers, representing two quantum dots, where the charges can aggregate. Thus, by properly positioning the molecules, four quantum dots can be obtained in the corners of a square.

A molecule specifically synthesized for MQCA is the bisferrocene [9], which is shown in figure 1.7. This molecule is composed by two ferrocenes (DOT 1 and DOT 2) connected by a carbazole bridge (DOT 3) and a thiol (DOT 4) which is able to bind a gold surface thanks to the high affinity between gold and sulphur. The molecule is oxidized, therefore it presents a positive unitary charge that can be moved within the molecule through two electric fields. Applying a vertically directed electric field, called clock field, the charge can be shifted down or up in the molecule. When the charge is shifted down, the molecule is in the RESET state. In this case even applying a horizontal switching field the charge will remain within DOT 3 and DOT 4. When the charge is pushed up by the clock field, the molecule is "enabled". In this case the charge can be moved in DOT 1 or in DOT 2 (associating thus the two logical states '0' or '1') applying the horizontal switching field.

In practice, the switching field on a bisferrocene molecule is generated by another one molecule placed next to it, which has to be in one of the two logical states '0' or '1'. Hence, by arranging the molecules in a row it is possible to propagate the logical information from one molecule to another in a domino style.

Figure 1.8 shows an implementation of a MQCA wire. The structure consists of a silicon trench where a gold wire has grown at the bottom. Above this wire, a row of bisferrocene molecules is placed. Gold electrodes are placed above the

two silicon walls in order to divide the wire in three clock zones. The information travels from one molecule to another in a domino style thanks to the Coulomb repulsion. This means for example that, if the first molecule of the wire has the charge within DOT 1, in the second the charge will be in DOT 2, in the third will be in DOT 1 and so on. As explained in the previous section, to ensure the correct propagation, the wire is divided into clock zones. To apply the vertically clock field, a voltage is applied between the clock electrodes and the wire at the bottom of the trench.

Actually each bisferrocene molecule in the wire does not influence only the following molecule, but each molecule influences all the others with more or less intensity depending on the distance. To take this effect into account during the information propagation, a sophisticated and efficient algorithm called SCERPA has been developed [10, 11].

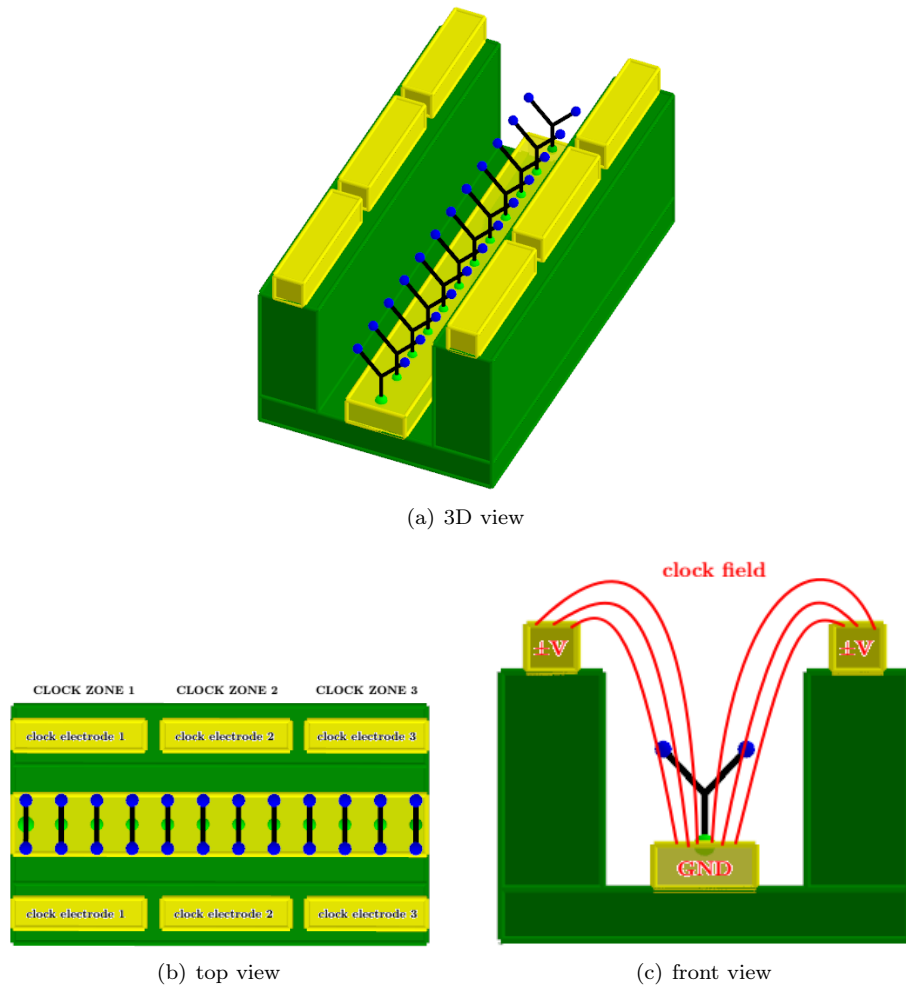


Figure 1.8: Implementation of a MQCA wire. In dark green is shown a silicon trench and in yellow the gold clock electrodes and the gold wire at the bottom of the trench. Aligned bisferrocene molecules are placed above the gold wire. In each bisferrocene, light green points represent the sulphur atom and blue points represent the DOT 1 and DOT 2.

Chapter 2

Molecular Dynamics Simulations

The molecular dynamics (MD) is a computational chemistry technique that allows to simulate the motion of single atoms in atomic or molecular systems [12]. The complete description of the motion of a particle system can be performed solving the Schrödinger's equation for each particle in the system. This approach is employed by ab initio methods and it is very accurate but also too much expensive from computational point of view; it requires a huge amount of time and CPU memory, that is why it can be used only for a small number of atoms.

The molecular dynamics enables to simulate complex molecular systems containing several thousands atoms, obviously the accuracy is much less respect to ab initio methods. Using MD it is possible understanding the behaviour of a system which is not accessible to experimental techniques [12]. For example when experimental and simulated results are agree it is reasonable to claim that the experimental results can be explained by the simulation model [13]. Moreover MD can be used as exploratory tool to help gain an initial understanding of a problem [13].

Thus, the main feature of MD is that allow you to simulate complex systems, but the obtained results should be critically analyzed because they may not be right. MD results should be compared with experimental ones if available.

In the following there will be a description of the molecular dynamics algorithm.

2.1 Molecular Dynamics Algorithm

In a molecular dynamics simulation you have a given number N of atoms, and the goal is simulate how these atoms will be move according to time.

Step 1

The first step of the molecular dynamics method is providing the initial configuration of the system. This means that you have to know the initial position and velocity of each atoms.

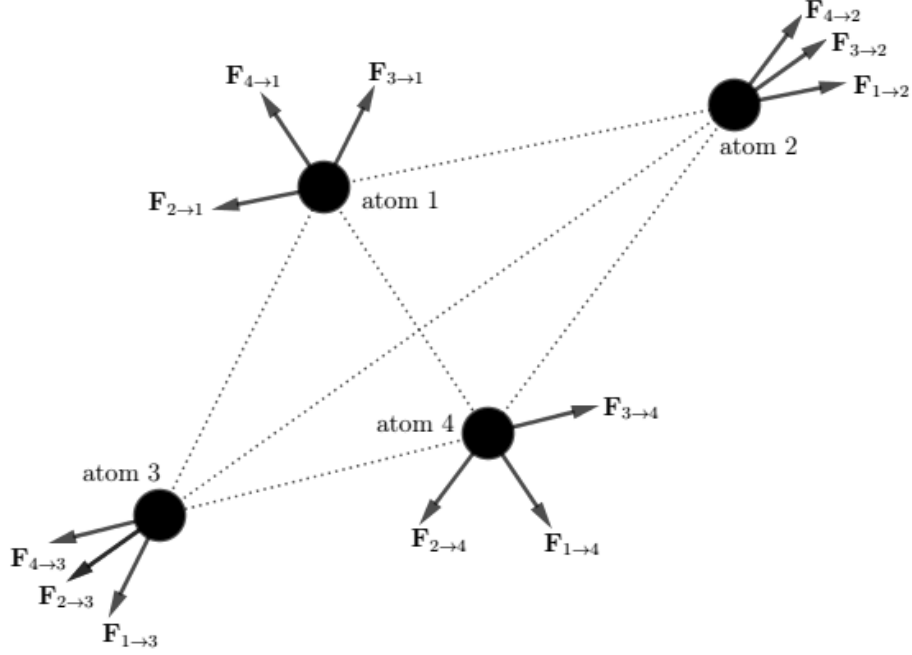


Figure 2.1:

Step 2

Each atom in the simulation applies a force on the others. We will denote as $\mathbf{F}_{i \rightarrow j}$ the total force that the atom i applies on the atom j . This force could be constituted by several factors, this depends on the force field used. For example, if the interactions among atoms are only coulombic and Lennard-Jones (LJ) types, then $\mathbf{F}_{i \rightarrow j} = \mathbf{F}_{i \rightarrow j}^{Coul} + \mathbf{F}_{i \rightarrow j}^{LJ}$, where $\mathbf{F}_{i \rightarrow j}^{Coul}$ is the coulombic force that atom i applies on atom j and $\mathbf{F}_{i \rightarrow j}^{LJ}$ is the Lennard-Jones force that atom i applies on atom j . $\mathbf{F}_{i \rightarrow j}^{Coul}$ and $\mathbf{F}_{i \rightarrow j}^{LJ}$ depend on the distance r_{ij} between atoms i and j (for $\mathbf{F}_{i \rightarrow j}^{Coul}$ you need also the charge associated to the atoms). In general $\mathbf{F}_{i \rightarrow j}$ can be constituted by others factors depending on the model (force field) used. Every factor depends on the distance between atoms. This means, whatever force field is used, if you know the distance r_{ij} between two atoms i and j , you can compute $\mathbf{F}_{i \rightarrow j}$ and $\mathbf{F}_{j \rightarrow i}$ (because $\mathbf{F}_{i \rightarrow j}$ is a function of r_{ij} and $\mathbf{F}_{j \rightarrow i}$ is a function of $r_{ji} = r_{ij}$). Actually if you know $\mathbf{F}_{i \rightarrow j}$, for the action-reaction principle (Newton's third law) you know also $\mathbf{F}_{j \rightarrow i}$ because $\mathbf{F}_{i \rightarrow j} = -\mathbf{F}_{j \rightarrow i}$.

The aim of this step is to compute the total force acting on each atom. To better understand the problem consider to have a system consisting of only four atoms as depicted in figure 2.1. The total force acting on the generic atom i is given by:

$$\mathbf{F}_i = \sum_{\substack{j=1 \\ j \neq i}}^N \mathbf{F}_{j \rightarrow i} \quad (2.1)$$

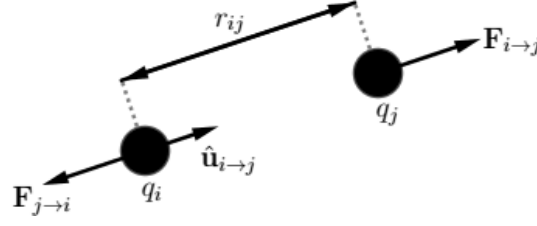


Figure 2.2:

Indeed using eq.2.1 the total forces for each atom in our example (with $N = 4$) are:

$$\mathbf{F}_1 = \mathbf{F}_{2 \rightarrow 1} + \mathbf{F}_{3 \rightarrow 1} + \mathbf{F}_{4 \rightarrow 1} \quad (2.2)$$

$$\mathbf{F}_2 = \mathbf{F}_{1 \rightarrow 2} + \mathbf{F}_{3 \rightarrow 2} + \mathbf{F}_{4 \rightarrow 2} \quad (2.3)$$

$$\mathbf{F}_3 = \mathbf{F}_{1 \rightarrow 3} + \mathbf{F}_{2 \rightarrow 3} + \mathbf{F}_{4 \rightarrow 3} \quad (2.4)$$

$$\mathbf{F}_4 = \mathbf{F}_{1 \rightarrow 4} + \mathbf{F}_{2 \rightarrow 4} + \mathbf{F}_{3 \rightarrow 4} \quad (2.5)$$

The choice of the force field means choosing what are the formulas to compute $\mathbf{F}_{i \rightarrow j}$ as a function of the interatomic distance r_{ij} . Actually in molecular dynamics you work in terms of potential energy. To each force corresponds a potential energy. When you choose the force field, actually, you choose the formulas to compute the interatomic energies. For example consider that $\mathbf{F}_{i \rightarrow j}$ has only the coulombic contribute so that $\mathbf{F}_{i \rightarrow j} = \mathbf{F}_{i \rightarrow j}^{Coul} = \frac{1}{4\pi\epsilon_0} \frac{q_i q_j}{r_{ij}^2} \hat{\mathbf{u}}_{i \rightarrow j}$ where q_i and q_j are the charges associated to atoms i and j , r_{ij} is the interatomic distance and $\hat{\mathbf{u}}_{i \rightarrow j}$ is the versor directed from atom i to atom j (figure 2.2). When you choose the force field, you do not set the formula for $\mathbf{F}_{i \rightarrow j}$ but you set the formula of the associated potential energy. In our example we will set the formula of the electrostatic pairwise potential energy $U_{ij} = \frac{1}{4\pi\epsilon_0} \frac{q_i q_j}{r_{ij}}$ and from this we will compute the force using the formula:

$$\mathbf{F}_{i \rightarrow j} = -\nabla U_{ij}(r_{ij}) = -\left. \frac{\partial U_{ij}(r_{ij})}{\partial r_{ij}} \right|_{r_{ij}} \hat{\mathbf{u}}_{i \rightarrow j} \quad (2.6)$$

Note that during derivative operation, r_{ij} is treated as independent variable. The result of the derivative is evaluated for r_{ij} value that it is known.

After the calculation of all $\mathbf{F}_{i \rightarrow j}$, using the equation 2.1 (and remembering that $\mathbf{F}_{i \rightarrow j} = -\mathbf{F}_{j \rightarrow i}$), you can compute the total force \mathbf{F}_i acting on each atom.

Generally, molecular dynamics simulators compute also the potential energy of the entire system during this step. The total potential energy is defined as the sum of the interatomic energies U_{ij} over all pairs [13]. For instance, considering our example with four atoms (figure 2.1), the potential energy of the system is given by:

$$U_{tot}^{N=4} = U_{12} + U_{13} + U_{14} + U_{23} + U_{24} + U_{34} \quad (2.7)$$

This expression can be written for a general number N of atoms as:

$$U_{tot} = \sum_{i < j} U_{ij} \quad (2.8)$$

Since $U_{ij} = U_{ji}$ the equation 2.8 can also be written as:

$$U_{tot} = \frac{1}{2} \sum_{\substack{i,j=1 \\ i \neq j}}^N U_{ij} \quad (2.9)$$

The meaning of the interatomic energy U_{ij} is the energy needed to bring the atoms i and j at infinite distance from each other. Therefore, you can imagine U_{tot} as the energy needed to break up the system (in the sense that each atom is brought at an infinite distance from the others).

Step 3

At this step, you know the total force \mathbf{F}_i acting on each atom, you know also the mass m_i of each atom, thus you can compute the acceleration of each atom as:

$$\mathbf{a}_i = \frac{\mathbf{F}_i}{m_i} \quad (2.10)$$

The goal of this step is computing position and velocity of each atom after a small increment of time Δt . This is done integrating Newton's law of motion (eq.2.10). There are many numerical methods, the main idea is always to do a Taylor expansion of position and velocity [12]. For example, considering the first-order Taylor expansion you can compute velocity and position of each atom i after the increment of time Δt as:

$$\mathbf{v}_i(\Delta t) = \mathbf{v}_i(0) + \left. \frac{\partial \mathbf{v}_i(t)}{\partial t} \right|_{t=0} \Delta t \quad (2.11)$$

$$\mathbf{r}_i(\Delta t) = \mathbf{r}_i(0) + \left. \frac{\partial \mathbf{r}_i(t)}{\partial t} \right|_{t=0} \Delta t \quad (2.12)$$

Since $\mathbf{a}_i(t) = \frac{\partial \mathbf{v}_i(t)}{\partial t}$ and $\mathbf{v}_i(t) = \frac{\partial \mathbf{r}_i(t)}{\partial t}$, you obtain:

$$\mathbf{v}_i(\Delta t) = \mathbf{v}_i(0) + \mathbf{a}_i(0) \cdot \Delta t \quad (2.13)$$

$$\mathbf{r}_i(\Delta t) = \mathbf{r}_i(0) + \mathbf{v}_i(0) \cdot \Delta t \quad (2.14)$$

Actually, in MD are usually used algorithms that employ Taylor expansion up to the third order because it has been observed that low-order algorithms are inaccurate while those of higher order are too expensive from computational point of view [12]. The most used algorithm is that of Verlet [12, 14] which exploits the following formulas:

$$\mathbf{r}_i(t + \Delta t) = -\mathbf{r}_i(t - \Delta t) + 2\mathbf{r}_i(t) + \frac{(\Delta t)^2}{m_i} \mathbf{F}_i(t) \quad (2.15)$$

$$\mathbf{v}_i(t) = \frac{1}{2\Delta t} [\mathbf{r}_i(t + \Delta t) - \mathbf{r}_i(t - \Delta t)] \quad (2.16)$$

With this scheme the error on the position and on the velocity are respectively of the order (Δt^4) and of (Δt^3) .

A variant of this integration scheme is the *leap-frog*:

$$\mathbf{v}_i(t + \Delta t) = \mathbf{v}_i\left(t - \frac{\Delta t}{2}\right) + \frac{\mathbf{F}_i(t)}{\Delta t} \quad (2.17)$$

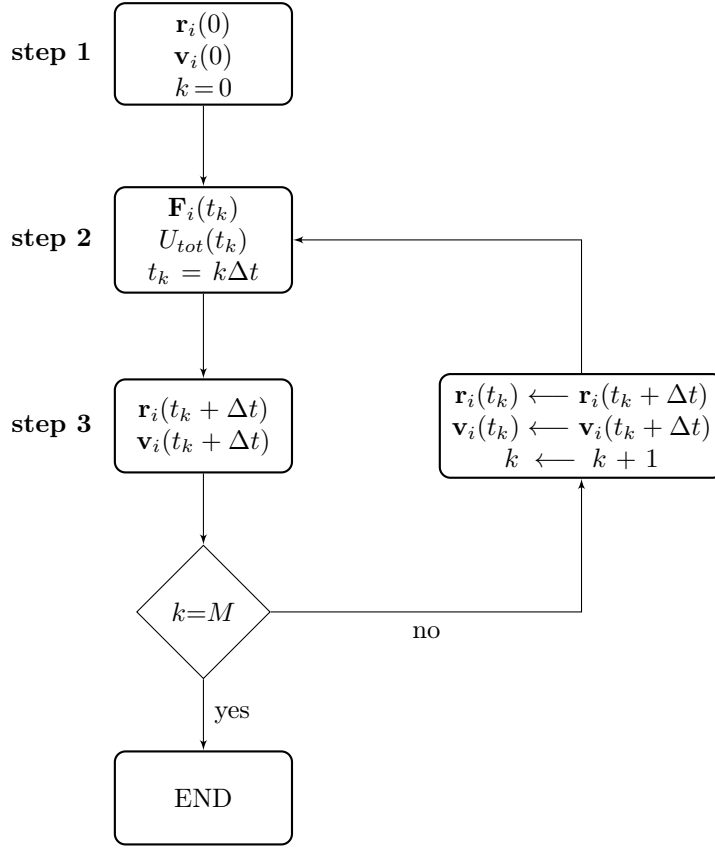


Figure 2.3: MD algorithm scheme.

$$\mathbf{r}_i(t + \Delta t) = \mathbf{r}_i(t) + \mathbf{v}_i(t + \Delta t)\Delta t \quad (2.18)$$

The choice of the Δt value is important because it must be small enough to guarantee an acceptable error. This choice depends of the type of system that you are simulating. For example if you have a system with atoms moving very fast you will need to choose a small Δt , but if the atoms are moving slower, then you can use a larger value of Δt . Typically for systems that we will simulate in this thesis Δt is around 1 fs.

At this point, you have to update position and velocity of each atom and repeating step 2 and 3 as many times as you want. Thus, in the second cycle the initial position and velocity will be $\mathbf{r}_i(\Delta t)$ and $\mathbf{v}_i(\Delta t)$; at the end of this cycle $\mathbf{r}_i(2\Delta t)$ and $\mathbf{v}_i(2\Delta t)$ will be computed. Then, at the end of the third cycle $\mathbf{r}_i(3\Delta t)$ and $\mathbf{v}_i(3\Delta t)$ will be computed and so on.

Figure 2.3 summarizes the MD algorithm. In the scheme k is a counter and the number of cycles is $M + 1$. At the end of the loop position and velocity of each atom will be collected at each timestep ($\mathbf{r}_i(t_k)$ and $\mathbf{v}_i(t_k)$ where $t_k = k\Delta t$ and $k = 0, 1, \dots, M$). In other words, the position of each atom has been obtained according to time (trajectory).

Note that considering a timestep of 1 fs, if you want to simulate a system for 1 ns, you need one million cycles that takes some time if the system contains several thousand atoms. Long MD simulation are usually roughly tens of nanoseconds.

Thermodynamic quantities

During step 2 of the MD algorithm, different quantities can be calculated apart from the total potential energy U_{tot} such as the kinetic energy K_{tot} , the temperature T and the pressure P of the system.

The kinetic energy of a single atom i at the timestep t_k is given by:

$$K_i(t_k) = \frac{1}{2} m_i \mathbf{v}_i^2(t_k) \quad (2.19)$$

The kinetic energy of the entire system K_{tot} at the timestep t_k is given summing that of all (N) atoms:

$$K_{tot}(t_k) = \sum_{i=1}^N \frac{1}{2} m_i \mathbf{v}_i^2(t_k) \quad (2.20)$$

The temperature T of the system at the timestep t_k is related to the kinetic energy by the following formula:

$$K_{tot}(t_k) = \frac{3}{2} k_B T(t_k) \quad (2.21)$$

where $k_B = 1.381 \cdot 10^{-23} J/K$ is the Boltzmann constant.

The total energy of the system E_{tot} at the timestep t_k is given by the sum of the total potential and kinetic energy:

$$E_{tot}(t_k) = U_{tot}(t_k) + K_{tot}(t_k) \quad (2.22)$$

The pressure P of the system can be computed at each timestep using the formula [15]:

$$P = \frac{N k_B T}{V} + \frac{\sum_{i=1}^N \mathbf{r}_i \cdot \mathbf{F}_i}{3V} \quad (2.23)$$

where N is the number of atoms and V the volume of the system. Note that $\mathbf{r}_i \cdot \mathbf{F}_i$ is a scalar product.

The volume of the system is the space occupied by the atoms. The existence of a pressure means that on the surface S that encloses the volume V acts an external force \mathbf{F}_{ext} . This force acts only on the surface S and not inside the volume V . Therefore only the atoms on the surface will be affected by this force. For a perfect gas the atoms do not interact with each others (except when they collide), therefore $\mathbf{F}_i = 0$ and the equation 2.23 becomes the state equation for ideal gas ($PV = N k_B T = nRT$).

MD simulations cannot give any informations about electronic properties because details of the electrons are not described. In MD atoms are treated as point bodies with a certain mass and eventually a charge can be associated.

Molecular systems

Until now, only systems where there are not molecules have been considered. We have considered only systems with atoms that are not bonded to each other. If you have a system without molecules (bonded atoms) with three atoms types C, H and S, you have only to define the interactions between all pairs of atoms. In this case you have to say what is the interatomic energy between the pairs C-C, C-H, C-S, H-H and H-S as a function of the distance between the two atoms.

Things change slightly if in this system you have also bonded atoms. For example it is clear that if there are two hydrogen molecules, two H atoms belonging to the same molecule cannot have the same interaction between two H atoms in two different hydrogen molecules. Also in this case you have to define the interatomic energy between all pairs of atoms but this formulas are valid only if the two atoms are not bonded. To compute the interatomic energy for bonded atoms you have to define different formulas that represent the bond energy between the two atoms as a function of their distance. For example if in the system there are only H₂ and CH₄ molecules means that there are two bond types that are H with H and C with H. Thus you have to define formulas for this two bonds as a function of the distance between the two bonded atoms (bond length).

To distinguish between bonded atoms and non-bonded, in a MD simulation you have to say which are all bonded atoms.

Usually in the molecules there are also angles and dihedrals that contribute to the energy of the molecule. In this case you have to set also the formulas to compute angle and dihedral energies and you have to say to the simulator which are all angles and dihedrals.

2.2 LAMMPS Molecular Dynamics Simulator

LAMMPS (Large-scale Atomic/Molecular Massively Parallel Simulator) is the molecular dynamics simulator used in this thesis. Since there is not a graphical interface, to run LAMMPS you have to write an input script file with all the instructions. LAMMPS takes your input files and executes all the instructions line by line. To run any simulation, in the input files there must be the two main ingredients for a molecular dynamics simulation that is the initial configuration of the system and all the interactions among the atoms (force field). The initial configuration of the system can be written in a external file in the LAMMPS format or can be generate with some LAMMPS commands. To generate the initial configuration it is also possible to use others software such as Avogadro, Moltemplate or Packmol. If the initial configuration is written in a external file in LAMMPS format, it can be read using the command "read_data". To set the interactions among atoms commands "pair_style" and "pair_coeff" are used. Details, syntax and examples for all commands can be found in the LAMMPS manual [16].

Some LAMMPS advantages are that it is an open source software continuously updated. In recent years it has improved a lot, also the installation is much easier than a few years ago. Then when you download LAMMPS there is a folder containing many simulation examples that can be very useful especially if you are a beginner. There is also a folder containing potential parameters for

various types of atoms.

In the following, the neighbor list, the boundary conditions and the ensembles are described which are some practical aspects that should be known.

2.2.1 Neighbor List

In a MD simulation most of the time is spent in calculating the non-bonded interactions [12]. This is why if you have N atoms the number of pairs that you have to consider is $\sum_{i=1}^{N-1} i = N(N-1)$. If each atom in the system has four bonds with other atoms, the number of bonded interaction is $4N$. Thus the number of non-bonded interaction increases quadratically when the number of atoms increases while the number of non-bonded interactions increases linearly (in the worst case because the system could not have bonds).

Thus to save computational time, you have to speed up the calculation of non-bonded interactions. To do this consider that non-bonded interactions become negligible when the interatomic distance is large enough. For example assume that you can model the non-bonded interactions with Lennard-Jones potential which has the following expression:

$$U^{LJ} = 4\varepsilon \left[\left(\frac{\sigma}{r} \right)^{12} - \left(\frac{\sigma}{r} \right)^6 \right] \quad (2.24)$$

Assuming $\varepsilon = 0.118$ kcal/mol and $\sigma = 3.905$ Å the potential is shown in figure 2.4. As you can see from figure 2.4 after a certain value of interatomic distance r , the interatomic energy between a pair of atoms becomes negligible. For this reason a cutoff distance r_c is applied to non-bonded interactions that means if the interatomic distance r is greater than r_c the interatomic energy is considered null. For instance in figure 2.4 the cutoff r_c could be chosen equal to 7 Å. Thus interactions among atoms are computed only if their distance is less r_c . In this way the number of non-bonded interactions to be calculated is reduced a lot saving a lot of computational time. An example is shown in figure 2.5: the red point is the atom i whose interactions we want to calculate, blue points inside the circle of radius r_c centered on the atom i are the atoms that interact on the atom i . These atoms are called neighbors of atom i . You note that atom i has 23 neighbors that is also the number of interactions that you have to compute for it. In a system you can have also several thousands atoms, this means that the number of interactions to compute is reduced considerably. From a practical point of view, in a molecular dynamics simulation, a data structure called neighbor list is built at each timestep. This structure stores for each atom its neighbors. When interactions of a generic atom have to be computed, its neighbors can be found in the neighbor list.

Since the configuration of the system changes at each timestep, the neighbor list should be always rebuilt. To avoid building the neighbor list at each timestep you can build one greater than necessary. To do this consider a skin distance r_{skin} and a sphere of radius $r_c + r_{skin}$ centered at the atom i (figure 2.5). The neighbors of the atom i will be that inside the sphere of radius $r_c + r_{skin}$. In this way more interactions than necessary are computed because atoms between the two spheres (that of radius r_c and that of radius $r_c + r_{skin}$) have a negligible interaction with the atom i . If you are sure that atoms in the system cannot be moved more than r_{skin} in M timestep then you can build the neighbor list

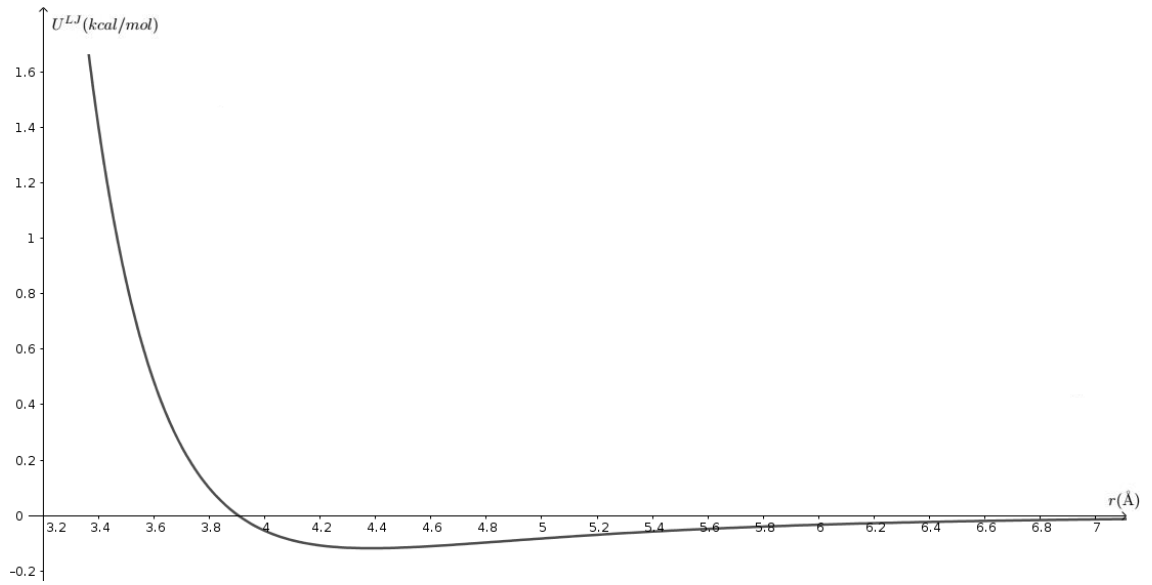


Figure 2.4: Lennard-Jones potential for $\varepsilon = 0.118$ kcal/mol and $\sigma = 3.905$ Å.

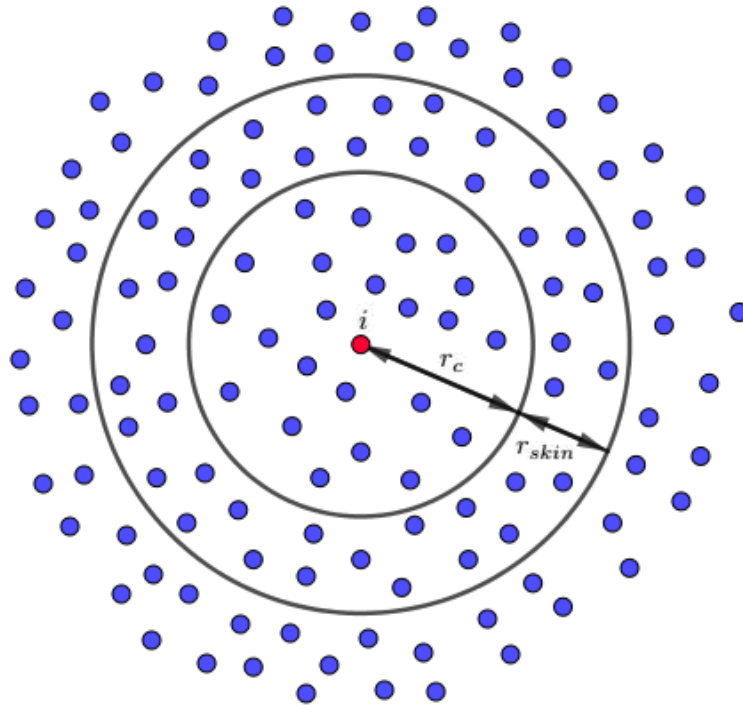


Figure 2.5: the red point is the atom i , the blue points are the other atoms.

every M timestep. This is why the neglected interactions are those with the atoms outside the sphere of radius $r_c + r_{skin}$. If in M timestep these atoms cannot move than r_{skin} , they cannot will enter in the sphere of radius r_c , thus their interactions with the atom i will still be negligible.

Note that as the skin distance increases more negligible interactions will be computed but the neighbor list can be rebuilt less often. Thus the choice of r_{skin} value is a trade-off.

2.2.2 Boundary Conditions

In LAMMPS the volume where the atoms are contained is called simulation box. The box used by LAMMPS is in the shape of a cube and you have to define the edges in all dimensions (x, y and z). Then you have also to define the boundary conditions that is you have to tell the simulator what happens when an atom reaches a edge of the box. For example in LAMMPS you can decide that if an atom exceeds any edge of the box it will be removed from the simulation or you can also decide that if an atom collides with an edge it bounces in an elastic way.

To limit the effect of the box surface, another approach is to use periodic boundary conditions. In this case the simulation box is surrounded by 26 identical replicas of itself [12] as shown in figure 2.6. Note that in figure 2.6 there are only 8 boxes around the central one because the picture is 2D, but in 3D case there are 18 more boxes. With periodic boundary conditions the total force \mathbf{F}_i acting on each atom is computed at each timestep only for the atoms in the central box. The neighbors of a generic atom in the central box can be also atoms in the boxes surrounding the central one. An example is shown in figure 2.6: the atom i (red point) has four neighbors where two of these are not inside the central box. After that \mathbf{F}_i for atoms in the central box is computed, their position after the small increment of time Δt is obtained integrating the equation of motion. Atoms' position in the other boxes is not computed, it simply follows that in the central box at each timestep.

When you use periodic boundary conditions it is easy to notice from figure 2.6 that you must have $L > 2r_c$ where L is the box length and r_c the cutoff [13].

Using periodic boundary conditions, during the course of the simulation if an atom crosses an edge of the simulation box, it reenters from the opposite side. In LAMMPS you can choose to use periodic boundary conditions in one, two or all three spatial dimensions.

2.2.3 Ensembles

In the MD algorithm considered until now the total energy E_{tot} of the system is constant over time. This is why we are not considered the effect that the outside world has on the system. In the algorithm each atom is affected only by the other atoms in the system and not by the external world. Thus it is like we have an isolated system.

According to the MD algorithm each atom i in the system moves under the effect of a conservative force \mathbf{F}_i therefore its mechanical energy (the sum of its potential and kinetic energy) is constant. Since the total energy of each atom is constant, also the total energy of the entire system is constant. You can prove this with LAMMPS but you have to be careful that atoms in the system

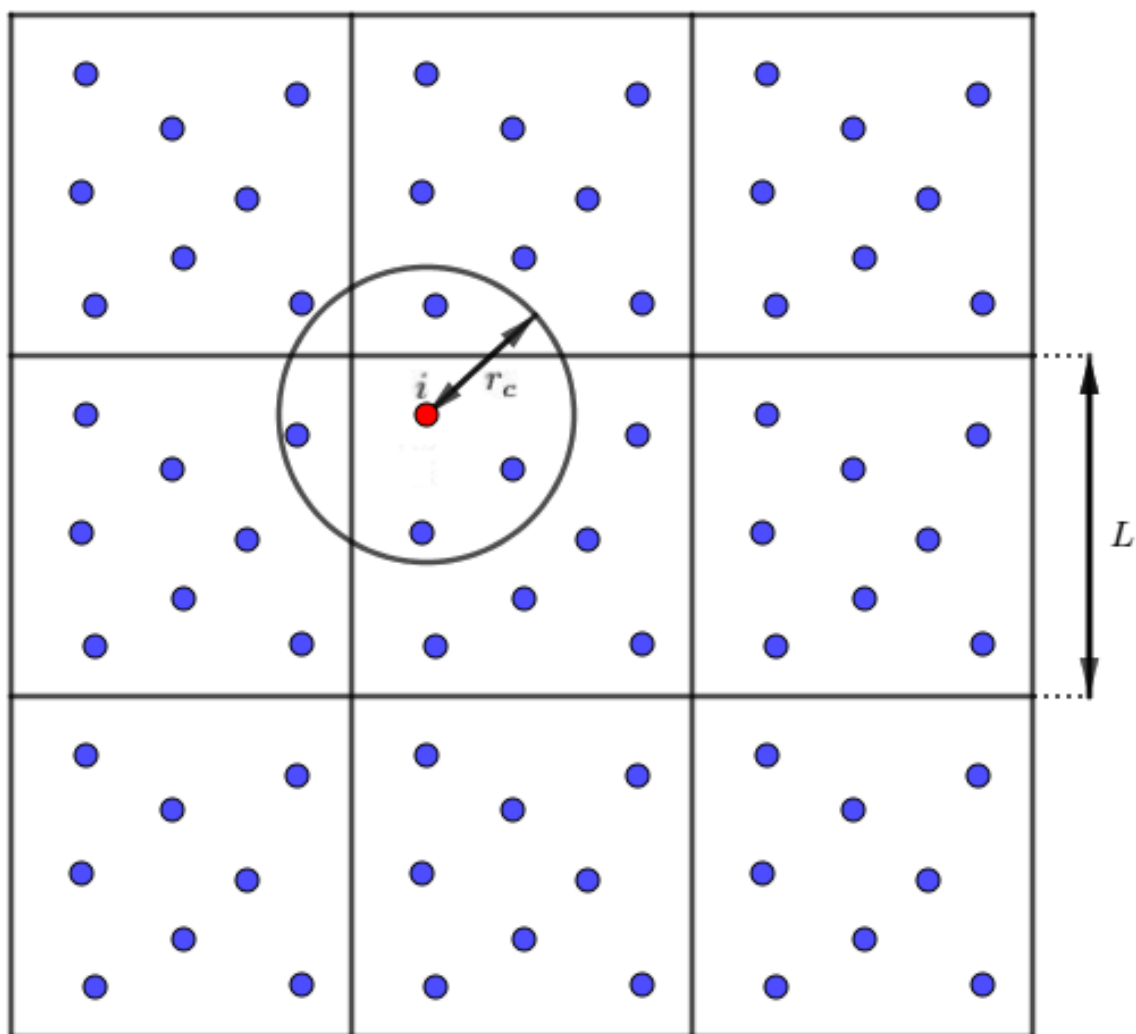


Figure 2.6: Periodic boundary conditions.

do not interact with the edges of the simulation box (for instance making the volume of the box very large).

A system characterized by a number of atoms N , volume V and total energy E_{tot} constant is called microcanonical ensemble (NVE). This type of system cannot reproduce many experimental data because these are usually obtained under constant temperature and pressure. To keep constant these quantities in a experiment, the system somehow interacts with the external world.

In a MD simulation, to maintain constant the temperature, the simplest method is that of Woodcock. It consists to compute at each timestep an appropriate factor, that multiplied by atoms' velocities, allows to obtain the required value of temperature [12]. This method exploits simply equations 2.20 and 2.21. Note that if the temperature is held constant, the total energy of the system will be not constant anymore; if the temperature is fixed the total energy will be change and viceversa.

In LAMMPS, to keep constant the temperature, a more advanced method is used, that of Nose-Hoover [17].

When you perform a simulation keeping number of atoms N , volume V and temperature T constant, the system is in the so-called canonical ensemble (NVT). Finally in LAMMPS you can simulate a system where number of atoms N , pressure P and temperature T are constant. This type of system is called isothermal-isobaric ensemble (NPT). The principle to fix the pressure to the required value in a MD simulation is to vary the volume step by step according to the equation 2.23 (you know pressure and temperature therefore you can obtain the volume). Note that in a MD simulation if the pressure is fixed the volume will be change and viceversa.

When you perform a simulation with LAMMPS, you have to tell which ensemble each atom belongs to, otherwise the atoms will be not integrated.

2.3 LAMMPS Results & VMD

Results of LAMMPS simulations are written in txt files. You can decide what quantities to store every an arbitrary number M of timestep. For example you can generate a txt file that stores thermodynamic quantities of the system such as temperature, pressure, volume, kinetic and potential energy every M timestep. Then you can also produce an other txt file that stores atoms' position every M timestep. The first is the LAMMPS log file while the second is usually called trajectory file because contains the evolution of the atoms' position according to time. Note that if the system contains several thousand atoms and many timestep are stored, the trajectory file will be huge and it will take up a lot of memory.

If you want, you can write some programs, for example a Matlab script, in order to read the output files of LAMMPS and elaborate the informations in it, generating some graphs for instance. Fortunately such programs already exist, one of these, that used in this thesis, is VMD (Visual Molecular Dynamics). VMD is able to take the trajectory file generated by LAMMPS as input and display in a 3D view each frame stored in it. Frames can also be displayed sequentially thus obtaining a movie of the evolution of the system.

In VMD it is also possible to set representation, dimension and colour of the atoms. Then you can select which atoms to show, this is very useful for complex

systems or if you want to see some details.

VMD can also be used to visualize results generated by other software since it support over 60 molecular file formats.

Since LAMMPS does not have a graphical interface, having a software like VMD, that show graphically the evolution of the system, is essential for debugging. In this way you can check if the initial configuration of the system is set correctly or if during the evolution of the system something definitely wrong happens.

In order to elaborate output results, several Matlab script are available in the LAMMPS directory tools/matlab. One of these reads thermodynamic quantities from the LAMMPS log file so that these can be processed.

Chapter 3

Force Field Computation with Density Functional Theory

In the previous chapter, we have seen that to run a MD simulation the two main ingredients are the initial configuration of the system and what are the interactions among the atoms (force field). The latter is the most problematic to obtain and can be considered the heart of a MD simulation since everything depends on it.

Interactions among atoms depend on atom types and on the particular type of simulation. For example the energy of C–H bond is different from that of C–C bond, but also the energy of C–C bond is different from that of a double bond C=C, and then the energy of a single bond C–C is different if the bond is in a linear molecule like an hexanethiol (figure 4.2) or in a "ring" molecule like benzene. Thus, find the right force field for the simulation it is not a trivial task and, if the choice is not adequate, the simulation will be wrong.

Many efforts have been made by researchers to develop force fields for many situations. For instance OPLS, AMBER, CHARMM and GROMOS are force fields that can be used to model interactions among atoms within a molecule, then, there are also force fields like EAM (embedded-atom method) or MEAM (modified embedded-atom method) to model pairwise interactions for metals and metal alloys. The hard task is always to understand if a force field is suitable for our case and in any case find the parameters in literature.

In this thesis we will often use force field parameters found in research papers but we will also obtain some parameters from ourselves. To do this, we use a method that needs to solve the Schrödinger equation for the electrons in a molecule. This is done with the software ORCA that is able to solve the Schrödinger equation applying the density functional theory (DFT).

In this chapter, first of all, a simple explanation of the DFT will be introduced, then the method used in this thesis to evaluate force field parameters for bonds, angles and dihedrals within a molecule is described. Finally, there are some examples in which some parameters, that will be used next for some MD simulations, are computed.



Figure 3.1: DFT as a black box.

3.1 Density Functional Theory

In this section a brief explanation of density functional theory (DFT) is given. Many details will be skipped since we are only interested in applying DFT and not in the whole theory. To get a deeper understanding about DFT please refer to [18].

DFT is a method that is able to obtain the ground state energy E_0 of a generic system constituted by a number M of nuclei and a number N of electrons. It can be seen as a black box (figure 3.1) that needs the number M of nuclei, the atomic number Z and the position R of each nucleus and the number N of the electrons as input and delivers the ground state energy E_0 and the associate electron density ρ_0 (that we will see later what it is).

3.1.1 Many-body Schrödinger Equation

A system constituted by a number M of nuclei and a number N of electrons can be associated to the many-body Schrödinger equation

$$\hat{H}\Psi_i(\vec{x}_1, \vec{x}_2, \dots, \vec{x}_N, \vec{R}_1, \vec{R}_2, \dots, \vec{R}_M) = E_i\Psi_i(\vec{x}_1, \vec{x}_2, \dots, \vec{x}_N, \vec{R}_1, \vec{R}_2, \dots, \vec{R}_M) \quad (3.1)$$

where $\Psi_i(\vec{x}_1, \vec{x}_2, \dots, \vec{x}_N, \vec{R}_1, \vec{R}_2, \dots, \vec{R}_M)$ stands for the wave function of the i 'th state of the system and E_i is the numerical value of the energy of the state described by Ψ_i . Each electron i is described by three spatial coordinates and one spin coordinate which are collected in $\vec{x}_i = (x_{i_x}, x_{i_y}, x_{i_z}, s_i)$ while each nucleus A is described with only three spatial coordinates collected in $\vec{R}_A = (R_{A_x}, R_{A_y}, R_{A_z})$. \hat{H} is a differential operator, called Hamiltonian, representing the total energy of the system:

$$\hat{H} = -\frac{\hbar^2}{2m_e} \sum_{i=1}^N \nabla_i^2 - \frac{\hbar^2}{2} \sum_{A=1}^M \frac{1}{M_A} \nabla_A^2 - \frac{q^2}{4\pi\epsilon_0} \sum_{i=1}^N \sum_{A=1}^M \frac{Z_A}{r_{iA}} + \frac{q^2}{4\pi\epsilon_0} \sum_{i=1}^N \sum_{j>i}^N \frac{1}{r_{ij}} + \frac{q^2}{4\pi\epsilon_0} \sum_{A=1}^M \sum_{B>A}^M \frac{Z_A Z_B}{R_{AB}} \quad (3.2)$$

Here, A and B run over the M nuclei while i and j denote the N electrons in the system. The first two terms describe the kinetic energy of the electrons and nuclei respectively, where m_e is the mass of electron, M_A is the mass of nucleus A , ∇_i^2 and ∇_A^2 are Laplace operators defined as:

$$\nabla_i^2 = \frac{\partial^2}{\partial x_{i_x}^2} + \frac{\partial^2}{\partial x_{i_y}^2} + \frac{\partial^2}{\partial x_{i_z}^2} \quad (3.3)$$

$$\nabla_A^2 = \frac{\partial^2}{\partial R_{A_x}^2} + \frac{\partial^2}{\partial R_{A_y}^2} + \frac{\partial^2}{\partial R_{A_z}^2} \quad (3.4)$$

The remaining three terms define the potential part of the Hamiltonian and represent the attractive electrostatic interaction between the nuclei and the electrons and the repulsive potential due to the electron-electron and nucleus-nucleus interactions, respectively. $r_{iA} = |\vec{x}_i - \vec{R}_A|$, $r_{ij} = |\vec{x}_i - \vec{x}_j|$ and $R_{AB} = |\vec{R}_A - \vec{R}_B|$ are respectively the distances between electron-nucleus, electron-electron and nucleus-nucleus, q is the elementary charge, ε_0 is the vacuum permittivity, \hbar is reduced Planck's constant and Z_A is the atomic number of nucleus A [18].

A first approximation to solve the Schrödinger equation is that of Born-Oppenheimer which considers the nuclei fixed in space. This approximation is justified since the nuclei are much heavier than electrons, therefore, they also move much slower. If the nuclei are fixed in space, their kinetic energy is zero and the potential energy due to nucleus-nucleus repulsion is a constant [18]. Thus, the complete Hamiltonian given in equation 3.2 reduces to the so-called electronic Hamiltonian

$$\hat{H}_{elec} = -\frac{\hbar^2}{2m_e} \sum_{i=1}^N \nabla_i^2 - \frac{q^2}{4\pi\varepsilon_0} \sum_{i=1}^N \sum_{A=1}^M \frac{Z_A}{r_{iA}} + \frac{q^2}{4\pi\varepsilon_0} \sum_{i=1}^N \sum_{j>i}^N \frac{1}{r_{ij}} = \hat{T} + \hat{V}_{Ne} + \hat{V}_{ee} \quad (3.5)$$

The solution of the Schrödinger equation with \hat{H}_{elec} is the electronic wave function of the i 'th state $\Psi_{i_{elec}}$, which depends only on the electron coordinates and not on the nuclei ones, and its associated energy $E_{i_{elec}}$:

$$\hat{H}_{elec} \Psi_{i_{elec}}(\vec{x}_1, \vec{x}_2, \dots, \vec{x}_N) = E_{i_{elec}} \Psi_{i_{elec}}(\vec{x}_1, \vec{x}_2, \dots, \vec{x}_N) \quad (3.6)$$

The total energy of the i 'th state of the system is given by

$$E_{i_{tot}} = E_{i_{elec}} + E_{nuc} \quad (3.7)$$

where

$$E_{nuc} = \frac{q^2}{4\pi\varepsilon_0} \sum_{A=1}^M \sum_{B>A}^M \frac{Z_A Z_B}{R_{AB}} \quad (3.8)$$

is the constant nuclear repulsion term [18].

From now on we will only consider the electronic problem of equations 3.5, 3.6, 3.7, 3.8 and the subscript 'elec' will be dropped.

A physical interpretation of the wave function Ψ_i can only be associated with its squared modulus in that

$$|\Psi_i(\vec{x}_1, \vec{x}_2, \dots, \vec{x}_N)|^2 d\vec{x}_1 d\vec{x}_2 \dots d\vec{x}_N \quad (3.9)$$

represents the probability that electrons 1, 2, ..., N are found simultaneously in volume $d\vec{x}_1 d\vec{x}_2 \dots d\vec{x}_N$.

The probability of finding the N electrons anywhere in space must be exactly unity, i.e.

$$\int \dots \int |\Psi_i(\vec{x}_1, \vec{x}_2, \dots, \vec{x}_N)|^2 d\vec{x}_1 d\vec{x}_2 \dots d\vec{x}_N = 1 \quad (3.10)$$

A wave function which satisfies equation 3.10 is said to be normalized [18].

3.1.2 The Variational Principle

Apart from a few trivial exceptions, no strategy to solve the Schrödinger equation exactly for atomic and molecular systems is known [18]. Nevertheless the wave function of the ground state Ψ_0 and the associated energy E_0 can be found thanks to the variational principle that it is one of the DFT's cornerstone.

Before going on we recall that the expectation value of a particular observable represented by the appropriate operator \hat{O} is given by

$$\langle \hat{O} \rangle = \int \cdots \int \Psi_i^* \hat{O} \Psi_i d\vec{x}_1 d\vec{x}_2 \dots d\vec{x}_N \equiv \langle \Psi_i | \hat{O} | \Psi_i \rangle \quad (3.11)$$

where Ψ_i must satisfy the normalization condition 3.10 and the star in Ψ_i^* indicates the complex-conjugate of Ψ_i [18].

The variational principle now states that the energy computed via equation 3.11 as the expectation value of the Hamiltonian operator \hat{H} from any guessed Ψ_{trial} will be an upper bound to the true energy of the ground state, i. e.,

$$\langle \Psi_{trial} | \hat{H} | \Psi_{trial} \rangle = E_{trial} \geq E_0 = \langle \Psi_0 | \hat{H} | \Psi_0 \rangle \quad (3.12)$$

where the equality holds if and only if Ψ_{trial} is identical to Ψ_0 [18].

This means (at least in principle) that you can insert all the acceptable wave function in 3.12 and the minimum value of energy obtained corresponds to the ground state energy E_0 . Acceptable means in this context that the trial functions Ψ_{trial} must be continuous everywhere and be quadratic integrable in order to satisfy the equation 3.10. Obviously the trial function used to obtain E_0 corresponds to the ground state wave function Ψ_0 .

A rule such that as that given through 3.11 or 3.12, which assigns a number, e. g. E_{trial} , to a function, e.g. Ψ_{trial} , is called a functional. Other examples of functionals, where the input is a function and the output is a number, can be the derivative evaluated in a point or a definite integral of a function. To distinguish a functional from a function in writing, one usually employs square brackets for the argument. Hence, $f(x)$ is a function of the variable x while $F[f]$ is a functional of the function f [18].

The variational principle in equation 3.12 can now be written as

$$E_0 = \min (E[\Psi_{trial}]) = \min (\langle \Psi_{trial} | \hat{H} | \Psi_{trial} \rangle) = \min (\langle \Psi_{trial} | \hat{T} + \hat{V}_{Ne} + \hat{V}_{ee} | \Psi_{trial} \rangle) \quad (3.13)$$

Thus the functional $E[\Psi_{trial}]$ must be minimized searching over all eligible functions Ψ_{trial} in order to find E_0 .

Obviously is not possible searching over all possible wave function Ψ_{trial} to minimize $E[\Psi_{trial}]$. This problem can be solved using the Hartree-Fock (HF) approximation which consists to search the wave function in a suitable subset that offers a physically reasonable approximation to the exact wave function. In the HF approximation this subset includes wave functions that can be described by a Slater determinant (see [18]).

However the HF approximation is still very complicated because it needs to manage the wave functions that depends on $3N$ spatial plus N spin variables. The systems we are interested contain many atoms and many more electrons, thus, the wave function has an unmanageable size.

To simplify the problem, one wonders if the variational principle can be applied

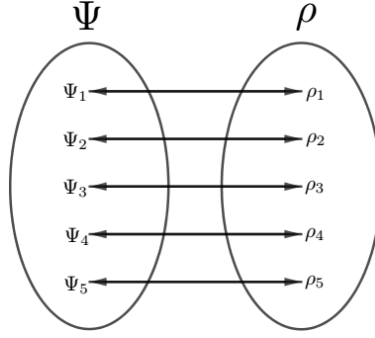


Figure 3.2: first Hohenberg-Kohn theorem consequence.

to obtain the ground state energy E_0 using a simpler function related to the wave function. The answer to this question is yes, and, this function is the electron density which we will see below.

3.1.3 The Electron Density & Hohenberg-Kohn Theorems

The electron density $\rho(\vec{r})$ is defined as the following multiple integral over the spin coordinates of all electrons and over all but one of the spatial variables

$$\rho(\vec{r}) = N \int \cdots \int |\Psi(\vec{x}_1, \vec{x}_2, \dots, \vec{x}_N)|^2 ds_1 d\vec{x}_2 d\vec{x}_3 \dots d\vec{x}_N \quad (3.14)$$

$\rho(\vec{r})$ determines the probability of finding any of the N electrons within the volume element $d\vec{r}$ (which is the infinitesimal volume centered at the position pointed by \vec{r}) but with arbitrary spin while the other $N-1$ electrons have arbitrary positions and spin in the state represented by Ψ [18].

The integral of the electron density over all the space is equal to the number of the electron:

$$\int \rho(\vec{r}) d\vec{r} = N \quad (3.15)$$

The wave function depends on $4N$ variables and returns a complex number while the electron density depends on only three spatial coordinates and returns a real number, thus, it is considerably much more simpler. Moreover, Unlike the wave function, the electron density is an observable and can be measured experimentally [18].

Hence, it would be very convenient using the the electron density instead of the wave function, but this is possible only if the electron density contains the same information as the wave function. The answer to this question was given by the first Hohenberg-Kohn theorem which is an other DFT's milestone. The very surprising consequence of this theorem is that there is one-to-one correspondence between the wave function and the electron density. In other words the function that connects the wave function to the electron density is bijective that means that to each wave function corresponds exactly one electron density, and to each electron density corresponds exactly one wave function (figure 3.2).

Thanks to this one-to-one correspondence, it can be stated that the electron density contains the same information as the wave function. Now, one wonders

if the variational principle can be applied with the electron density in order to find the energy ground state. The answer to this question was given by the second Hohenberg-Kohn theorem. This theorem states that the functional

$$E[\rho] = E_{Ne}[\rho] + F_{HK}[\rho] \quad (3.16)$$

delivers the lowest energy if and only if the input density is the true ground state density ρ_0 . This is nothing else than the variational principle that can be expressed as [18]

$$E_0 \leq E[\rho] = E_{Ne}[\rho] + F_{HK}[\rho] \quad (3.17)$$

where in equations 3.16 and 3.17 the functional E_{Ne} is the system dependent part and the F_{HK} is the Hohenberg-Kohn functional which is universally valid. The first is given by

$$E_{Ne}[\rho] = \int \rho(\vec{r}) V_{Ne} d\vec{r} \quad (3.18)$$

with

$$V_{Ne} = -\frac{q^2}{4\pi\epsilon_0} \sum_{i=1}^N \sum_{A=1}^M \frac{Z_A}{r_{iA}} \quad (3.19)$$

and the Hohenberg-Kohn functional equal to

$$F_{HK}[\rho] = T[\rho] + E_{ee}[\rho] \quad (3.20)$$

contains the functional for the kinetic energy $T[\rho]$ and that for the electron-electron interaction $E_{ee}[\rho]$. The explicit form of both these functionals is unfortunately unknown. However, from the latter we can extract at least the classical Coulomb part $J[\rho]$ [18]

$$E_{ee}[\rho] = \frac{1}{2} \int \int \frac{\rho(\vec{r}_1)\rho(\vec{r}_2)}{r_{12}} d\vec{r}_1 d\vec{r}_2 + E_{ncl}[\rho] = J[\rho] + E_{ncl}[\rho] \quad (3.21)$$

E_{ncl} is the non-classical contribution to the electron-electron interaction containing all the effects of self-interaction correction and exchange and Coulomb correlation [18].

3.1.4 The Kohn-Sham Approach

Hohenberg-Kohn theorems give us not a practical way to compute the ground state energy E_0 of a system since, in the functional $F_{HK}[\rho] = T[\rho] + J[\rho] + E_{ncl}[\rho]$, only $J[\rho]$ is known, while the explicit forms of the other two contributions remain a mystery.

To solve this problem Kohn and Sham introduced the concept of a non-interacting reference system built from a set of orbitals (i.e., one electron functions) such that the major part of the kinetic energy T can be computed to good accuracy [18]. In this context the kinetic energy T consists of two terms, that of the non-interacting system T_S and the residual part of the true kinetic energy T_C :

$$T[\rho] = T_S[\rho] + T_C[\rho] \quad (3.22)$$

Thus, the Hohenberg-Kohn functional can be written as:

$$F_{HK}[\rho] = T_S[\rho] + T_C[\rho] + J[\rho] + E_{ncl}[\rho] = T_S[\rho] + J[\rho] + E_{XC}[\rho] \quad (3.23)$$

where E_{XC} is the so-called exchange-correlation energy

$$E_{XC}[\rho] \equiv T_C[\rho] + E_{ncl}[\rho] \quad (3.24)$$

which contains everything that is unknown.

Now, it can be proved [19] that in order to minimize the energy expression 3.16 to compute the ground state energy E_0 (this is the variational principle as already said above), you have to solve the following Kohn-Sham equations:

$$\left(-\frac{1}{2}\nabla^2 + V_{eff}(\vec{r}_1) \right) \phi_i = \varepsilon_i \phi_i \quad i = 1, 2, \dots, N \quad (3.25)$$

where

$$V_{eff}(\vec{r}_1) = \int \frac{\rho(\vec{r}_2)}{|\vec{r}_1 - \vec{r}_2|} d\vec{r}_2 + V_{XC}(\vec{r}_1) - \sum_A^M \frac{Z_A}{r_{1A}} \quad (3.26)$$

$$V_{XC} = \frac{\delta E_{XC}}{\delta \rho} \quad (3.27)$$

$$\langle \phi_i | \phi_j \rangle = \delta_{ij} \quad (3.28)$$

After solving equations 3.25, the electron density that delivers the ground state energy is

$$\rho_0(\vec{r}) = \sum_i^N \sum_s |\phi_i(\vec{r}, s)|^2 \quad (3.29)$$

Finally the ground state energy is

$$E_0 = \int \rho_0(\vec{r}) V_{Ne} d\vec{r} + T_S[\rho_0] + J[\rho_0] + E_{XC}[\rho_0] \quad (3.30)$$

where

$$J[\rho_0] = \frac{1}{2} \int \int \frac{\rho(\vec{r}_1)\rho(\vec{r}_2)}{r_{12}} d\vec{r}_1 d\vec{r}_2 \quad (3.31)$$

$$T_S = -\frac{1}{2} \sum_i^N \langle \phi_i | \nabla^2 | \phi_i \rangle \quad (3.32)$$

Regarding the exchange-correlation energy E_{XC} , if its exact form is known, the Kohn-Sham strategy would lead to the exact energy! This is why the Kohn-Sham approach does not contain any approximation. The approximation only enters when we have to decide on an explicit form of the unknown functional for E_{XC} . The central goal of modern density functional theory is therefore to find better and better approximation of E_{XC} [18].

It is important to note that the electron density appears in Kohn-Sham equations (3.25) through $V_{eff}(\vec{r}_1)$ complicating our problem. Thus you have to proceed iteratively in order to find ρ_0 . An initial guess for ρ_0 is chosen, then V_{eff} is computed, then Kohn-Sham equations are solved, then ρ_0 is computed and if it is different within a certain threshold from the initial one, then it is the right density otherwise the cycle is repeated (figure 6.6).

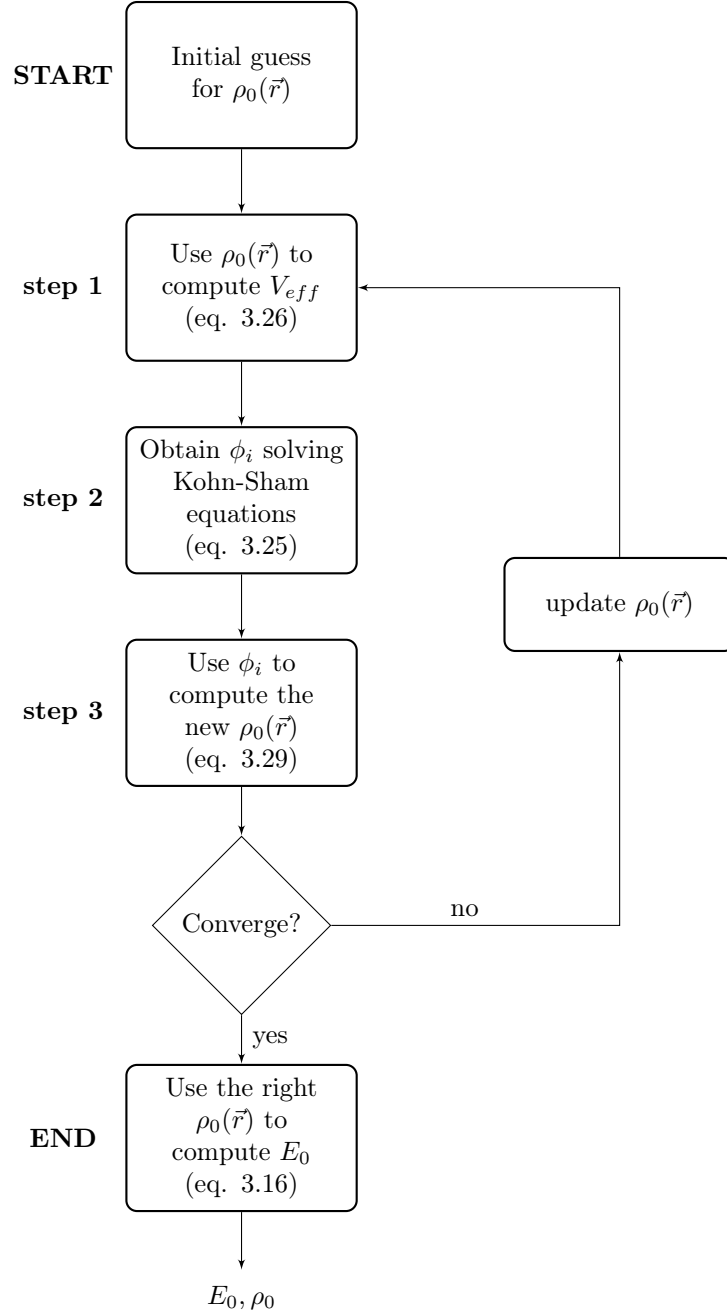


Figure 3.3: DFT algorithm scheme.

Sumarizing, DFT allows us to obtain the ground state energy of a system solving N one electron Kohn-Sham equations instead of the much more complicated many-body Schrödinger equation. In theory, there is no loss of information in this transformation if the exact form of E_{XC} is known, however, since E_{XC} is not known we have to decide on an explicit form for it, thus introducing an approximation. Kohn-Sham equations can be solved, in a relatively simple way, with numerical method that are implemented in computer codes e.g. VASP, Quantum ESPRESSO or ORCA. Then a loop is required to compute the ground state density since it appears in the Kohn-Sham equations. Finally, after the ground state density is found, the ground state energy will be computed. Note that there is no the wave function in density functional theory, the outputs are only ρ_0 and E_0 .

3.2 Force Field Evaluation

With reference to the figure 3.1, position and type of each atom in a molecule corresponds respectively to the position R and the atomic number Z of each nucleus. Then, the number M of nuclei is also the number of atoms and the number N of electrons is the sum of all nuclei's atomic numbers. Hence, if you know position and type of each atom that constitute a molecule, you can compute its energy. In other words the energy E of a molecule is function of the coordinates of the atoms that we collect in the vector \mathbf{x} :

$$E = E(\mathbf{x}) \quad (3.33)$$

Knowing $E(\mathbf{x})$ means that the molecule energy is known in each conformation, therefore, it is possible to find the conformation of minimum energy. The function that approximates $E(\mathbf{x})$ is called force field.

Cartesian coordinates of the atoms are not the best choice to describe the $E(\mathbf{x})$ function, since, the dipendence of $E(\mathbf{x})$ from them is complex. Indeed moving a single Cartesian coordinate, bond lengths, bond angles and torsional angles are simultaneously deformed. Moreover if the molecule translates or rotates, every Cartesian coordinates changes but the geometry of the molecule and then, also the energy, do not change.

Internal coordinates (see appendix A) do not have the problems just mentioned, therefore they are more appropriate to describe $E(\mathbf{x})$. To fix the geometry¹ of a molecule, and thus its energy, $3N - 6$ internal coordinates are required where N is the number of atoms (see appendix A). Hence, the energy E of the molecule is function of $3N - 6$ variables:

$$\mathbf{x} = (x_1, x_2, \dots, x_{3N-6}) \quad (3.34)$$

In principle, for each conformation of the molecule, which is defined by a certain value of the vector \mathbf{x} , the energy E of the molecule can be computed via DFT method. Thus the function $E(\mathbf{x})$ could be obtained computing many points. However, a small number of atom N is enough to have a considerable number of variables ($3N - 6$), doing that a myriad number of points is required to trace $E(\mathbf{x})$ accurately, making this method not applicable.

¹fix the geometry means that the molecule can translate or rotate in the space but its structure remains unchanged.

The strategy used in this thesis to evaluate force field parameters of a molecule starts from the equilibrium structure of the molecule itself. One might think that this does not make sense because to find the equilibrium position of a molecule you should minimize $E(\mathbf{x})$ that it is what we want to find. Actually the equilibrium geometry of the most recurring molecules is known, because in literature several force fields are developed with which the structure of many molecules can be optimized minimizing $E(\mathbf{x})$.

To find the equilibrium position of a molecule, we will use the software Avogadro, in which it is possible to draw a molecule, and then optimizing its geometry using the available force fields. The default force field is UFF (Universal Force Field) which is capable of reproducing the most structural features across the periodic table. However, depending on the molecule being tested, other force fields may be better suited to optimize the molecular parameters. Moreover, in Avogadro a lot of molecules are available already optimized.

Once the equilibrium structure of the molecule is obtained, its Z-matrix (see appendix A) is computed. There are many different Z-matrix that can describe the equilibrium structure of the molecule, this is why the position of each atom is defined relatively with respect to other three atoms and their choice is completely arbitrary. However, it is not recommended writing the Z-matrix randomly, but it is convenient using distances and angles among atoms actually linked by a chemical bonds. This is useful because what we are going to do is see how the energy of the molecule changes when a single parameter of the Z-matrix changes. Thus, choosing the bond distances and the bond angles (and not any distances and angles), we can obtain characteristics similar to some already present in literature, thus having a feedback or an indication about what has been obtained. Moreover, in this way we can export the obtained parameters and use them again in other molecules with similar bonds and angles.

Once the Z-matrix of the molecule at the equilibrium is written, all its parameters are collected in

$$\mathbf{x}_{eq} = (x_{1_{eq}}, x_{2_{eq}}, \dots, x_{3N-6_{eq}}) \quad (3.35)$$

The minimum energy of the molecule is obtained for $\mathbf{x} = \mathbf{x}_{eq}$

$$E_{min} = E(\mathbf{x}_{eq}) \quad (3.36)$$

At this point we evaluate how the energy varies when the conformation of the molecule moves from that of equilibrium. This is done using ORCA, an ab initio quantum chemistry program package, in which the DFT method is implemented. ORCA requires position and type of each atom that constitute the molecule as input and returns the corresponding energy of the system. With ORCA the energy of the system (the molecule) is computed varying the $3N - 6$ parameters one at a time while the other parameters are fixed to the equilibrium value, thus

the following functions are obtained:

$$\begin{aligned}
 &E(x_1, x_2 = x_{2_{eq}}, x_3 = x_{3_{eq}}, \dots, x_{3N-6} = x_{3N-6_{eq}}) \\
 &E(x_1 = x_{1_{eq}}, x_2, x_3 = x_{3_{eq}}, \dots, x_{3N-6} = x_{3N-6_{eq}}) \\
 &\vdots \\
 &E(x_1 = x_{1_{eq}}, x_2 = x_{2_{eq}}, x_3 = x_{3_{eq}}, \dots, x_{3N-6})
 \end{aligned} \tag{3.37}$$

which are $3N - 6$ functions of only one variable.

From now on, we will written the functions in equation 3.37 in the following compact way:

$$E(x_i) \quad i = 1, 2, \dots, 3N - 6 \quad \& \quad x_j = x_{j_{eq}} \quad \text{for } \forall j \neq i \tag{3.38}$$

These functions evaluated in $x_{i_{eq}}$ returns the minimum energy

$$E(x_i = x_{i_{eq}}) = E_{min} \quad \forall i = 1, 2, \dots, 3N - 6 \tag{3.39}$$

After their computation, the $E(x_i)$ functions are shifted down by the quantity E_{min} . It is like fixing E_{min} equal to zero. In this way $E(x_i = \bar{x})$ represent the energy needed to move the variable x_i from the equilibrium value $x_{i_{eq}}$ to the non equilibrium value \bar{x} while the other variables $x_j \neq x_i$ are fixed to their equilibrium value $x_{j_{eq}}$.

In our model, the $E(x_i)$ functions are those that we will give to LAMMPS to compute bonds, angles and dihedrals energies of the molecule. In other words, the $E(x_i)$ functions define the force field to describe the molecule. In this context, the forces between atoms within the molecule are computed by LAMMPS using the formula

$$F_i = -\frac{dE(x_i)}{dx_i} \tag{3.40}$$

If the molecule is in equilibrium then $F_i = 0 \quad \forall i$, otherwise the forces F_i are different to zero and they act to restore the equilibrium position.

Note that each force F_i related to the variable x_i is exact only if the other variables $x_j \neq x_i$ are set to their equilibrium value. In any case, we will use the same expression for the F_i force even if the $x_j \neq x_i$ variables are not set to their equilibrium value, this is obviously an approximation.

In LAMMPS, the energy of the molecule is given summing up the energies of all bonds, angles and dihedrals, that means

$$E_{molecule} = E_{bonds} + E_{angles} + E_{dihedrals} = \sum_{i=1}^{3N-6} E(x_i) \tag{3.41}$$

The meaning of this energy is the energy required to move the molecule from its equilibrium position to the non equilibrium position defined by the x_i variables (this is why the E_{min} value is fixed to zero). Also in this case, the non trivial implicit approximation done, is that each function $E(x_i)$ is valid even if the other $x_j \neq x_i$ variables are not equal to their equilibrium value.

In the following there are examples where the force field parameters for some bonds, angles and dihedrals are evaluated. The evaluated parameters will be used next in this thesis for some MD simulations.

3.2.1 Butane-1-thiol

Figure 3.4 shows the structure of a butane-1-thiol or 1-butanethiol molecule.

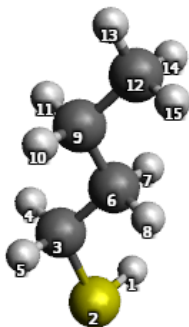


Figure 3.4: 1-Butanethiol or butane-1-thiol molecule ($C_4H_{10}S$). Dark grey is carbon (C), light grey is hydrogen (H) and yellow is sulphur (S).

Labels of the atoms in figure 3.4 are relative to the Z-matrix reported below:

1	H							
2	S	1			1.308			
3	C	2	1		{2-3}	100.2		
4	H	3	2	1	1.106	110.5	67.1	
5	H	3	2	1	1.108	104.8	-179.2	
6	C	3	2	1	{3-6}	114.7	-57.9	
7	H	6	3	2	1.109	110.1	61.0	
8	H	6	3	2	1.109	110.2	-55.2	
9	C	6	3	2	{6-9}	111.1	-177.2	
10	H	9	6	3	1.108	109.9	58.1	
11	H	9	6	3	1.108	110.0	-57.6	
12	C	9	6	3	{9-12}	111.3	-179.8	
13	H	12	9	6	1.097	111.2	180.0	
14	H	12	9	6	1.098	111.7	60.0	
15	H	12	9	6	1.098	111.6	-60.1	

where $\{2-3\} = 1.817$, $\{3-6\} = 1.517$, $\{6-9\} = 1.521$ and $\{9-12\} = 1.512$. In general $\{i-j\}$ terms denote the distance between atom i and atom j . Distances and angles in the Z-matrix are given respectively in angstrom and degree.

Here we are interested in the bond energy between the atom pairs 2-3, 6-9 and 9-12. The pair 2-3 corresponds to the C-S bond, pairs 6-9 and 9-12 correspond both to C-C bond, but in the former there are two CH_2 groups and in the latter there is one CH_2 group and one CH_3 group.

To compute the bond energy of the pair 2-3, the energy of the whole molecule is computed with ORCA leaving all parameters of the Z-matrix fixed except $\{2-3\}$ which is the distance between atom 2 and 3. For each value of $\{2-3\}$ the corresponding energy value is obtained with a DFT simulation. When enough points are obtained they are fitted in order to find an analytic function that describes the bond energy of the pair. This is shown in figure 3.5(a) where the red points obtained with ORCA are fitted with the blue curve. The points are

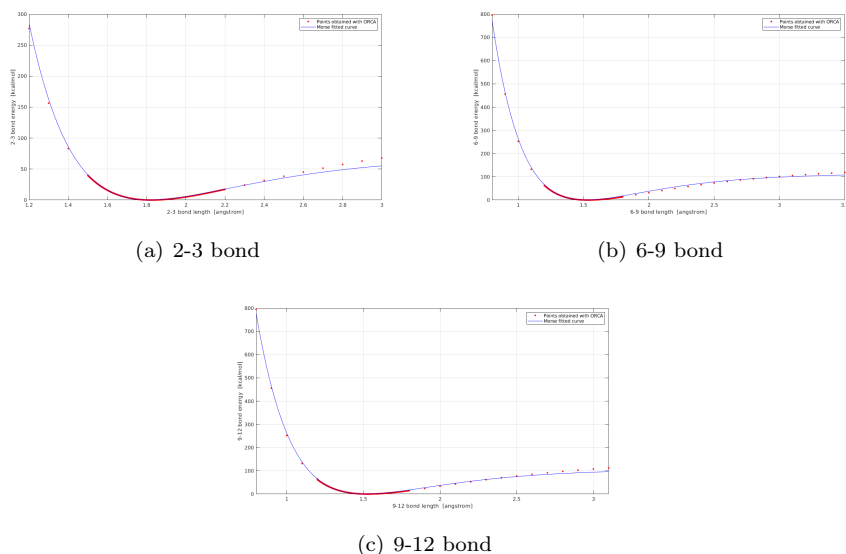


Figure 3.5: Energies of 2-3, 6-9 and 9-12 bonds in butane-1-thiol. Red points are obtained with ORCA and they are interpolated using a Morse potential (blue curve).

Bond	D [kcal/mol]	α [$1/\text{\AA}$]	r_0 [\AA]
2-3	71.4123	1.7857	1.8152
6-9	114.1394	1.7865	1.5179
9-12	108.1007	1.8249	1.5148

Table 3.1: Morse parameters.

fitted with a Morse potential which uses the function

$$E = D \left[1 - e^{-\alpha(r-r_0)} \right]^2 \quad (3.42)$$

where D , α and r_0 are estimated by fitting. The fitting is done with Matlab using the non-linear least squares method.

The same procedure is used to find the bond energy for the pairs 6-9 and 9-12 (see figures 3.5(b) and 3.5(c)). The fitting parameters for each bond are reported in table 3.1.

Very often the bond between two atom is modeled as two masses connected by a spring. When the distance between the two atoms is larger than that of equilibrium the two atoms attract each other while when the distance is shorter than that of equilibrium the two atoms repel each other. This behavior is modeled with the parabolic or harmonic energy function

$$E = K(r - r_0)^2 \quad (3.43)$$

Figure 3.6 shows the fitting using this parabolic function and in table 3.2 are reported the fitting parameters. You can see from the figure 3.6 that the fitting is good only if the bond length does not differ too much from the equilibrium

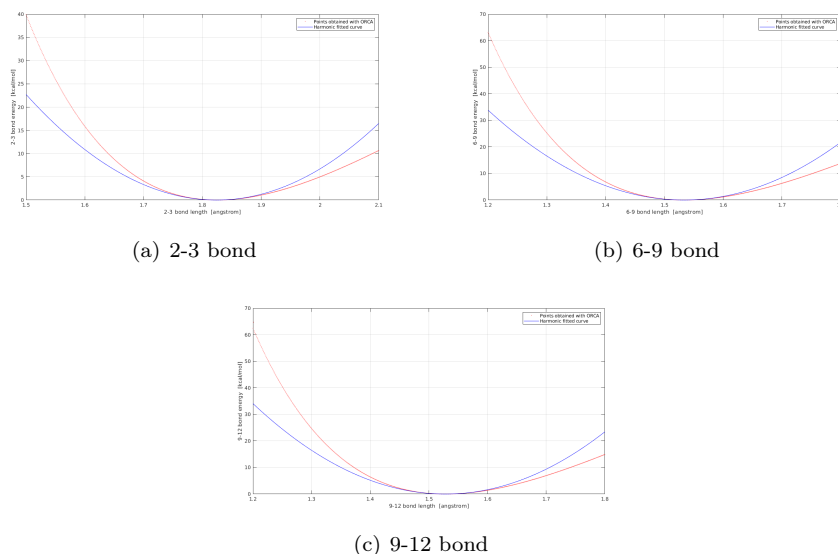


Figure 3.6: Energies of 2-3, 6-9 and 9-12 bonds in butane-1-thiol. Red points are obtained with ORCA and they are interpolated using a harmonic potential (blue curve).

Bond	K [kcal/(mol·Å ²)]	r_0 [Å]
2-3	216.6061	1.824
6-9	305.5069	1.533
9-12	316.8778	1.528

Table 3.2: Harmonic parameters.

one (that of minimum energy). Even if this model is less accurate than the Morse one, it is simpler, more intuitive and less expensive from a computational point of view.

3.2.2 Carbazole

Figure 3.7 shows the carbazole molecule. In the previous example, the corresponding Z-matrix of the molecule has been reported just for clarity, from now on it will not be reported anymore.

Here, we are interested in the energy of the dihedral angles defined by atoms 1-2-3-4, 2-3-4-5, 3-4-7-8, 4-7-8-9, 5-4-3-6 and 6-3-4-7.

Similar to the previous example, the dihedral energy is obtained computing the energy of the molecule with ORCA varying a specific dihedral angles in the Z-matrix while all other parameters are fixed to the equilibrium position. For each dihedral angle, figure 3.8 shows with red points the values obtained with ORCA and with the blue curve the interpolation. The chosen interpolating function is a 4th-order Fourier series

$$E = K_1 [1 + \cos(\phi - \theta_1)] + K_2 [1 + \cos(2\phi - \theta_2)] + K_3 [1 + \cos(3\phi - \theta_3)] + K_4 [1 + \cos(4\phi - \theta_4)] \quad (3.44)$$

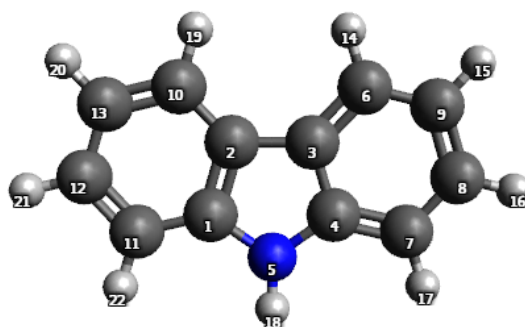
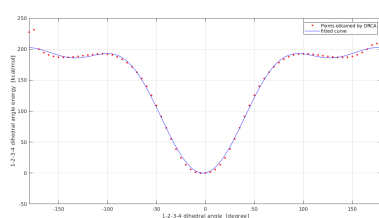
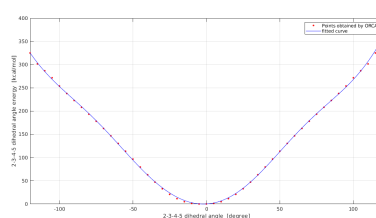


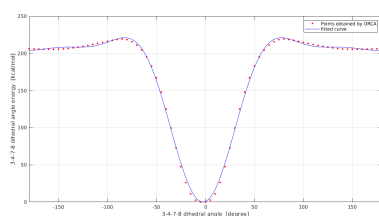
Figure 3.7: Carbazole molecule ($C_{12}H_9N$). Dark grey is carbon (C), light grey is hydrogen (H) and blue is nitrogen (N).



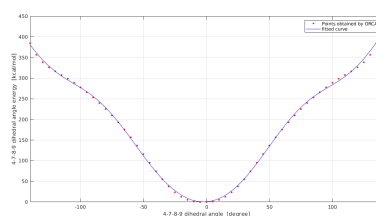
(a) 1-2-3-4 dihedral angle



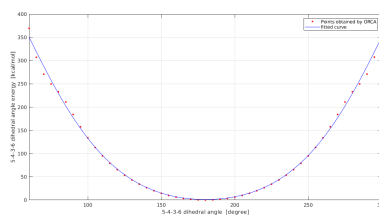
(b) 2-3-4-5 dihedral angle



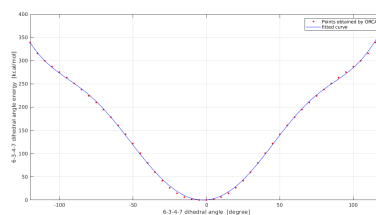
(c) 3-4-7-8 dihedral angle



(d) 4-7-8-9 dihedral angle



(e) 5-4-3-6 dihedral angle



(f) 6-3-4-7 dihedral angle

Figure 3.8: Energies of 1-2-3-4, 2-3-4-5, 3-4-7-8, 4-7-8-9, 5-4-3-6 and 6-3-4-7 dihedral angles in carbazole. Red points are obtained with ORCA and they are interpolated using a 4th-order Fourier series (blue curve).

dihedral angle	[kcal/mol]				[degrees]			
	K_1	K_2	K_3	K_4	θ_1	θ_2	θ_3	θ_4
1-2-3-4	81.9826	45.0545	19.4072	-2.1842	537.4788	535.0071	172.4028	527.9216
2-3-4-5	281.3017	-45.2561	39.7361	-9.3575	537.0570	530.8345	168.2937	519.2620
3-4-7-8	70.4130	58.2787	31.5986	10.3750	537.4985	174.9999	172.5071	529.9564
4-7-8-9	225.5927	0.9903	34.0419	-11.3127	537.2720	234.7042	169.7634	522.7246
5-4-3-6	298.4083	-64.7147	7.1256	0.6355	359.9917	539.9463	-360.2642	719.8252
6-3-4-7	305.1911	-54.7976	60.2354	-14.4461	537.1595	1252.0857	170.1422	524.0986

Table 3.3: Fourier parameters.

where ϕ is the dihedral angle while K_i and θ_i coefficients have been evaluated by fitting in Matlab using the non-linear least squares method and are reported in table 3.3.

3.2.3 Isobutane

Here we want to compute the energy of the bond defined by atoms 1-2 and that of the angle defined by atoms 3-1-4 in the isobutane molecule shown in figure 3.9.

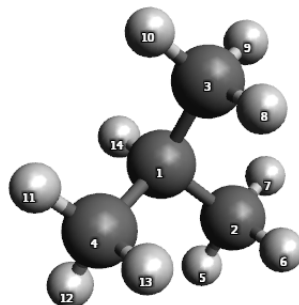


Figure 3.9: Isobutane molecule ($\text{HC}(\text{CH}_3)_3$). Dark grey is carbon (C) and light grey is hydrogen (H).

The 1-2 bond energy and the 3-1-4 angle energy have been computed in ORCA as in the previous examples and the results are shown in figure 3.10. Red points are the energy values obtained by ORCA. For the 1-2 bond energy, they are interpolated using both harmonic potential (green curve) and Morse potential (blue curve). The second one leads to have a better interpolation and the fitting parameters estimated with Matlab are $D = 93.4681$ kcal/mol, $\alpha = 2.0415$ 1/Å and $r_0 = 1.4736$ Å.

The 3-1-4 angle energy has been interpolated using a quartic function of the form

$$E = K_2(\theta - \theta_0)^2 + K_3(\theta - \theta_0)^3 + K_4(\theta - \theta_0)^4 \quad (3.45)$$

where θ is the angle, θ_0 is its equilibrium value and K_2 , K_3 , K_4 are coefficients. The values of θ_0 and K coefficients estimated by fitting in Matlab are $\theta_0 =$

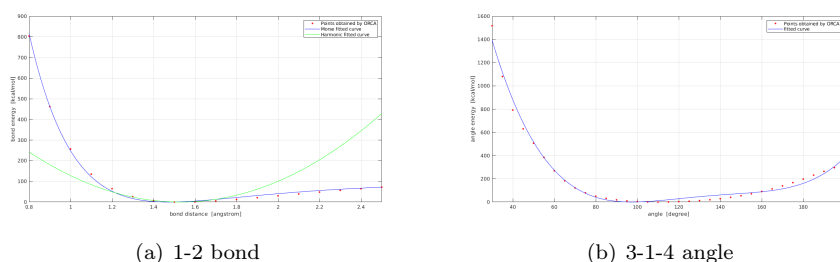


Figure 3.10: 1-2 bond energy and 3-1-4 angle energy. Red points are obtained with ORCA. For the 1-2 bond energy, the interpolation has been made using both harmonic potential (green curve) and Morse potential (blue curve). For the 3-1-4 angle energy, the interpolation has been made with the quartic function in equation 3.45.

97.3384° , $K_2 = 0.0969$ kcal/mol, $K_3 = -0.0021$ kcal/mol and $K_4 = 0.000014949$ kcal/mol.

3.2.4 Alkylcarbazole

Figure 3.11 shows an alkylcarbazole molecule with a hydrocarbon chain made up of six carbon atoms.

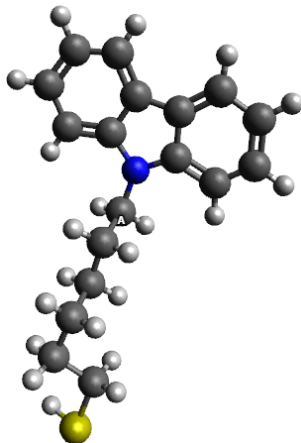


Figure 3.11: Alkylcarbazole molecule. Dark grey is carbon (C), light grey is hydrogen (H), yellow is sulphur S and blue is nitrogen N.

Here, we are interested in the bond energy between nitrogen (blue atom) and the last carbon atom in the hydrocarbon chain (the one labeled with letter A in figure 3.11).

This energy has been computed with ORCA as in the previous examples and the result is shown in figure 3.12. Red points are the energy values obtained with ORCA. These points are interpolated both with Lennard-Jones and Morse potentials. The second one leads to have a better interpolation and the fitting

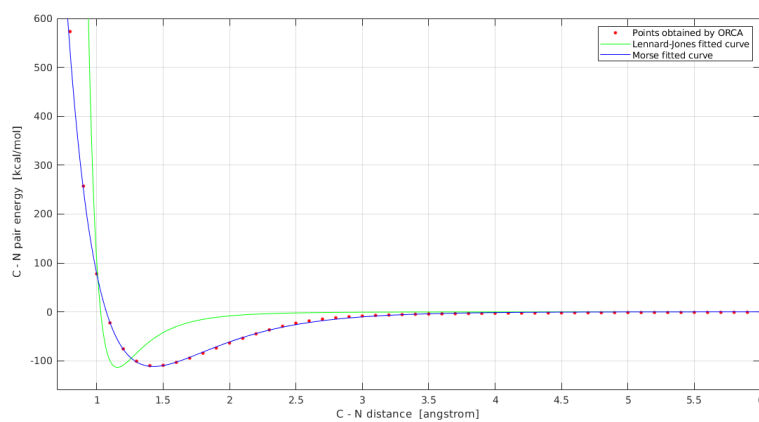


Figure 3.12: Bond energy between nitrogen and the last atom in the hydrocarbon chain (the one labeled with letter A in figure 3.11). Red points are obtained with ORCA and they are interpolated both with Lennard-Jones (green curve) and Morse potential (blue curve).

parameters estimated with Matlab are $D = 111.6791$ kcal/mol, $\alpha = 1.9449$ 1/Å and $r_0 = 1.4291$ Å.

Chapter 4

Self-Assembled Monolayer of Alkanethiols on Gold (111)

Self-assembly is a method that has attracted significant interest in physics, chemistry, and biology, because it provides a convenient and simple way of creating a highly ordered thin molecular film [20].

In a self-assembly process, an ultra-thin molecular layer is formed by the adsorption of molecules from solution onto a solid surface. Then the adsorbates spontaneously arrange themselves until finally a completely ordered molecular monolayer is formed, a so-called Self-Assembled Monolayer (SAM) [20].

Figure 4.1 shows common preparation scheme of a SAM [20]. SAMs are prepared by immersion of a substrate into a solution of organic molecules.

Molecules that form SAMs typically consist of three units:

- A headgroup that binds to the substrate. The molecules are immobilized on the surfaces via an interaction between the headgroup and the substrate forming a chemical bond.
- A spacer or backbone that connects headgroup and tailgroup. This part affects the intermolecular interaction, molecular orientation and can provide a well-defined thickness of the SAM.
- A tailgroup that constitutes the outer surface of the film [20].

In this thesis we are interested in SAMs of alkanethiols on gold. An alkanethiol is a thiol in which an alkyl group (R) is attached to a sulfhydryl group (SH), thus its chemical formula is $\text{CH}_3(\text{CH}_2)_n\text{SH}$. A simple alkanethiol molecule, called 1-hexanethiol or hexane-1-thiol or also simply hexanethiol, is shown in figure 4.2. The SH group is the headgroup, the spacer is made up of five methylene groups (CH_2) and the tailgroup is a methyl group (CH_3).

The used substrate is made of gold. The most important reason for choosing gold is that it binds thiols with a high affinity. Other advantages are that it is easy to prepare thin films of gold by physical vapor deposition, sputtering, or electrodeposition. Then, gold is exceptionally easy to pattern by a combination of lithographic tools and chemical etchants. Moreover gold is a reasonably inert metal: it does not oxidize at temperatures below its melting point; it does not

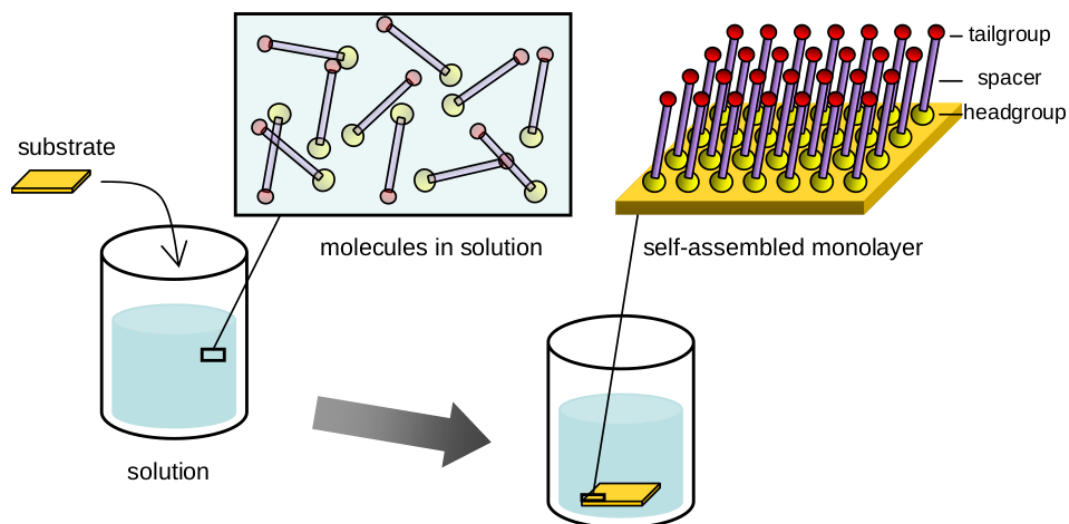


Figure 4.1: Schematic preparation of a SAM [20].

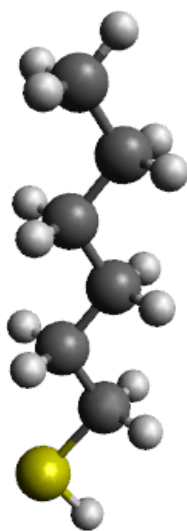


Figure 4.2: Alkanethiol with a hydrocarbon chain made up of six carbon atoms which is called 1-hexanethiol or hexane-1-thiol or also simply hexanethiol. Dark grey is carbon (C), light grey is hydrogen (H) and yellow is sulphur (S).

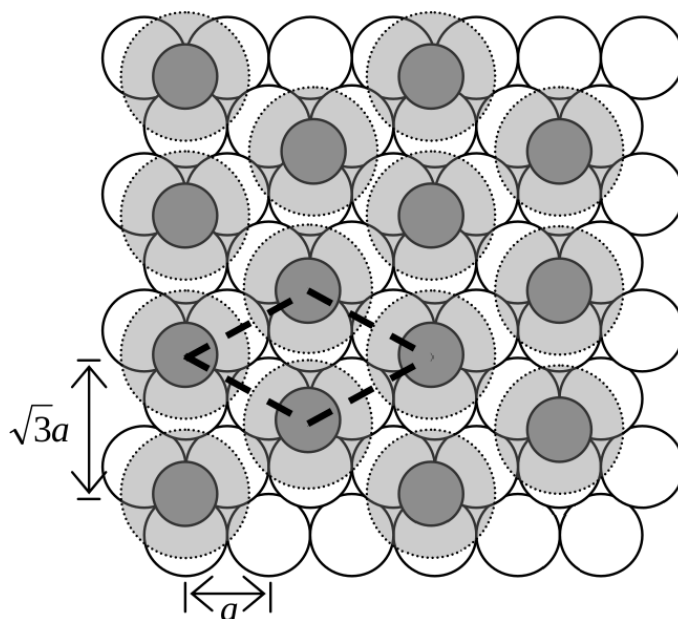


Figure 4.3: Arrangement of a monolayer formed by alkanethiols on a Au(111) surface, $a = 2.88 \text{ \AA}$. White circles are gold atoms, dark grey circles are sulphur atoms and the light grey circles with the dash lines is the area occupied by each alkanethiol [20].

react with atmospheric O_2 ; it does not react with most chemicals. These properties make it possible to handle and manipulate samples under atmospheric conditions [21].

The solvent most used is ethanol: it solvates a variety of alkanethiols, it is inexpensive, available in high purity and it has low toxicity [21]. The effects of the choice of a solvent on the kinetics of formation and the mechanism of assembly are complex and poorly understood. Studies on this topic have led to some qualitative understanding of how solvent can affect the assembly process [21].

The temperature has a role particularly relevant during the first few minutes of the formation of a SAM. Forming SAMs at temperatures above 25°C can improve the kinetics of formation and reduce the number of defects in them [21]. The immersion time of the substrate into the solution can be of several hours or a day [20]. Immersion time is inversely related to the concentration of the solution: low concentrations of alkanethiols in solution require long immersion times [21].

SAMs of alkanethiols on gold are extensively studied. Alkanethiols bind to gold surface via the formation of S–Au bond, then they arrange themselves to optimize the intermolecular interactions (van der Waals). Figure 4.3 shows position of alkanethiols on a gold surface (111) in a SAM [20].

The nature of S–Au bond is not completely understood. Studies showed that the formation of S–Au bond can take place either keeping intact or breaking the SH group of the alkanethiol. This can depend on the chain length of the alkanethiol and defects on the Au surface [22]. Breaking the SH group means

that hydrogen is lost from SH group and then the sulphur atom forms a chemical bond with Au.

4.1 MD Simulation of One Alkanethiol above Au(111) Surface Using Reactive Force Field

Before simulating a complete SAM, only one alkanethiol has been simulated in order to see if it binds to the Au(111) surface.

In the simulation the gold substrate is made of five layers. The x and y box length are respectively 27 Å and 23 Å. Periodic boundary conditions are used in x and y directions. The temperature is held at 300 K using time integration on Nose-Hoover style with a timestep of 1 fs. The alkanethiol is that shown in figure 4.2 and it is placed roughly 6.7 Å above the substrate at the start of the simulation.

The reactive force field (reaxFF) for Au–S–C–H systems developed by Järvi et al. in [23] has been used. ReaxFF is a bond order-based force field that is able to model chemical reactions where the formation and breaking of bonds takes place. Traditional force field cannot simulate chemical reactions because all bonds are defined from the beginning and remain intact for the whole duration of the simulation.

However this force field is not be able to simulate the loss of the hydrogen atom from SH group of the alkanethiol therefore it has been removed from the start of the simulation. Figure 4.4 shows some steps of the simulation, after about 150 ps the alkanethiol is well bonded to the surface and it remains there even after. When the alkanethiol is bond to the the surface, its hydrocarbon chains is oriented parallel to the surface in agreement with the experimental study done by Xu S. et al. in [24]. At a low surface coverage, the thiol molecule are physisorbed with their chains lying flat on the surface. As the surface coverage increases to near saturation, they stand up and form a compact SAM.

Figure 4.4(f) shows that the sulphur position on the substrate is in agreement with the theory (figure 4.3).

The energy associated to S–Au interaction can be thought as the energy between sulphur and all gold atoms because it corresponds to the energy to bring the sulphur atom to an infinite distance from the substrate. It can be computed as $\sum_i U_{Si}$ where U_{Si} is the energy between sulphur and a generic gold atom i . In LAMMPS it is not possible computing the energy between a specific pair of atoms using reaxFF. This is why reaxFF is not a standard force field that use a single function to compute the energy associated to a pair of atoms (U_{ij}). However it is possible to compute the potential energy of a generic atom i that is the sum of the energies between the atom i and all other atoms in the system. It corresponds to $\sum_{j=1}^N U_{ij}$ where N is the number of atoms in the system.

For this reason an other simulation was carried out in which the alkanethiol has been replaced with a single sulphur atom. When the sulphur atom binds to the surface, its potential energy has been calculated which corresponds to the bond energy between sulphur and gold substrate (as we have already said). The obtained result is of 87 kcal/mol which is reasonably strong.

The absorption of an alkanethiol can happen even without the loss of the hy-

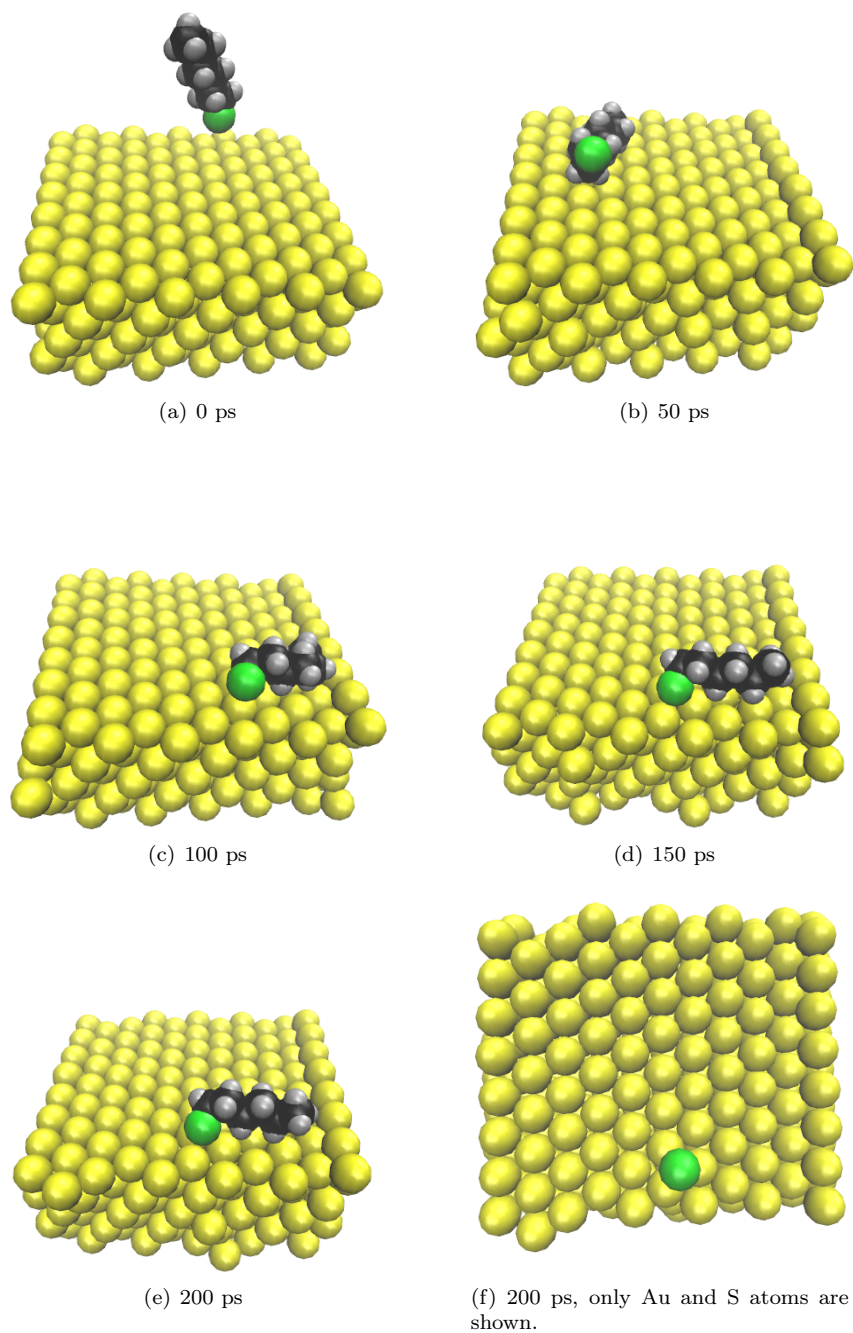


Figure 4.4: MD simulation of only one alkanethiol above Au(111) substrate using reaxFF for Au-S-C-H systems. Yellow is Au, green is S, black is C and grey is H.

drogen atom according to [22] but the used reaxFF cannot simulate it. I tried to simulate only one thiol without removing the hydrogen atom but it does not bind to Au(111) surface.

4.2 MD Simulation of a Self-Assembled Monolayer above Au(111) Surface

In the previously section only one alkanethiol has been simulated above Au(111) surface. Now we want to simulate many alkanethiols all together, that is, the formation of a SAM. This simulation cannot be done using the reaxFF, as in the previous case, because the number of atoms is much higher and the reaxFF is too expensive from the point of view of computational time. Moreover, in reaxFF you do not have to define all bonds, angles and dihedrals among atoms (unlike traditional force fields) and this could cause problems during the evolution of the simulation.

To do this simulation we were inspired by work of Kim H. et al. in [25]. The gold substrate consists of 1421 atoms. It has a height of three atomic layers and the top surface is (111) with an area of 6 nm by 6 nm. Gold atoms have been fixed in position to make simpler the simulation.

A mass of 216 hexanethiols (figure 4.2 shows the structure of a single molecule) has been prepared and it has been positioned roughly 6 Å above the substrate. The number of hexanethiols is not random, it is about 22% greater than the number of places available where the hexanethiols can bind to the surface (that it is one third of the gold atoms on the surface) in order to guarantee a SAM with a maximum coverage.

The CH₃, CH₂ and SH groups of hexanethiols are treated as united atoms. This means that each group is considered as a point body with a mass corresponding to that of the group. The united-atom model allows to make a faster simulation (because the number of atoms is reduced) and it produces SAM structures in agreement with those predicted from all-atom simulations [25].

The bond stretching interactions between the united atoms have been modeled by using the harmonic potentials, the parameters are the ones obtained in section 3.2.1 and they are listed in table 3.2. Also the bending angle interactions have been modeled using the harmonic potential and, the parameter listed in table 4.1, have been taken from the work of Hautman and Klein in [26]. The four-atom torsion potential (C-C-C-C or C-C-C-S) has been modeled with the function

$$E_t = a_0 + a_1 \cos(\phi) + a_2 \cos^2(\phi) + a_3 \cos^3(\phi) + a_4 \cos^4(\phi) + a_5 \cos^5(\phi) \quad (4.1)$$

where ϕ is the dihedral angle. The values of the coefficients are $a_0 = 2.2177$, $a_1 = 2.9053$, $a_2 = -3.1358$, $a_3 = -0.7313$, $a_4 = 6.2716$, $a_5 = -7.5275$ in units of kcal/mol [26, 27]. The non-bonded interatomic interactions have been taken to be the Lennard-Jones (LJ) potentials

$$E_{LJ} = 4\epsilon \left[\left(\frac{\sigma}{r} \right)^{12} - \left(\frac{\sigma}{r} \right)^6 \right] \quad (4.2)$$

Angle	K [kcal/(mol·rad ²)]	θ_0 [degree]
C–C–C	62.1002	109.5
S–C–C	62.1002	114.4

Table 4.1: Angle parameters

Pair	ε [kcal/mol]	σ [Å]
SH–SH	0.397	4.250
CH ₂ –CH ₂	0.118	3.905
CH ₃ –CH ₃	0.175	3.905
Au–Au	0.039	2.935

Table 4.2: Lennard-Jones parameters

where r is the interatomic distance. The σ and ε parameters have been taken from [28] and are listed in table 4.2. L-J parameters of the heteroatomic pairs have been obtained using Lorentz-Berthelot mixing rule

$$\varepsilon_{xy} = \sqrt{\varepsilon_{xx}\varepsilon_{yy}} \quad \sigma_{xy} = \frac{1}{2}(\sigma_{xx} + \sigma_{yy}) \quad (4.3)$$

The S–Au pair interaction, that describes the chemisorption, has been modeled by a Morse potential

$$E_{Morse}^{Au-S} = D_0 \left[e^{-2\alpha(r-r_0)} - 2e^{-\alpha(r-r_0)} \right] \quad (4.4)$$

where $D_0 = 8.763$ kcal/mol, $\alpha = 1.47$ Å⁻¹ and $r_0 = 2.65$ Å have been taken from [29].

The mass of 216 hexanethiols has been prepared initially placing the thiols in the points of a simple cubic lattice with a spacing of 10 Å. Since the thiols take up space, each thiol will be distant about 5 Å from the first neighbors. Then, a energy minimization of the system has been performed and finally the system has been equilibrated by running an NVT simulation at 300 K for 3 ns.

This mass of hexanethiols has been positionated roughly 6 Å above the gold substrate as already said above. After, an NVT simulation at 300 K for 75 ns and with a timestep of 1 fs was performed. Periodic boundary conditions are assumed in the planar x and y directions. During the whole simulation gold atoms have been fixed in position.

Figure 4.5 shows the spreading of the hexanethiols mass above the Au(111) surface. Most of the thiols bind to the surface in the first moments of SAM formation since there are many free sites where thiols can attach. At 5 ns almost all the available sites are occupied. From 5 ns the remaining free places are occupied in a longer time. At 25 ns all available places are filled, thus, from 25 ns to 75 ns nothing changes.

In figure 4.6 only the linked thiols at 25 ns are shown. The position of the sulphur atom (figures 4.6(c) and 4.6(d)) corresponds to that of the data found in literature (figure 4.3). Figure 4.6(d) shows the lack of a sulphur atom (red circle). This is a defect due to a linked thiol lying on the surface. This thiol, shown in figure 4.6(b), does not stay up because it is trapped by surrounding molecules.

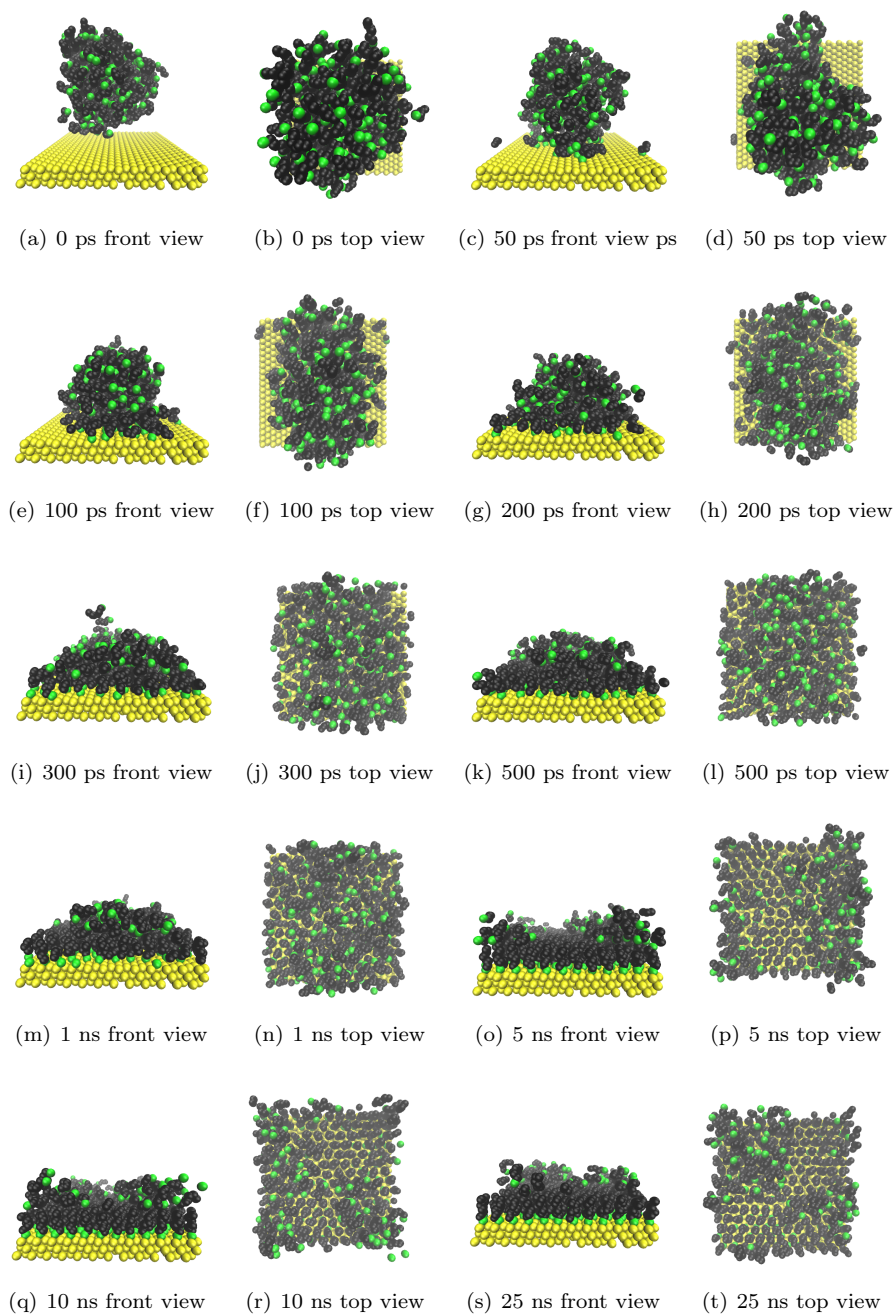


Figure 4.5: MD simulation of a self-assembled monolayer above Au(111) surface. Yellow is Au, green is S and black are both CH_2 and CH_3 groups.

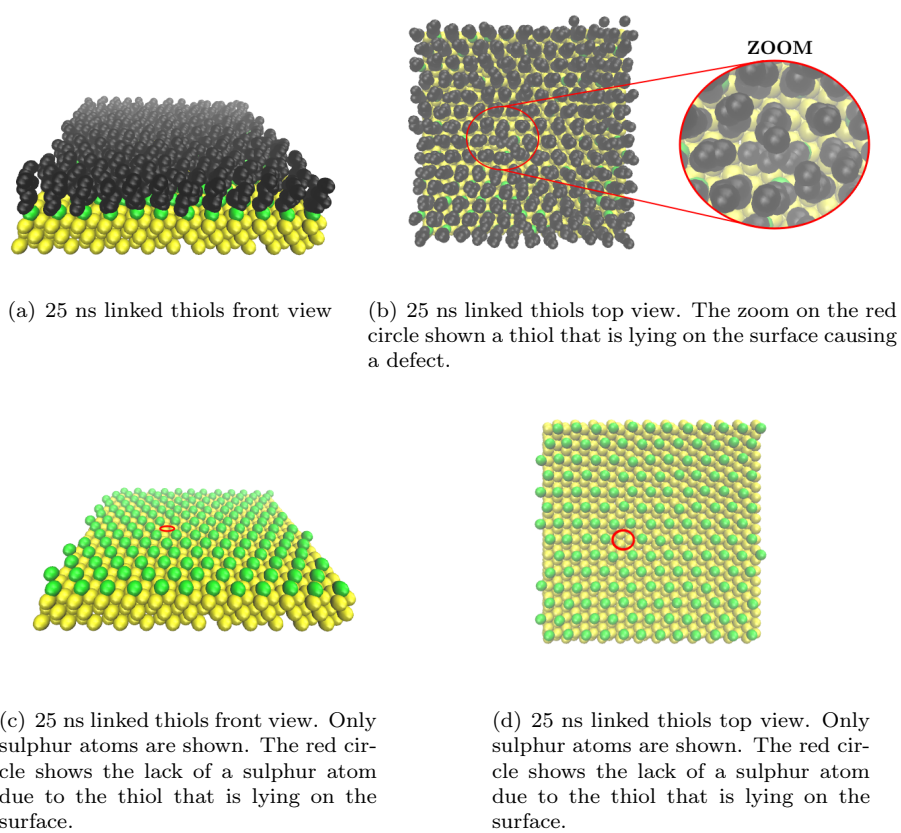


Figure 4.6: SAM formation at 25 ns where only linked thiols are shown. Yellow is Au, green is S and black are both CH_2 and CH_3 groups.

Chapter 5

Growth of an Au Thin Film above a Si Substrate

In the previous chapter, the formation of a SAM on a perfect (111) gold surface has been simulated. Now we want to simulate the formation of the gold layer through molecular dynamics in order to obtain a more realistic surface where the thiols bind.

If the gold atoms are deposited directly on the silicon substrate, via sputtering for example, the obtained layer will be disordered and it will contain a mixture of Si and Au on the top even for relatively thick films [30]. Silva et al. found experimentally in [30] that Au films, with properties resembling those of bulk Au(111), can be obtained interposing a Cu thin film between silicon and gold that prevent reactions between them. Thus, a thin film of Cu is first deposited on the silicon substrate and then the Au layer is deposited on the Cu.

This chapter is divided in three sections. In the first, the growth of an Au thin film on a Si substrate interposing in the middle a layer of Cu will be simulated. In the second, the growth of the Au thin film will be simulated depositing Au atoms directly on the Si substrate. In the third, the SAM of alkanethiols will be simulated again but using a non-ideal gold surface, that is a surface with defects, in order to see how positions of linked thiols change.

5.1 Growth of Au Thin Film on Si Substrate Interposing a Cu Buffer in the Middle

In this section the formation of the Au layer using a Cu thin film to separate the Au from the Si substrate will be simulated.

First a Cu film is deposited above a Si substrate with dimension 6 nm x 6 nm in the two planar x and y directions and with a height of 2.58 nm consisting in 20 atomic layers. The total number of Si atoms is 5065 and the top surface is (001). During the deposition, the substrate is held at 900 K except the bottom 3 layers that are fixed in position to prevent the moving of the substrate. The top surface is chosen (001) and the temperature to be 900 K because, according to [31], this would lead to a Cu film with a (111) top surface.

At the beginning of the simulation, the substrate is equilibrated at 900 K for

200 ps. Periodic boundary conditions are assumed in x and y directions and the timestep is 1 fs. Subsequently, the deposition begins inserting one Cu atom every 1 ps. The Cu atoms are inserted in a random position 7 nm above the silicon substrate. The inserted atoms are directed vertically toward the silicon surface with a velocity of 5.50 Å/ps. The selected velocity has been taken from [31] and it is in agreement with simulations of electron beam physical vapor deposition in [32]. At this velocity corresponds an incident energy of 0.1 eV. The total number of Cu atoms inserted is 7052 and they are assigned to the NVE ensemble. After all Cu atoms are inserted, the system is equilibrated for 0.5 ns (in this stage Si atoms are in the NVT ensemble while the Cu ones are in the NVE). Then, the whole system (both Si and Cu atoms) is equilibrated in the NVT ensemble at 900 K for 0.5 ns. The system is then cooled at 300 K in 2 ns and finally it is equilibrated at 300 K for 10 ns.

During the simulation, interactions between Cu atoms are modeled with the EAM potential developed by Foiles et al. in [33] and the parameters can be found in the potentials LAMMPS directory. Si–Si and Si–Cu interactions are instead modeled using Tersoff potential [31, 34].

The simulation is shown in figures 5.1, 5.2, 5.3 and 5.4. The first deposited atoms interact with the top layers of the silicon substrate, thus generating an interface between Si and Cu where both atoms are present. After all the atoms are deposited the top Cu surface is quite disorganized (figure 5.2(b)). During the cooling stage, the top surface begins to become more orderly (figure 5.3(d)). At the end of the equilibration at 300 K some areas are (100) but the most of the top surface resembles that of Cu(111) (figure 5.4(h)).

In figure 5.5 the percentage of Si atoms along z direction is shown. The graphic is obtained dividing the system along z direction in slices of thickness 2.5 Å. For each slice the percentage of Si atoms is computed as $\frac{N_{Si}}{N_{Si}+N_{Cu}} \cdot 100$, where N_{Si} and N_{Cu} are respectively the number of Si and Cu atoms in the slice. The black dashed line in figure represents the initial top surface of the silicon substrate. In this simulation Cu atoms penetrate until roughly 10 Å below the initial Si top surface and, above roughly 10 Å from this, only Cu atoms are present. Note that the intermixing behaviour depicted in figure 5.5 depends on the temperature. The higher the temperature is, the greater will be the thickness of the interface where both Si and Cu atoms are present.

Once the Cu layer is formed, the deposition of Au atoms begins inserting 4032 atoms, one every 1 ps. Au atoms are generated in a random position above 5 nm the top Cu surface with a velocity of 5.50 Å/ps vertically directed toward the Cu layer. At this velocity corresponds an incident energy of 0.31 eV. During the deposition Au atoms are assigned to the NVE ensemble while Si and Cu atoms belong to the NVT ensemble at a temperature of 300 K except the bottom three Si layers that, as done previously, are fixed in position. When the deposition ends, the system is equilibrated for 0.5 ns (in this stage Si and Cu atoms are in the NVT ensemble while Au ones are in the NVE). Then, the whole system (Si, Cu and Au atoms) is equilibrated for 5 ns in the NVT ensemble at 300 K. At this point, the top gold surface is quite disorganized, hence, an annealing process is performed in order to better rearrange the atoms position. The whole system is heated from 300 K to 800 K in 1 ns, then it is equilibrated at 800 K for 3 ns, then it is cooled again at 300 K in 2 ns and finally it is equilibrated at 300 K for 2 ns.

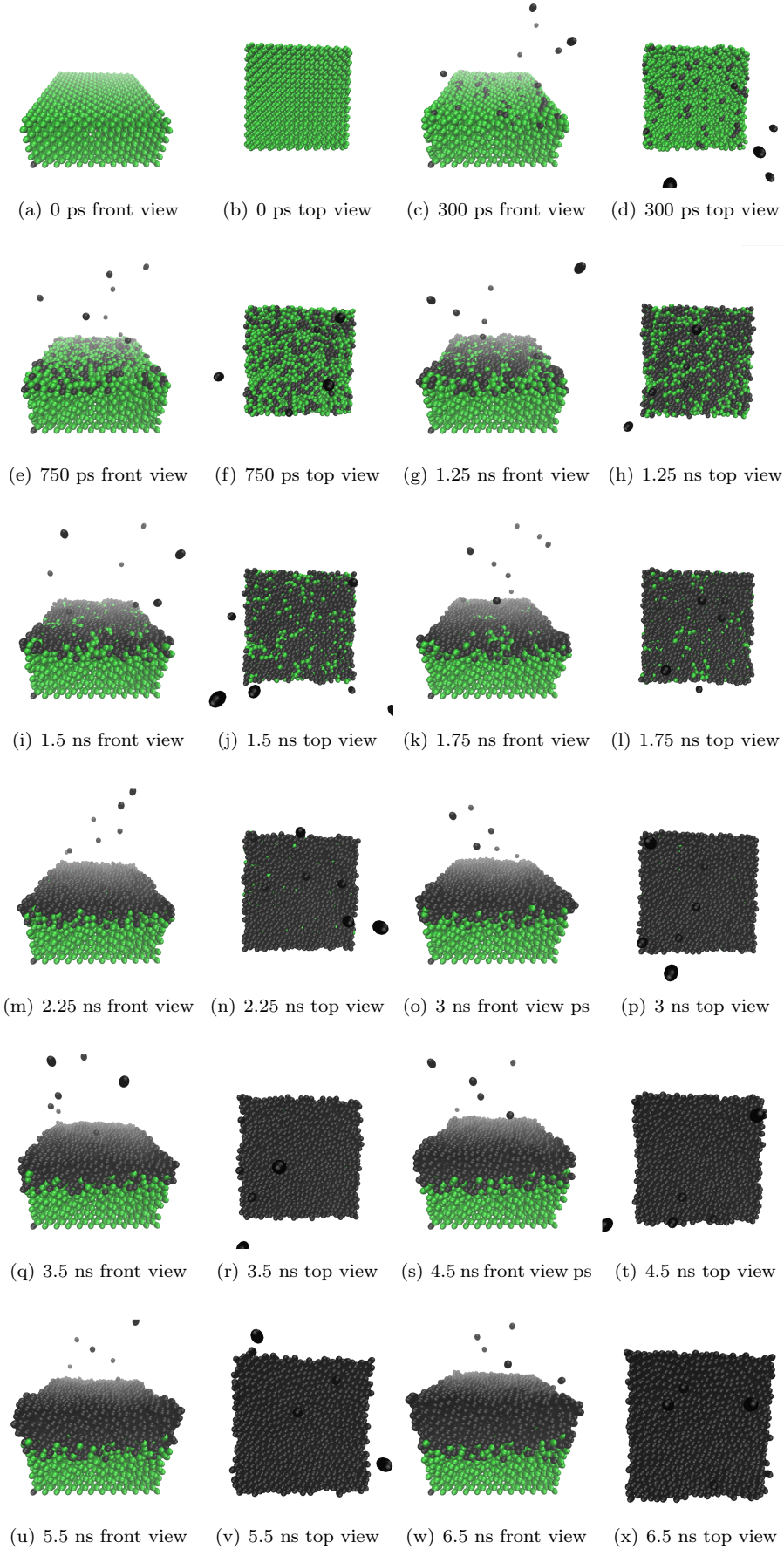


Figure 5.1: Cu deposition above Si(001). Green is Si and black is Cu.

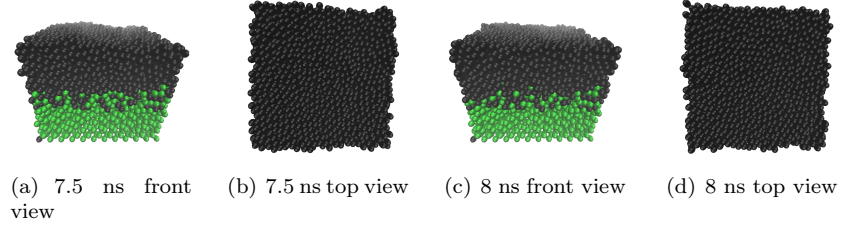


Figure 5.2: Equilibration at 900 K. Green is Si and black is Cu.

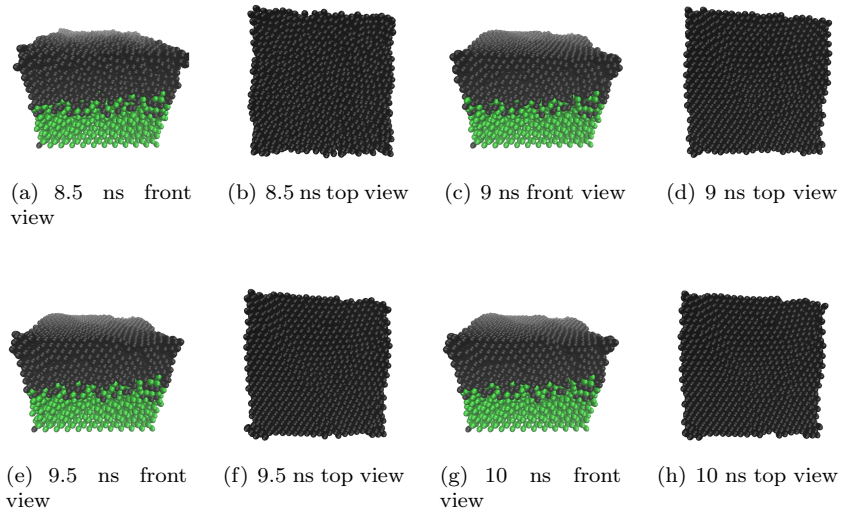


Figure 5.3: Cooling from 900 K to 300 K. Green is Si and black is Cu.

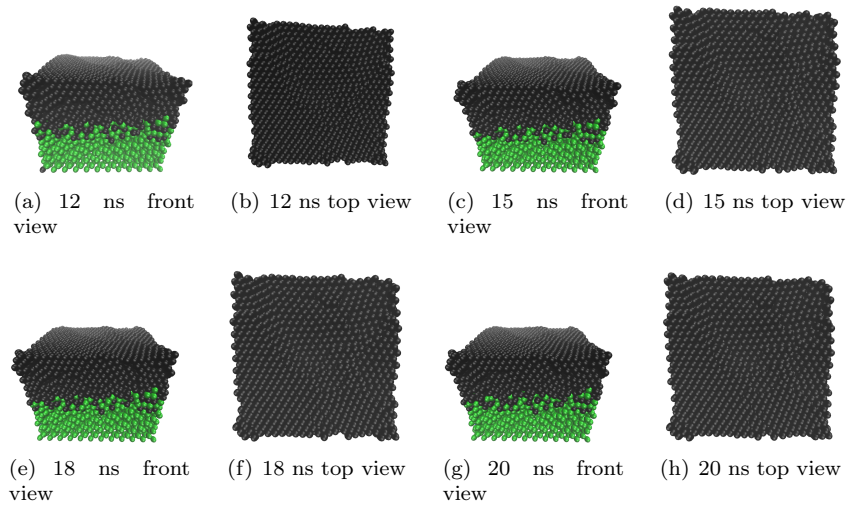


Figure 5.4: Equilibration at 300 K. Green is Si and black is Cu.

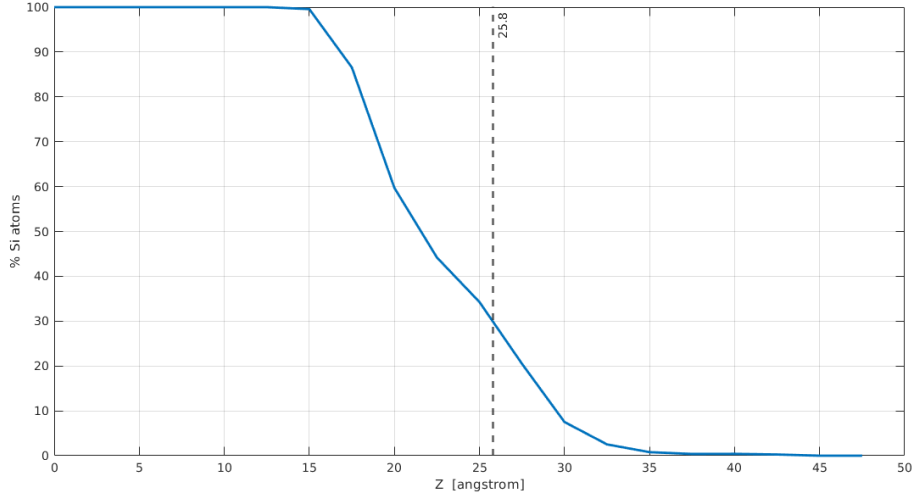


Figure 5.5: Percentage of Si atoms along z direction. The black dashed line represents the initial top surface of the silicon substrate.

Interactions between Au and Si atoms are neglected since they are separated by the Cu buffer, Cu–Cu and Au–Au interactions are modeled with the EAM potential, Si–Si and Si–Cu are modeled with the Tersoff potential.

The simulation is shown in figures 5.6, 5.7, 5.8, 5.9, 5.10 and 5.11. At the end of the deposition (figure 5.6(t)) and of the equilibration at 300 K (figure 5.7(h)), the top gold surface is quite disorganized. For this reason an annealing process at 800 K is performed (figures 5.8 and 5.9). Then, during the cooling stage (figure 5.10), the top gold surface begins to resemble that of Au(111). After the cooling stage, an other equilibration at 300 K is performed (figure 5.11) and the final result is shown in figure 5.11(d).

Figure 5.11(d) is better shown in figure 5.12(a), you can see that the top gold surface resembles that of Au(111) everywhere. In figure 5.12(b) the final result is shown from an other point of view in order to highlight qualitatively the height differences along the z axis. The height of the steps on the surface ranging roughly from 1.2 Å to 2.5 Å. To give a quantitative description of the height differences, a surface has been built with Matlab interpolating the atoms on the top gold layer. In figure 5.13 is shown the top view of this surface. The value of the surface for each coordinate (x, y) is represented by color and the color scale is reported on the right of the figure.

In figure 5.14 the percentage of Si, Cu and Au atoms is shown along the z axis. There are two intermixing interfaces with a certain thickness where in the first both Si and Cu atoms are present while in the second one both Cu and Au are present. After these interfaces the three material have a relatively good separation despite the high temperatures (900 K during the Cu deposition and 800 K during the annealing process after the Au deposition).

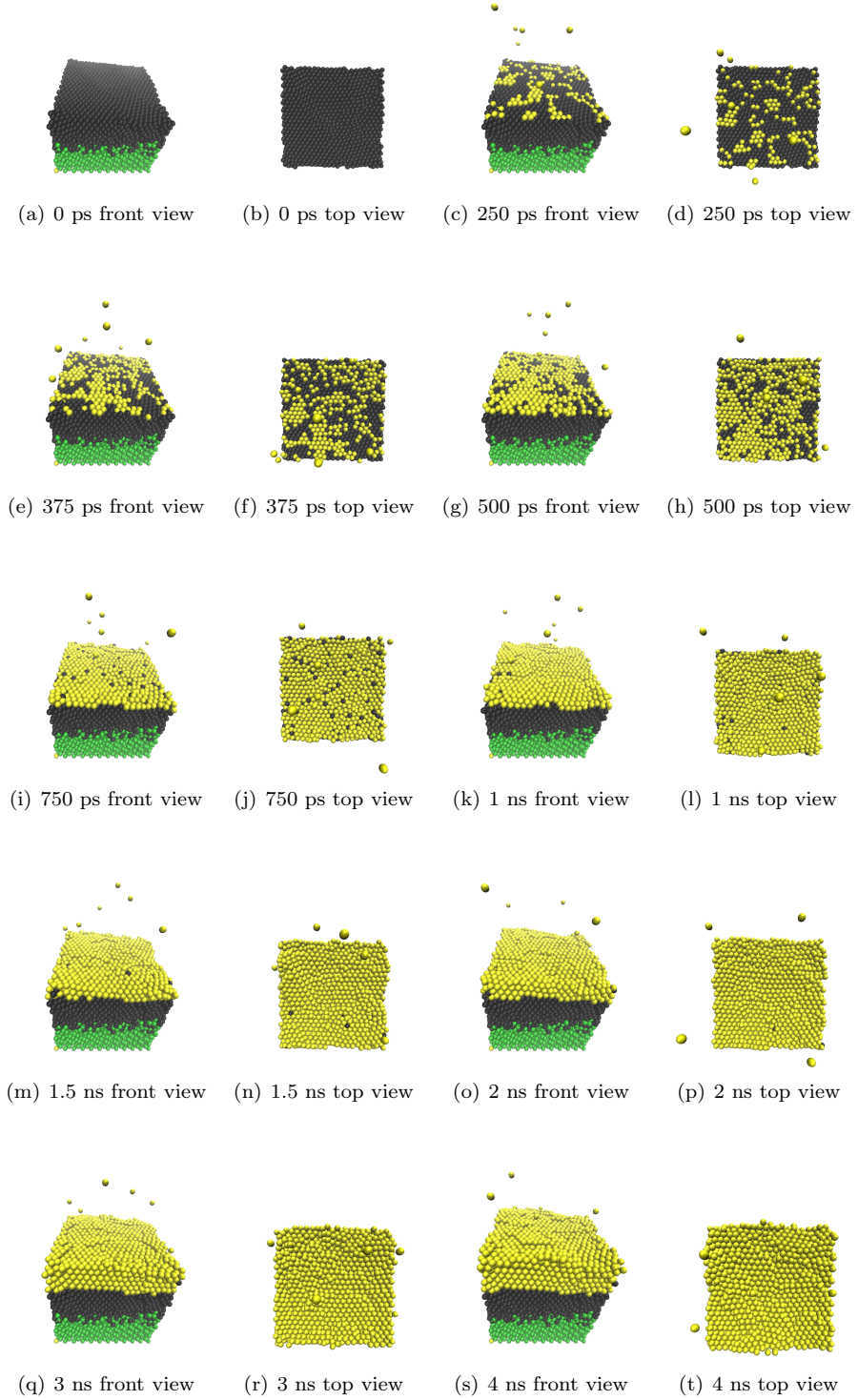


Figure 5.6: Au deposition above Cu buffer. Green is Si, black is Cu and yellow is Au.

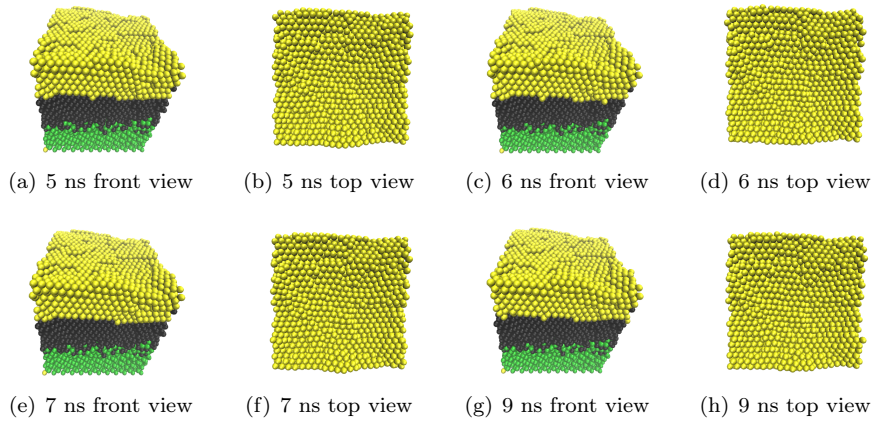


Figure 5.7: Equilibration at 300 K. Green is Si, black is Cu and yellow is Au.

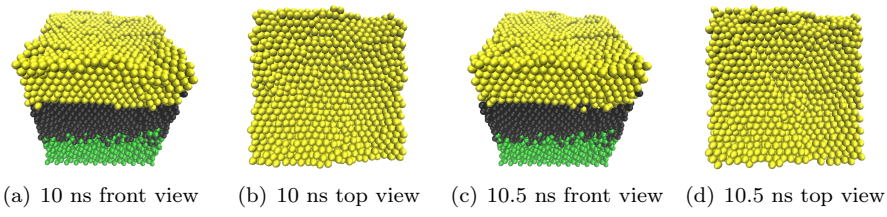


Figure 5.8: Heating from 300 K to 800 K. Green is Si, black is Cu and yellow is Au.

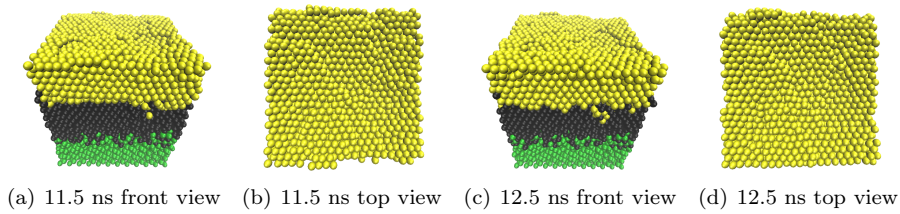


Figure 5.9: Equilibration at 800 K. Green is Si, black is Cu and yellow is Au.

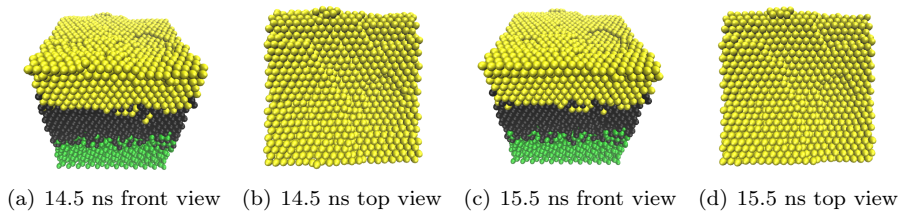


Figure 5.10: Cooling from 800 K to 300 K. Green is Si, black is Cu and yellow is Au.

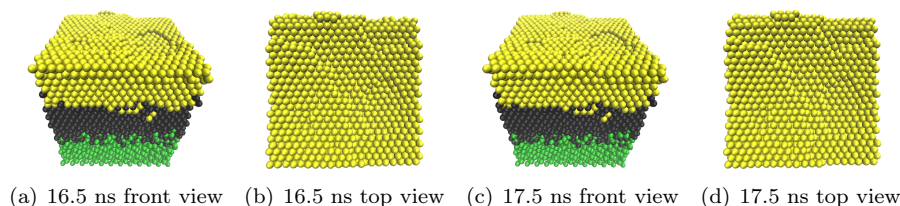


Figure 5.11: Equilibration at 300 K. Green is Si, black is Cu and yellow is Au.

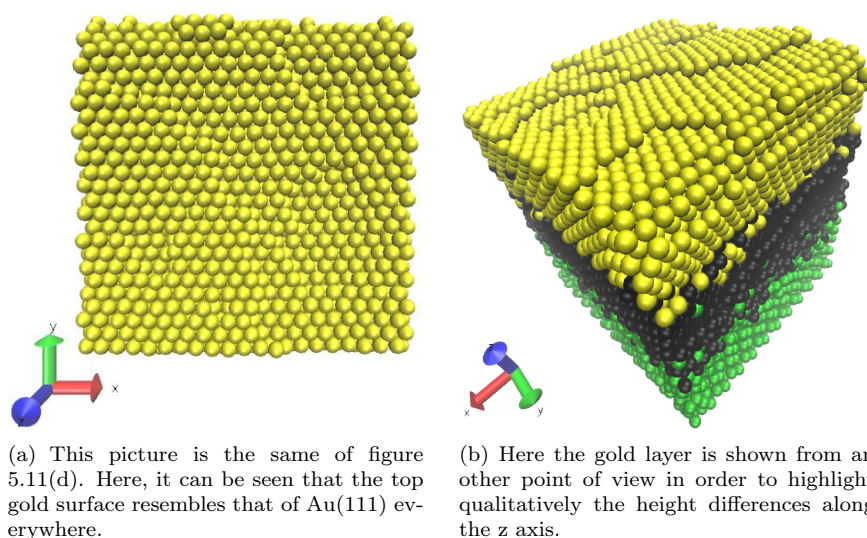


Figure 5.12: Gold layer formation final result. Green is Si, black is Cu and yellow is Au.

5.2 Growth of Au Thin Film Depositing Au Atoms Directly on the Si Substrate

In the previous section the formation of a Au layer has been simulated interposing a Cu buffer between the silicon substrate and the Au layer in order to prevent reactions between Si and Au. Now we want to simulate the formation of a Au layer depositing the Au atoms directly on the silicon substrate.

In this simulation the dimensions of the silicon substrate are 3 nm x 3 nm in the two planar x and y directions and the height is 2.5 nm. The top surface is (111) and the total number of Si atoms is 1254. The substrate is held at 300 K except the bottom two layers that are fixed in position to prevent the moving of the substrate.

At the beginning of the simulation, the substrate is equilibrated at 300 K for 50 ps. Periodic boundary conditions are assumed in x and y directions and the timestep is 0.25 fs. Subsequently, the deposition begins inserting one Au atom every 0.25 fs. Au atoms are inserted in a random position 7 nm above

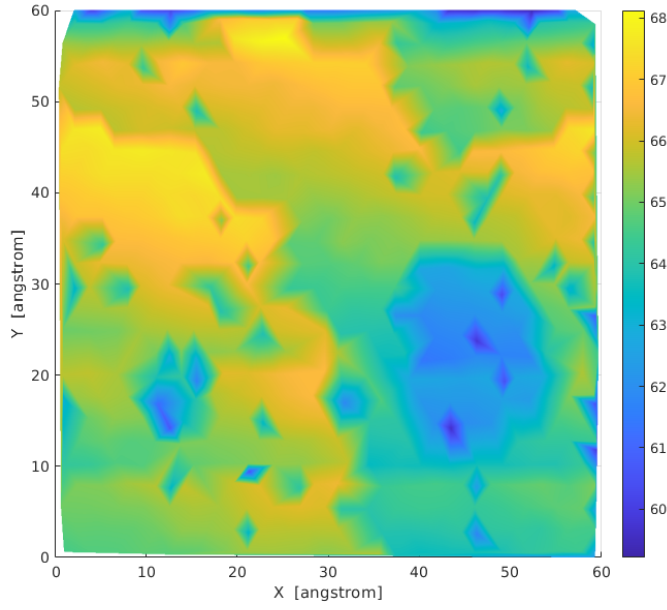


Figure 5.13: Interpolated gold surface.

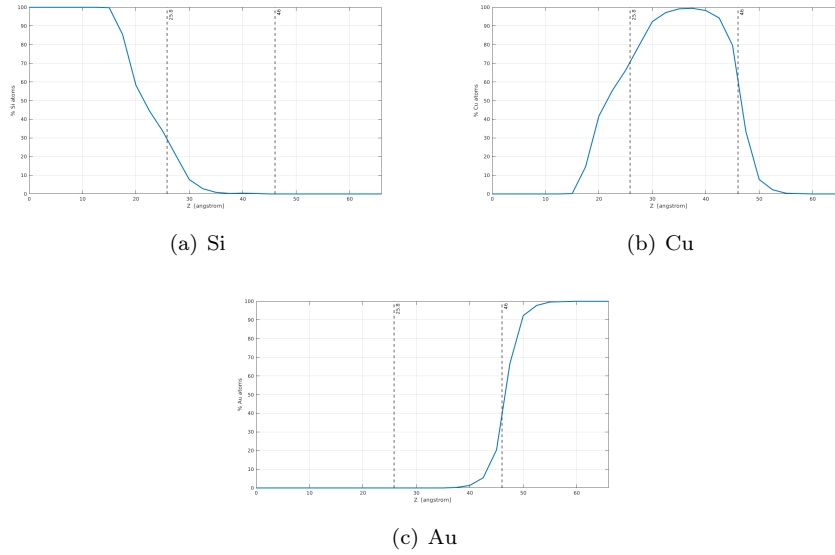


Figure 5.14: Percentage of Si, Cu and Au atoms along the z direction. The first black dashed line at 25.8 \AA represents the initial top surface of the silicon substrate. The second black dashed line represents the initial Cu top surface at the start of Au deposition; its value is roughly 46 \AA (it cannot be evaluated exactly due to the differences in height).

the silicon substrate with a velocity of 5.50 Å/ps directed vertically toward the silicon surface. At this velocity corresponds an incident energy of 0.31 eV. The total number of Au inserted atoms is 1486 and they are assigned to the NVE ensemble. The deposition is divided in two steps, 600 atoms are first inserted, then the system is equilibrated for 41.5 ps, then the deposition start again inserting the 886 remaining Au atoms. After all Au atoms are inserted, the system is equilibrated for 25 ps (in this stage Si atoms are in the NVT ensemble while the Au ones are in the NVE). Then, the whole system (both Si and Au atoms) is equilibrated in the NVT ensemble at 300 K for 1 ns.

Interactions between all pairs of atoms (Si–Si, Si–Au and Au–Au) are modeled with the MEAM potential developed by Seunghwa Ryu e Wei Cai in [35].

This first part of the simulation is shown in the figures 5.15 and 5.16.

Subsequently, to better rearrange the position of the atoms on the surface, an annealing process is performed. Here, the system is heated from 300 K to a certain temperature T in 1 ns, then it is equilibrated at this temperature for 3 ns, then it is cooled again to 300 K in 2 ns and finally it is equilibrated at 300 K for 2 ns. During the annealing process the timestep has been changed to 0.5 fs. To observe the effect of the temperature, the annealing process has been simulated many times with the heating temperature T ranging from 450 K to 1000 K with a step of 50 K. The final result of the annealing process at each temperature is shown in figures 5.17, 5.18 and 5.19. For each heating temperature the top and front view of the final configuration is shown. In the front view, the Au atoms are shown in transparency to highlight the presence of Si atoms on the surface (or close to it). Then, also the percentage of Si atoms along z direction, obtained as done previously, is shown. The black dashed line represents the initial top surface of the silicon substrate. The Si concentration profiles are all shown simultaneously in figure 5.20.

Figures show that Si and Au have a strong interaction, even at 450 K, the lowest heating temperature simulated, several Si atoms reach the upper gold layers. This phenomenon mainly depends on three factors: thickness of gold, heating temperature and time. In these simulations, the deposited gold layer has a thickness of 3 nm roughly, but if you increase it, will become harder for Si atoms to reach the top gold surface. Then, increasing the heating temperature (as shown in figures 5.17, 5.18 and 5.19), will become easier for Si atoms to reach the top gold surface since the thermal agitation is increased. Also the heating time, that is the time the system stays at the heating temperature, has a key role. Si atoms are able to move towards the top gold surface when they are heated, thus, reducing the heating time, will be more difficult for Si atoms reaching the upper gold layers.

In section 5.1, Cu deposition on Si substrate has been simulated (see figures 5.1, 5.2, 5.3 and 5.4). In that simulation the silicon substrate has been held at 900 K and, despite this high temperature, Si and Cu atoms do not mix so much unlike the case of Si and Au atoms (figures 5.19(d), 5.19(e) and 5.19(f)). This means that Cu has a much weaker interaction with Si than Au. Moreover, after the Cu deposition on the silicon substrate, an Au layer has been deposited on the Cu buffer, and then, an annealing process at 800 K has been simulated (see figures 5.8, 5.9 and 5.10). After this annealing process the three layers of material remained quite separate.

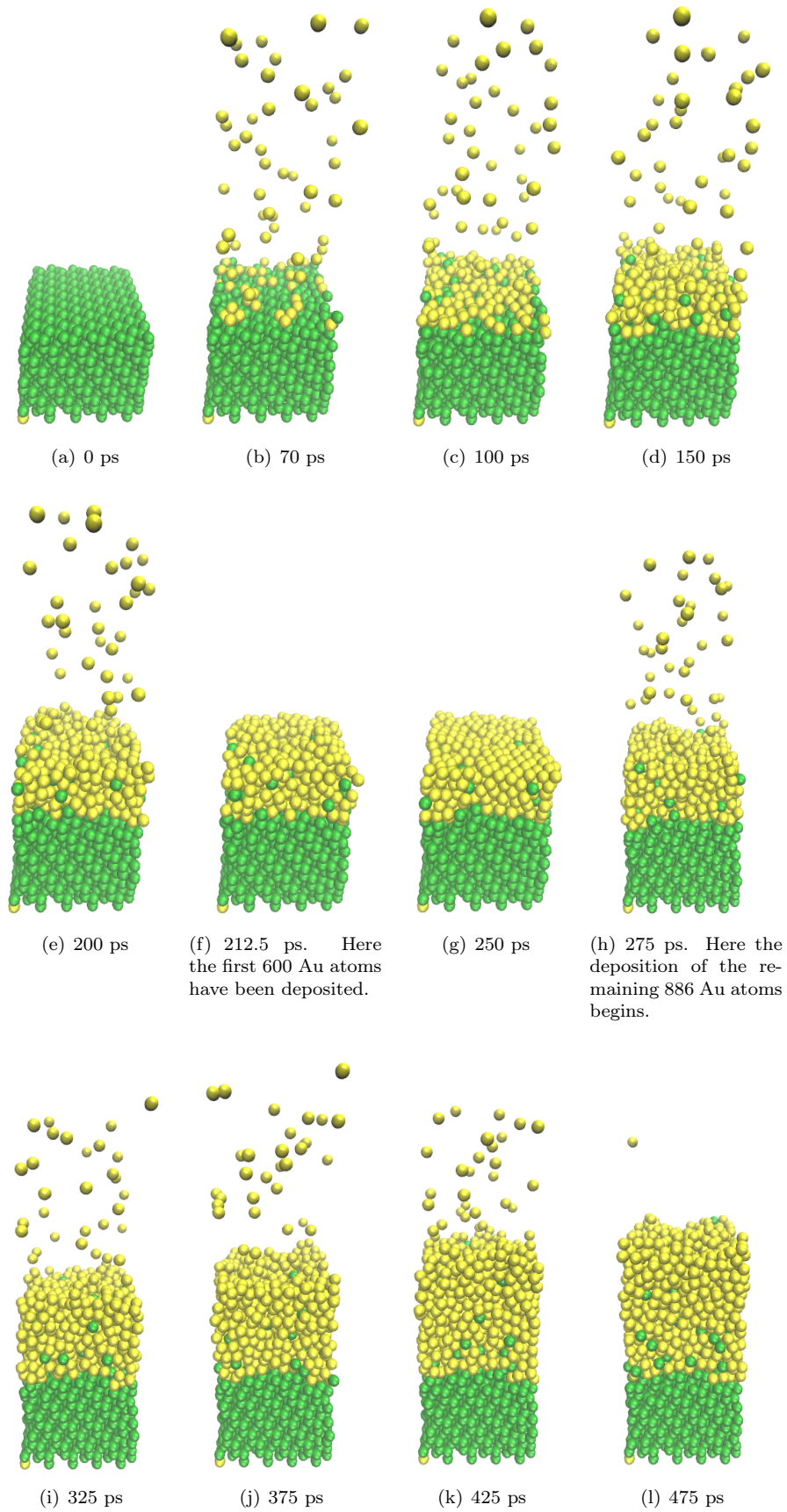


Figure 5.15: Au deposition above Si substrate. Green is Si and yellow is Au.

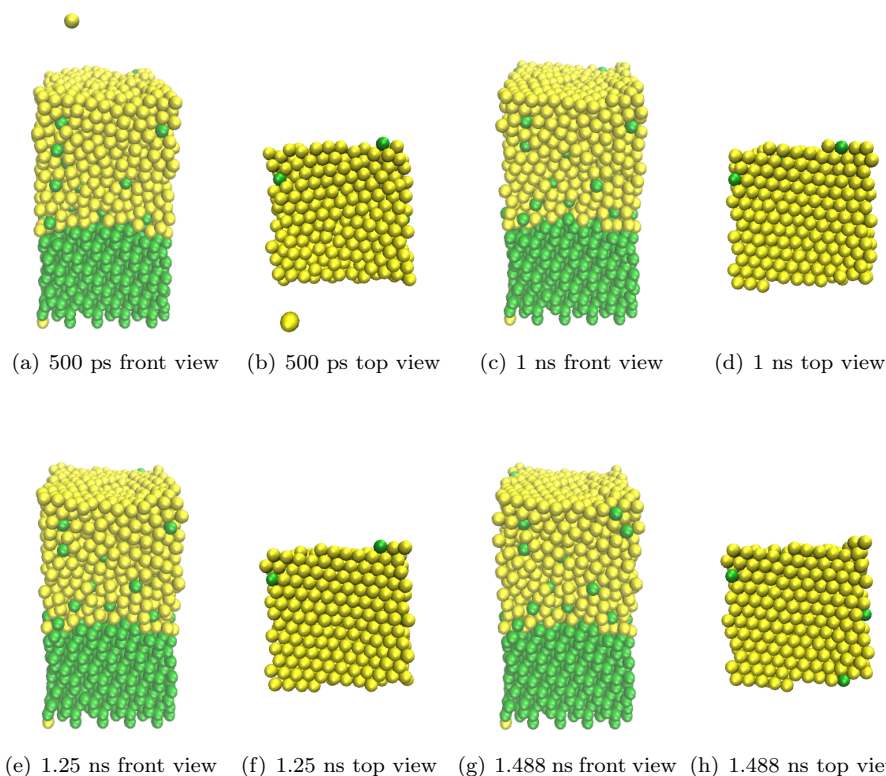


Figure 5.16: Equilibration at 300 K. Green is Si and yellow is Au.

These results agree with the experimental ones in [30], indeed, we have seen through molecular dynamics simulations that depositing Au directly on the silicon substrate leads to have Si atoms on the top gold surface or close to it. The Cu layer interposed between Si and Au acts like a shielding, preventing reactions between Si and Au, even at high temperatures.

5.3 Self-Assembled Monolayer of Alkanethiols on a Non-ideal Gold Surface

In this section, the simulation concerning the SAM formation performed in section 4.2, has been improved replacing the ideal gold surface with the non-ideal one obtained in section 5.1. Si and Cu atoms, like those of Au, have been fixed in position, thus, interactions between them have been neglected. Also interactions between Si or Cu with any other type of atom have been neglected since they are separated from the thiols by the Au layer. For the rest, the simulation has not changed and the final result (at 25 ns) is shown in figure 5.21.

From figure 5.21(d) you can see that sulphur atoms do not order perfectly as in the case of the ideal gold surface (see figure 4.6(d)). In any case we have an encouraging result because there is a good coverage of the gold substrate by

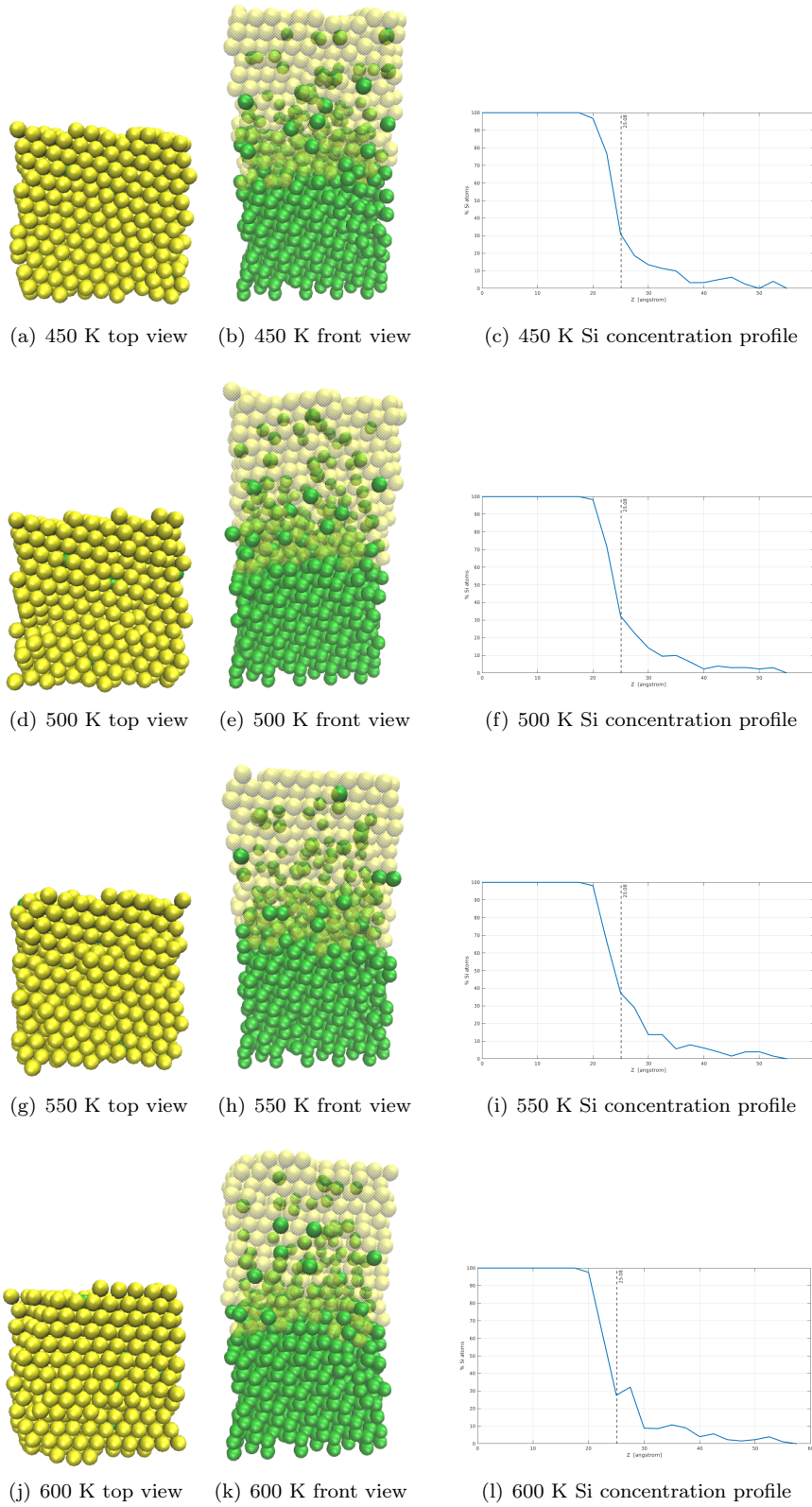


Figure 5.17: Final configuration of the system after the annealing process for heating temperature of 450 K, 500 K, 550 K and 600 K. Green is Si and yellow is Au. In the first two columns the top and the front view are respectively shown. In the front view gold atoms are transparent in order to highlight qualitatively the presence of Si atoms on the surface (or close to it). In the third column the percentage of Si along z direction is shown. The black dashed line represents the initial top surface of the silicon substrate.

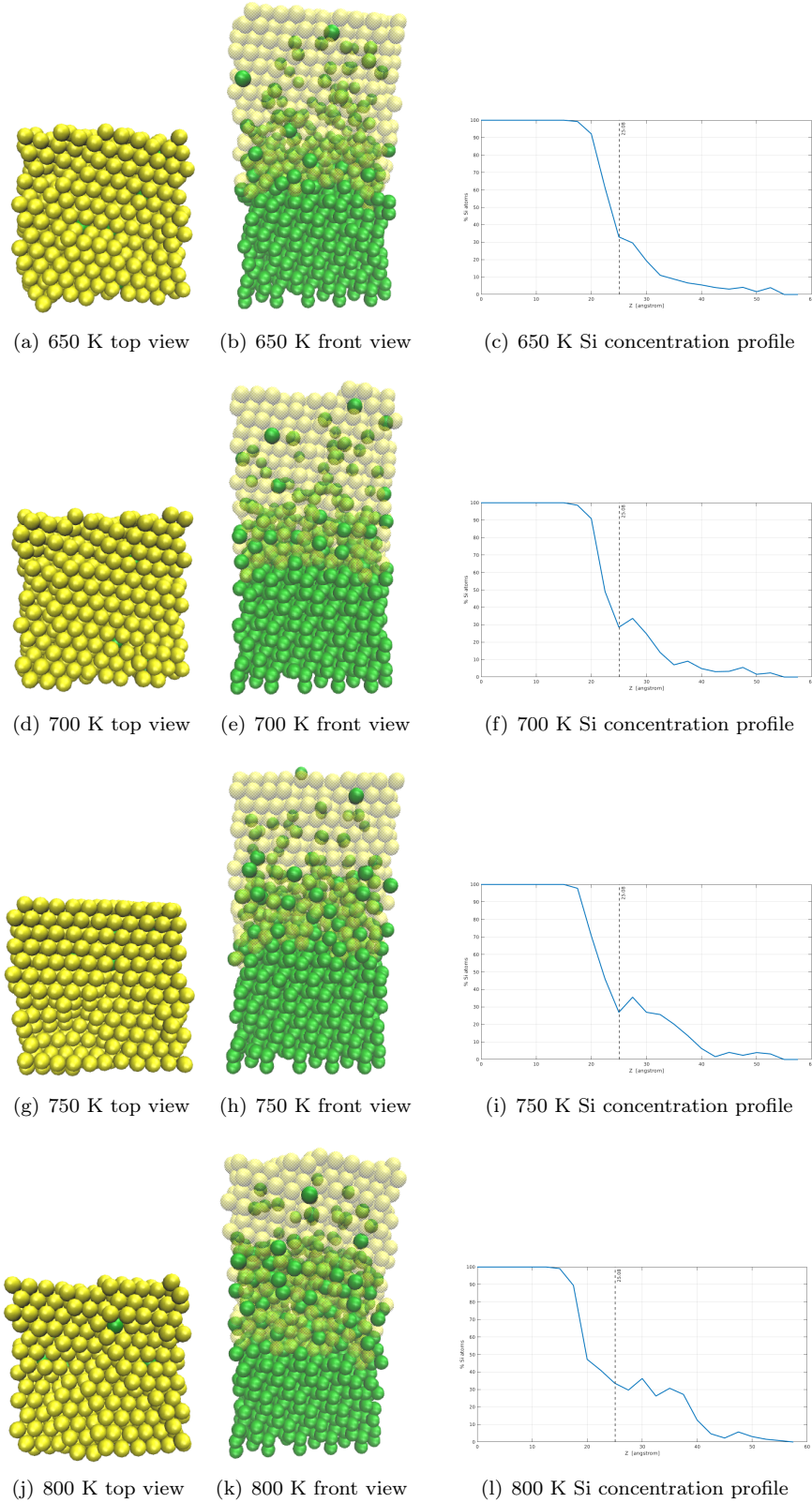


Figure 5.18: Final configuration of the system after the annealing process for heating temperature of 650 K, 700 K, 750 K and 800 K. Green is Si and yellow is Au. In the first two columns the top and the front view are respectively shown. In the front view gold atoms are transparent in order to highlight qualitatively the presence of Si atoms on the surface (or close to it). In the third column the percentage of Si along z direction is shown. The black dashed line represents the initial top surface of the silicon substrate.

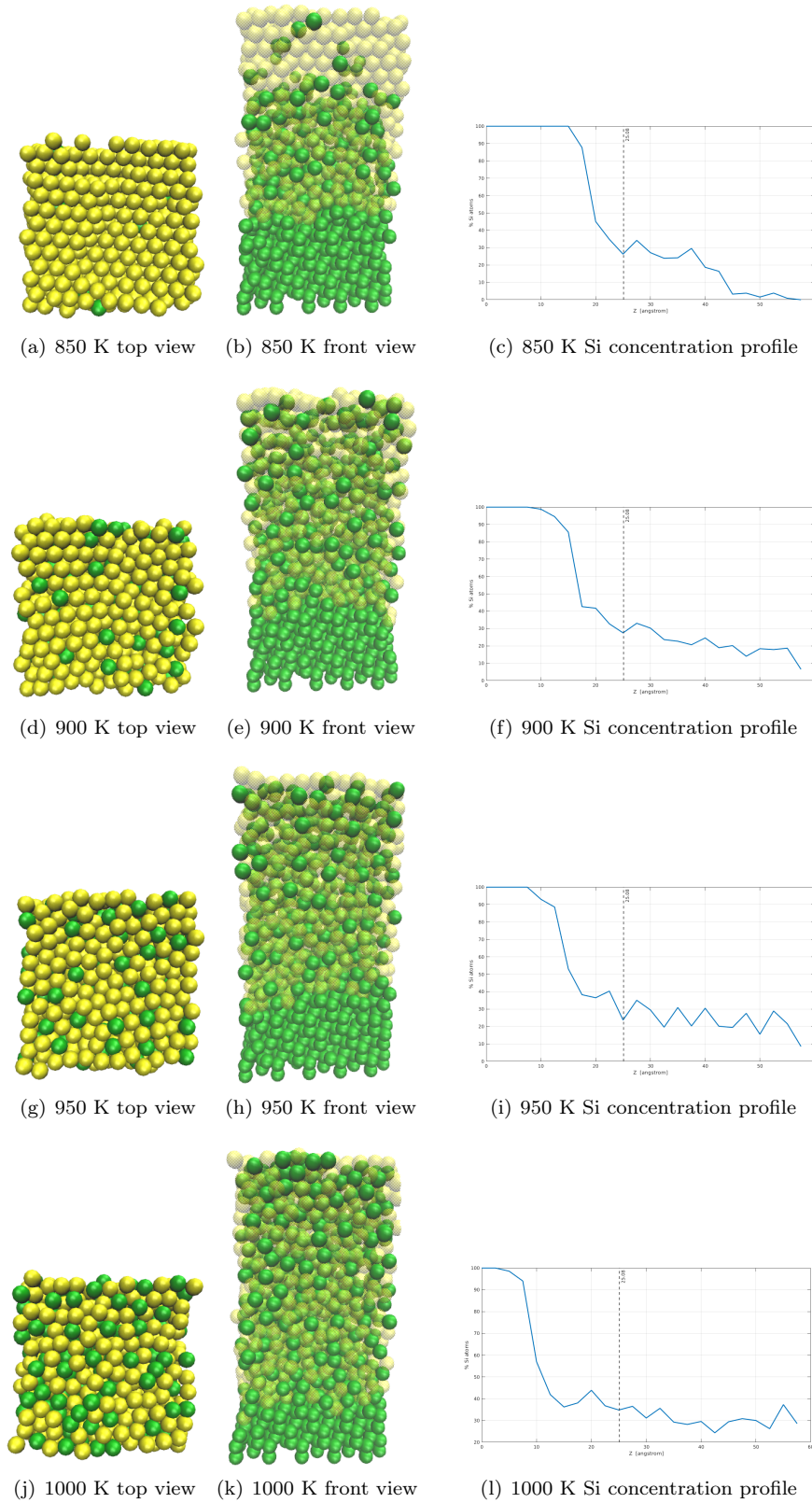


Figure 5.19: Final configuration of the system after the annealing process for heating temperature of 850 K, 900 K, 950 K and 1000 K. Green is Si and yellow is Au. In the first two columns the top and the front view are respectively shown. In the front view gold atoms are transparent in order to highlight qualitatively the presence of Si atoms on the surface (or close to it). In the third column the percentage of Si along z direction is shown. The black dashed line represents the initial top surface of the silicon substrate.

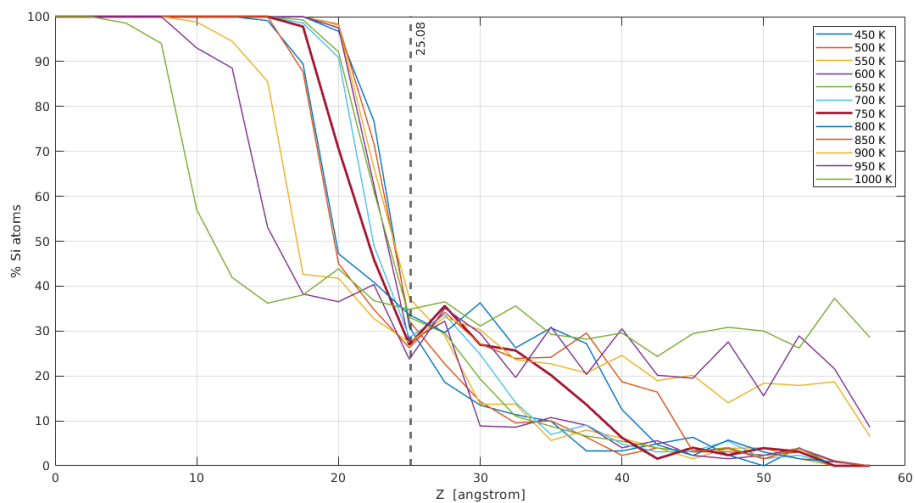


Figure 5.20: Percentage of Si atoms along z axis after the annealing process performed at temperature ranging from 450 K to 1000 K with a step of 50 K. The black dashed line represents the initial top surface of the silicon substrate.

thiols.

In figure 5.22 the interpolated gold surface is shown again (see figure 5.13), but also sulphur atom positions are represented in order to give an idea, thanks to the dimensioned axes, about the distance between the sulphur atoms. You can see that sulphur atoms are distant from each other on average about 5 Å, that is a distance for which the information can propagate correctly.

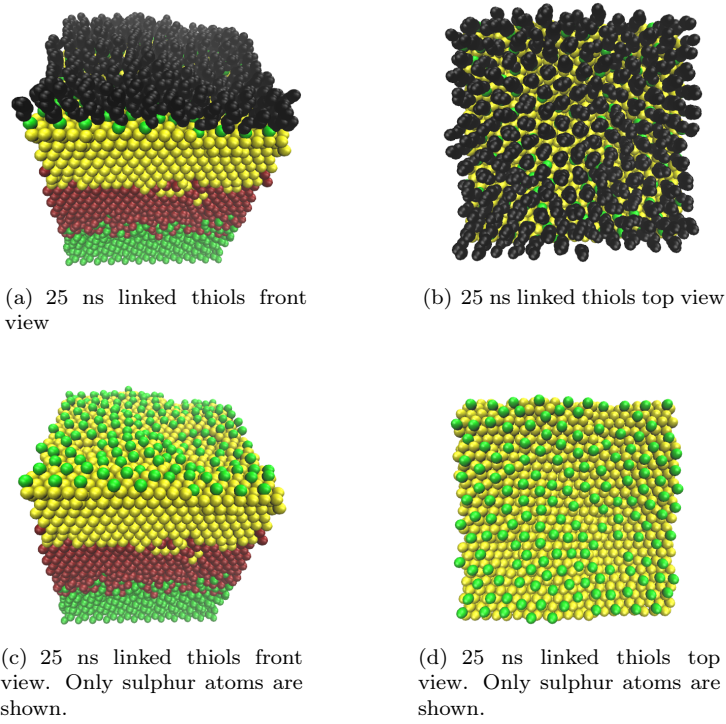


Figure 5.21: SAM formation above a non-ideal gold surface at 25 ns where only linked thiols are shown. Dark green is Si, burgundy is Cu, yellow is Au, light green is S and black are both CH_2 and CH_3 groups.

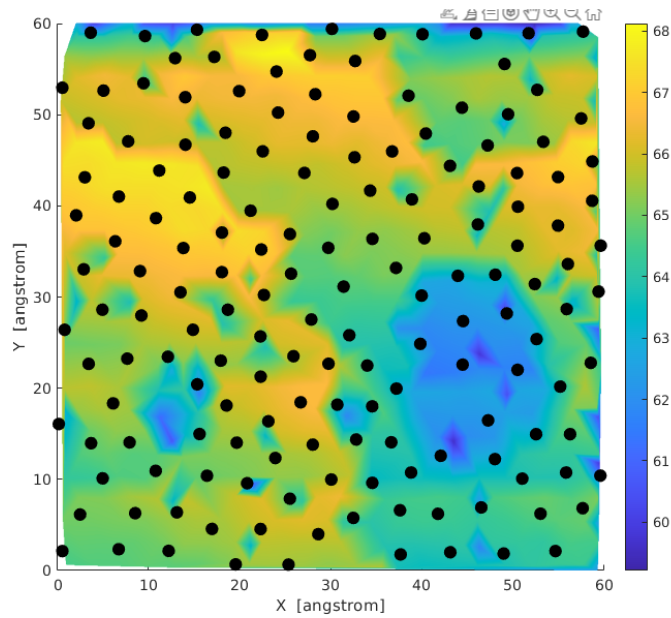


Figure 5.22: Interpolated gold surface (already represented in figure 5.13) with linked sulphur atoms represented by black circles.

Chapter 6

MD Simulations with Bisferrocene Molecules

In this chapter simulations with bisferrocene molecules will be performed. The main purpose is to understand how bisferrocenes organize themselves with respect to each other above a gold 2D substrate or a wire.

There is no scientific literature about a force field specially developed for bisferrocene molecules. For this reason, it is suggested to read the chapter critically because the force field used has been arranged by me, using parameters found in literature, others obtained in chapter 3 and making approximations. Certainly this force field can be greatly improved also because many parameters have been fixed.

6.1 Bisferrocenes without the Hydrocarbon Chain above a SAM

In this section we will try to simulate how bisferrocenes arrange themselves on a gold substrate. We will start from the SAM of hexanethiols on a ideal gold surface obtained in section 4.2. Roughly 5 Å above this SAM, a mass of 64 bisferrocenes without the hydrocarbon chain has been positioned.

Figure 6.1 shows the bisferrocene without the hydrocarbon chain used in the simulation. CH, CH₃ and NH groups are treated as united atoms for sake of simplicity to avoid to consider also hydrogen atoms.

The carbazole bonds have been fixed to 1.41 Å, the inner angles in the carbazole pentagon to 108° and the inner ones in the two carbazole hexagons to 120°. Carbazole dihedral angles have not been fixed since, differently from bonds and angle that I expect that they vary slightly around their equilibrium point, torsions in carbazole could be very pronounced. Thus, in my opinion, is more appropriate to use a force field for carbazole dihedral angles instead of fixing them. Therefore, they have been modeled with the 4th-order Fourier series in equation 3.44 and the parameters are those found out in the subsection 3.2.2 listed in table 3.3.

The two ferrocenes structure has been completely fixed and their equilibrium geometry taken from [36] is represented in figure 6.2.

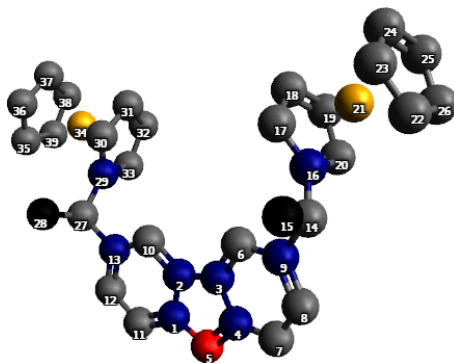


Figure 6.1: Bisferrocene without the hydrocarbon chain. Blue is C, grey is CH, black is CH₃, red is NH and orange is Fe.

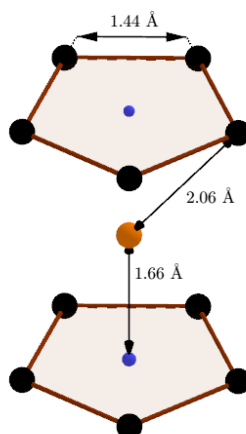


Figure 6.2: Ferrocene united atoms equilibrium geometry. Black points are CH groups, the orange point is Fe and the two small blue points represent the center of the two pentagons.

Pair	ε [kcal/mol]	σ [Å]
C–C	0.110	3.750
CH–CH	0.110	3.750
CH ₂ –CH ₂	0.118	3.905
CH ₃ –CH ₃	0.175	3.905
SH–SH	0.397	4.250
N–N	0.170	3.250
Au–Au	0.039	2.935
Fe–Fe	4.628	2.419

Table 6.1: Lennard-Jones parameters

The two "junctions" that connect carbazole to the two ferrocenes (numbers 9, 14, 15, 16 and 13, 27, 28, 29 in figure 6.1) have unfixed geometry. The bond stretching interactions between these groups of atoms has been modeled with Morse potential and the parameters are those obtained in subsection 3.2.3 for the isobutane molecule. Angle bending interactions and torsional angles have been modeled with the same potential used for the hexanethiols (that is described in the section 4.2).

The non-bonded interatomic interactions were taken to be the Lennard-Jones potentials and the parameters are listed in table 6.1. Parameters for CH₂, CH₃, SH and Au are the same used in the SAM above Au(111) simulation (section 4.2), those for C, CH and N are taken from the study of Jorgensen and Tirado-Rives in [37] and those for Fe from [38]. As done in section 4.2, Lennard-Jones parameters of the heteroatomic pairs were obtained using Lorentz-Berthelot mixing rule (eq. 4.3).

In order to link a bisferrocene without the hydrocarbon chain to a thiol of the SAM, a reaction between the carbazole NH group and the CH₃ tailgroup of the thiol has been modeled via Morse pair interaction and the parameters are those obtained in subsection 3.2.4. Thus, we have used the potential for the already formed molecule. This simplification has been done because this type of reaction may not be easy to realize in practice and in this preliminary simulation we are mainly interested how bisferrocenes arrange themselves on the SAM in relation to each other. In the following sections we will remove the question of the feasibility of this reaction starting directly from bisferrocene molecules already synthesized.

The mass of 64 bisferrocenes without the hydrocarbon chain has been prepared initially placing the molecules in the points of a simple cubic lattice with a spacing of 12 Å. Then, a energy minimization of the system has been performed and finally the system has been equilibrated by running an NVT simulation at 500 K for 3 ns.

As already said, this mass has been positioned roughly 5 Å above the SAM, after an NVT simulation at 500 K for 10 ns and with a timestep of 1 fs has been performed. Periodic boundary conditions are assumed in the two planar x and y directions and during the whole simulation gold atoms have been fixed in position. During this first part of the simulation an external force, cyclically directed along the x and y axis, has been applied every 100 timestep in order to spread the mass of bisferrocenes over the SAM (otherwise it would remain quite compact). Then, bisferrocenes that have not bound to any thiol have

been removed and the system has been equilibrated without any external force by running an NVT simulation at 500 K for 10 ns. The system is then cooled at 300 K in 5 ns and finally it is equilibrated at 300 K for 5 ns.

The simulation is shown in figure 6.3. In figures 6.3(a) and 6.3(b) is respectively shown the initial and the final configuration of the system. Figure 6.3(c) is simply a zoom of the 6.3(b). Figure 6.3(e) shows only the position of the N atom for each bisferrocene and figure 6.3(d) shows both N and Fe atoms. These last two figures are the most understandable and suggest that the bisferrocene molecules probably arrange and orient themselves randomly respecting some constraints of closeness.

6.2 Bisferrocenes above Au(111) Surface

In the previous section how bisferrocenes without the hydrocarbon chain organize themselves above a SAM has been simulated. The idea was to simulate a reaction between the NH group in carbazole and the CH₃ tailgroup of the thiol in order to form the bisferrocene molecule connected to the gold substrate. However, as already said, this type of reaction could be tricky to replicate in practice, therefore, it may not be a viable solution. For this reason, in this section we will try to simulate how bisferrocene molecules already synthesized organize themselves above an Au(111) surface.

Here, a mass of 63 bisferrocenes has been prepared and it has been positioned roughly 6 Å above a (111) gold surface. The gold substrate consists of 1439 atoms, it has a surface area of 6 nm by 6 nm and a height of three atomic layers. The mass of 63 bisferrocenes has been prepared initially placing the bisferrocenes in the points of a simple cubic lattice with a spacing of 15 Å. Then, a energy minimization of the system has been performed and finally the system has been equilibrated by running an NVT simulation at 500 K for 3 ns.

Figure 6.4 shows one single bisferrocene molecule used in the simulation. CH, CH₂, CH₃ and SH groups are treated as united atoms.

For the carbazole plus the two ferrocenes part of the molecule, the used force field is that in the previous section while for the thiol part is that in section 4.2. The non-bonded interactions are those in table 6.1.

After placement of the bisferrocene mass above the gold substrate, an NVT simulation at 500 K for 10 ns and with a timestep of 1 fs has been performed. Periodic boundary conditions are assumed in the two planar x and y directions and during the whole simulation gold atoms have been fixed in position. As done in the previous section, during this first part of the simulation, an external force as been applied in order to spread the mass of bisferrocenes over the gold surface. Subsequently, the external force has been removed and the system has been cooled at 300 K in 5 ns and then it has been equilibrated for 5 ns. Finally, bisferrocenes that have not bound to the gold substrate have been removed and the system has been equilibrated at 300 K for 10 ns.

The simulation is shown in figure 6.5. Figure 6.5(d), where only the position of the sulphur atoms above the Au surface is shown, suggests that bisferrocene molecules link the surface in random places but the distance between two sulphur atoms is always greater than roughly 5 Å. Figure 6.5(c) shows that bisferrocene molecules orient themselves quite casually. Moreover, differently from the previous simulation, some molecules tend to lie down on the surface even if there

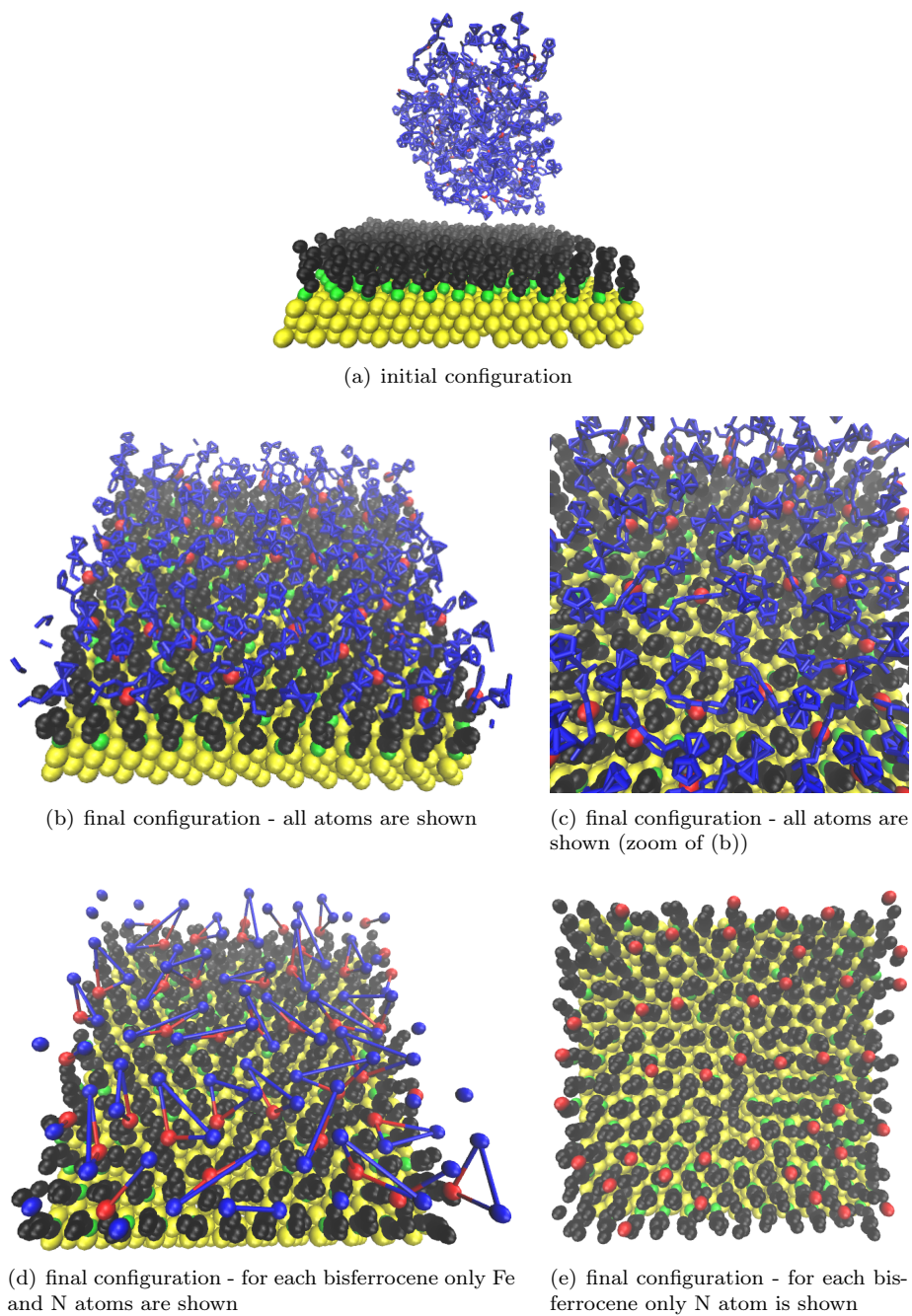


Figure 6.3: Simulation of bisferrocenes without the hydrocarbon chain above a SAM. Yellow is Au, green is S, black is the hydrocarbon chain of the thiols, red is N, blue are the atoms of all carbazoles (except N) and ferrocenes.

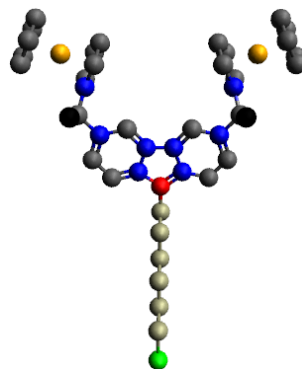


Figure 6.4: Bisferrocene molecule united atoms. Blue is C, dark grey is CH, black is CH₃, red is N, orange is Fe, light grey is CH₂ and green is SH.

are no molecule that are lying totally flat on the surface.

6.3 Bisferrocenes above an Au Wire

In the previous simulation we have seen that bisferrocene molecules organize themselves quite casually above the gold substrate. To force the molecules to arrange themselves better, in the following simulation the mass of 63 bisferrocenes has been placed roughly 6 Å above a gold wire which has a (111) top surface, it is extended along the entire box, it has a thickness of three atomic layers and a width of only 1 nm. The gold wire is placed manually above a silicon substrate with a (111) top surface. The structure constituted of Si and Au is kept frozen during the whole simulation. Here, we are avoiding the issue of how to get this structure. This is a difficult problem to solve, indeed, as seen in section 5.2, the interface between Si and Au has a certain thickness where both type of atoms are present. The biggest problem, however, is that patterning a wire of only one nanometer wide is not possible using photolithography processes. In any case, we assume to have this structure and the purpose is to see how bisferrocenes arrange themselves above.

The basic idea of this simulation is that since the gold wire is only one nanometer wide, some placements of the bisferrocenes are not allowed leading a more ordered final configuration. For instance, two bisferrocene molecules will not be able to position side by side as shown in figure 6.6(a). Anyway, as seen in chapter 4, since the minimum distance between two thiols is roughly 5 Å, the attachment points of two bisferrocenes (the SH group) could be side by side as shown for example in figure 6.6(b). To make sure that the attachment points of two bisferrocenes cannot be side by side, the width of the wire should be smaller than 5 Å, but this is not possible in practice.

The used force field for this simulation is the same as the previous one but with the addition of the non-bonded interactions for Si with the other types of atoms. The Lennard-Jones (LJ) parameters used for the Si-Si and Si-C pairs are taken from [39]. For the Si-CH, Si-CH₂ and Si-CH₃ pairs the used parameters are the same as in Si-C. LJ parameters for Si-S have been obtained applying the Lorentz-Berthelot mixing rules to the parameters of Si and S taken

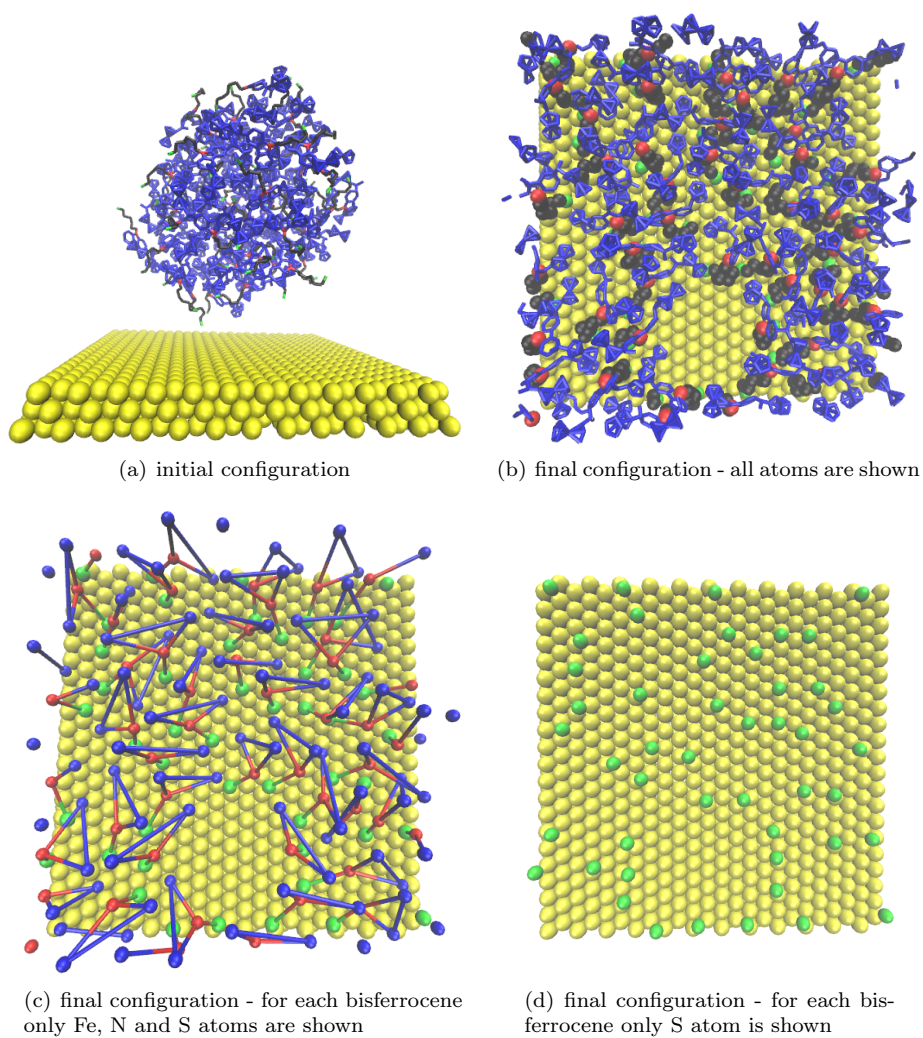


Figure 6.5: Simulation of bisferrocenes above Au(111) surface. Yellow is Au, green is S, black are the atoms of the hydrocarbon chains, red is N, blue are the atoms of all carbazoles (except N) and ferrocenes.

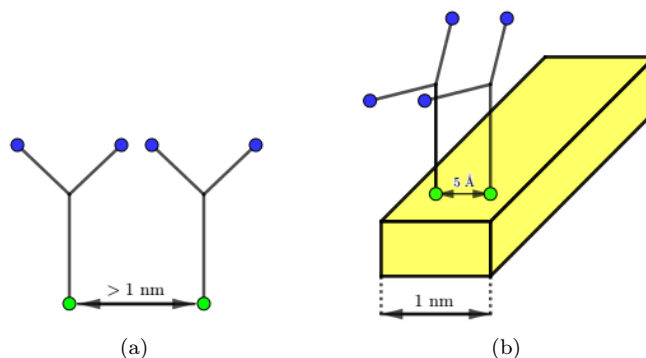


Figure 6.6:

from [40]. Finally parameters for Si–N, Si–Au and Si–Fe have been obtained with the mixing rules (where the parameters used for N, Au and Fe are those listed in table 6.1).

After the placement of the bisferrocene mass above the Au wire, an NVT simulation at 500 K for 15 ns and with a timestep of 1 fs has been performed. Periodic boundary conditions are assumed in the two planar x and y directions and unlike the previous simulation no external force has been applied to the bisferrocenes. Subsequently, the system has been cooled at 300 K in 5 ns and then it has been equilibrated for 5 ns. Finally, bisferrocenes that have not bound to the Au wire have been removed and the system has been equilibrated at 300 K for 10 ns.

The simulation is shown in figure 6.7. From figures 6.7(e), 6.7(f) and 6.7(g), it can be seen that the attachment points of the bisferrocenes are roughly aligned on the top surface of the wire but there are also bisferrocenes attached to the side walls. The orientation of the molecules on the top of the wire, shown in figures 6.7(c) and 6.7(d), is not the one hoped with the rised hydrocarbon chain and the two Fe atoms aligned in the direction of the width of the wire.

Bisferrocenes linked to the side walls of the wire could cause problems, thus, to prevent them from being there, the same simulation has been performed again, but starting with the wire surrounded by silicon. This simulation is shown in figure 6.8 and, as it can be seen from the initial configuration (figure 6.8(a)), only the top surface of the wire is exposed. From figure 6.8(d) you can see that the attachment points are not perfectly aligned. This because bisferrocene molecules can reach the wire from right and left.

To avoid this, an other simulation, where two silicon walls have been added to the sides of the wire, has been run. Thanks to the two silicon walls, bisferrocene molecules can reach the Au wire only from above. This simulation, shown in figure 6.9, is the same as the previous two but with longer simulation times. At the beginning of the simulation only 11 bisferrocene molecules, already equilibrated at 500 K, have been placed a few angstrom above the Au wire, then an NVT simulation at 500 K for 40 ns has been performed, then the system has been cooled at 300 K in 10 ns and then it has been equilibrated for

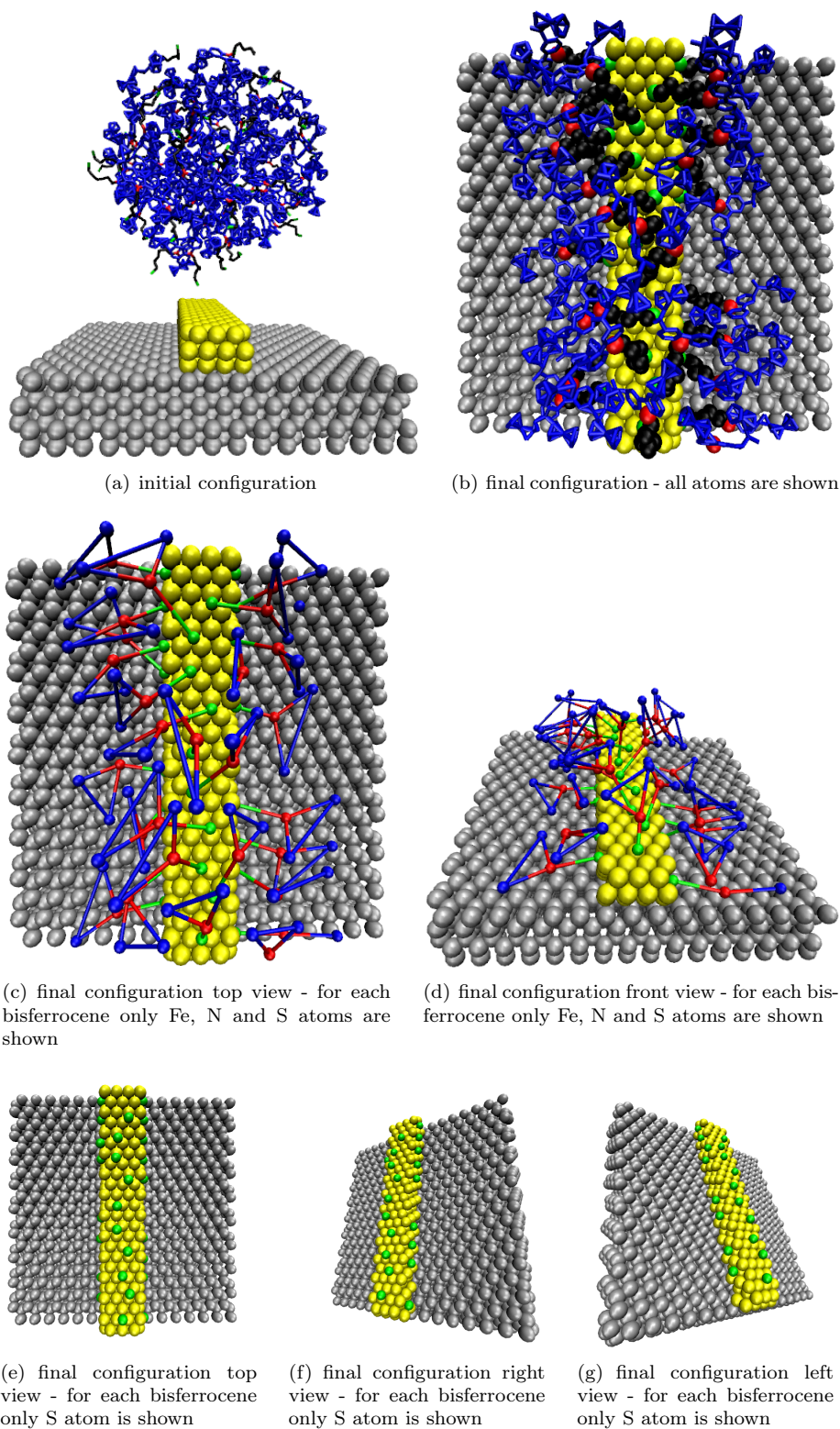


Figure 6.7: Simulation of bisferrocenes above an Au wire. Yellow is Au, silver-grey is Si, green is S, black are the atoms of the hydrocarbon chains, red is N, blue are the atoms of all carbazoles (except N) and ferrocenes.

15 ns. Finally, the only one bisferrocene that has not bound to the Au wire has been removed and the system has been equilibrated at 300 K for 25 ns.

Figure 6.9(d) shows that the attachment points of the bisferrocene molecules are quite aligned and this is a good result but the molecules orientation is not the desired one as you can see from figure 6.9(c).

6.4 Bisferrocenes Mixed with Thiols

In this section a mixed mass of bisferrocenes and thiols has been simulated above both a gold substrate and a gold wire with the only top surface exposed. The mass is composed by 45 bisferrocenes and 241 thiols and it has been equilibrated at 300 K for 3 ns.

After placing it roughly 5 Å above the substrate, an NVT simulation at 500 K for 15 ns and with a timestep of 1 fs has been performed. Subsequently, the system has been cooled at 300 K in 5 ns and then it has been equilibrated for 5 ns. Finally, bisferrocenes and thiols that have not bound to the gold substrate or the gold wire have been removed and the system has been equilibrated at 300 K for 15 ns.

No external force has been applied to bisferrocenes or thiols to help the spreading of the mass over the substrate. Periodic boundary conditions are assumed in the two planar x and y directions and during the whole simulation the substrate is kept frozen. The used force field is that of the previous simulations.

Figures 6.10 and 6.11 show respectively the simulations with the 2D gold substrate and with the wire. You can see that bisferrocenes are not at all regularly arranged. From the simulation with the 2D gold substrate, it can be noted that bisferrocenes do not tend to lie down on the surface. This is thanks to the thiols surrounding the bisferrocenes, that make the hydrocarbon chain of the bisferrocenes stay up. In the simulation with the Au wire, this does not happen because bisferrocene molecules are not completely surrounded by thiols.

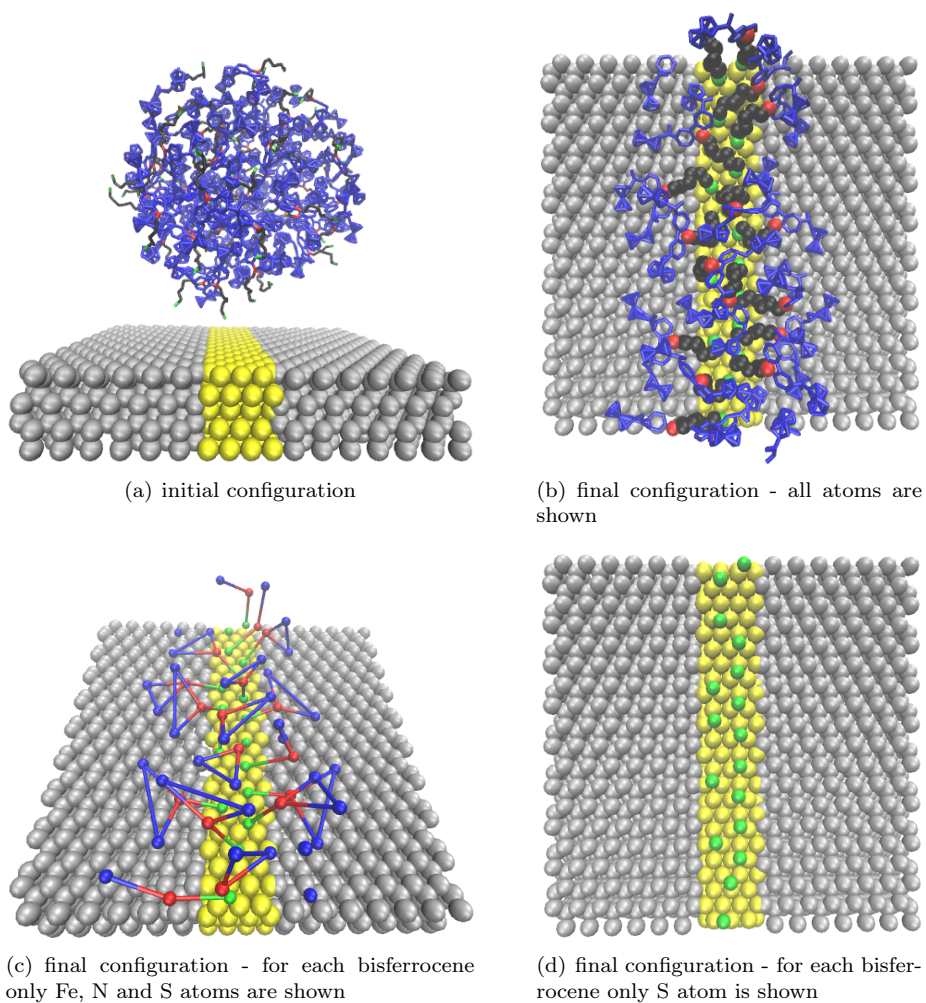


Figure 6.8: Simulation of bisferrocenes above an Au wire with the only top surface exposed. Yellow is Au, silver-grey is Si, green is S, black are the atoms of the hydrocarbon chains, red is N, blue are the atoms of all carbazoles (except N) and ferrocenes.

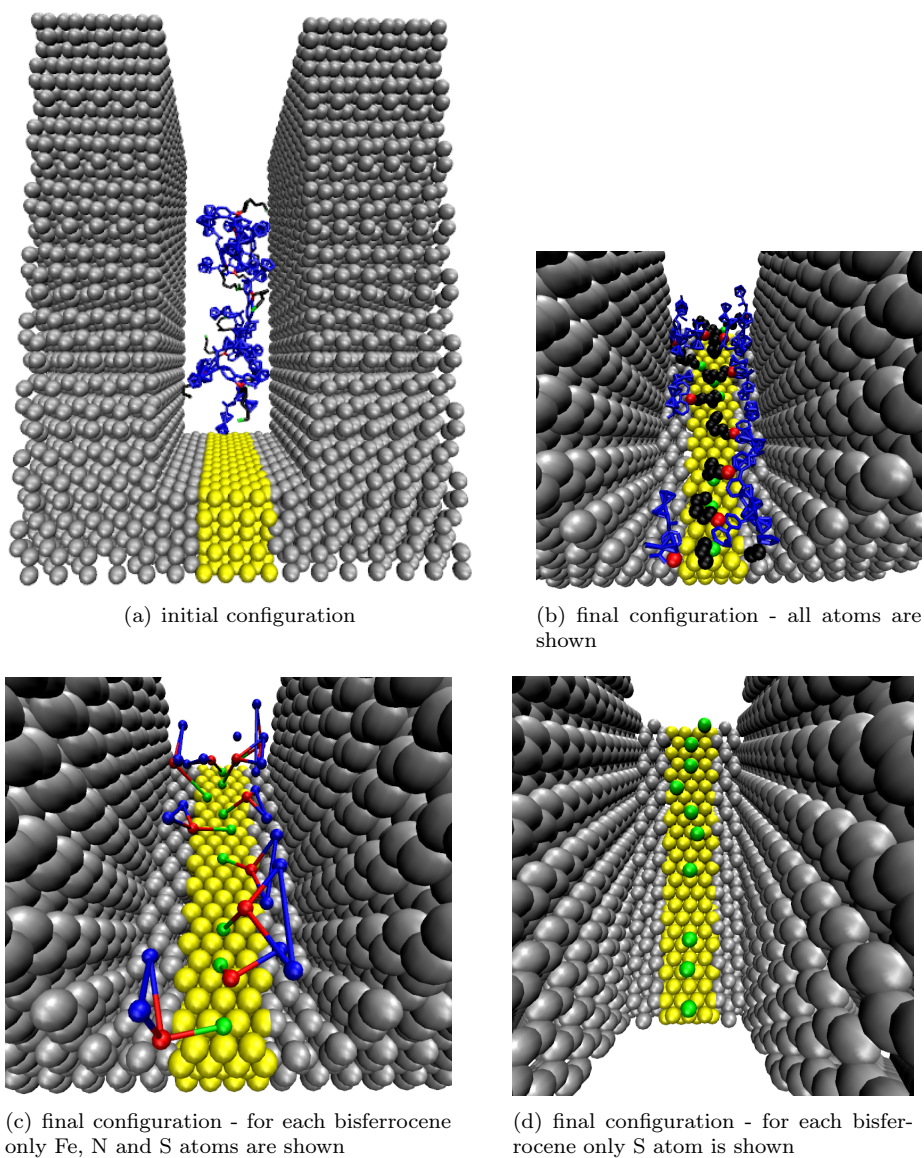
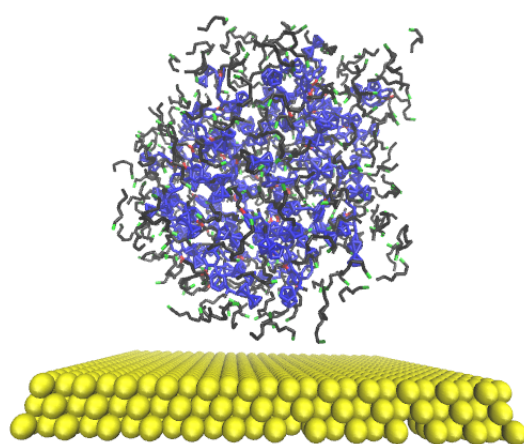
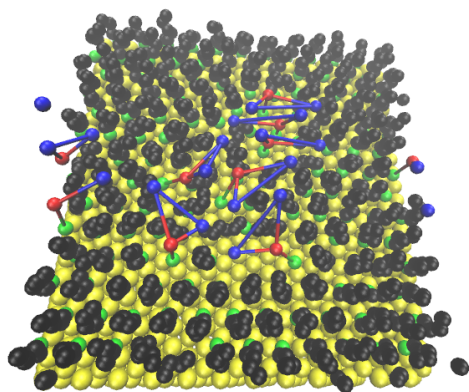


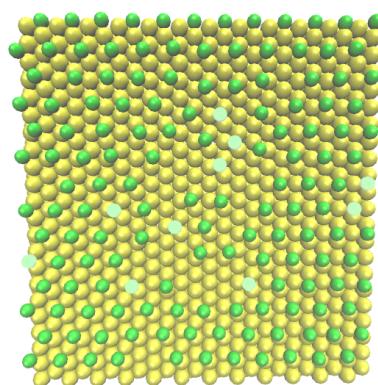
Figure 6.9: Simulation of bisferrocenes above an Au wire with the only top surface exposed and with two Si walls on either side. Yellow is Au, silver-grey is Si, green is S, black are the atoms of the hydrocarbon chains, red is N, blue are the atoms of all carbazoles (except N) and ferrocenes.



(a) initial configuration

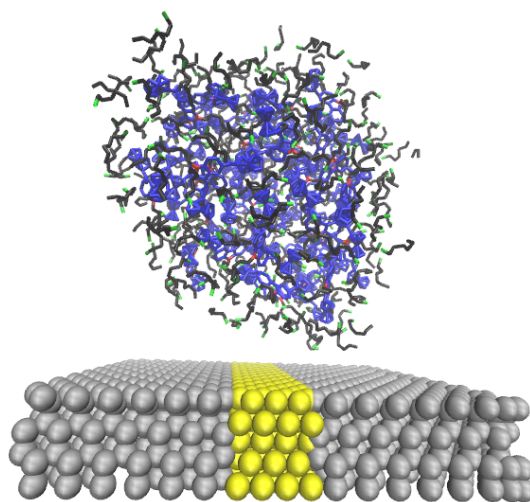


(b) final configuration - for each bisferrocene only Fe, N and S atoms are shown

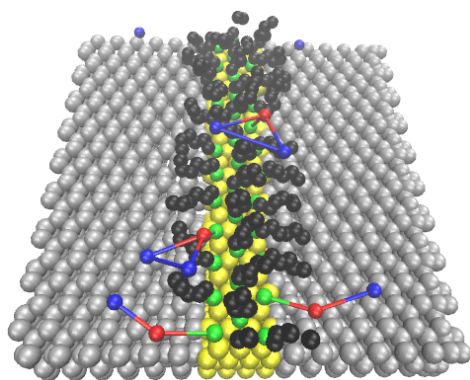


(c) final configuration - only S atoms are shown and those of the bisferrocenes are highlighted

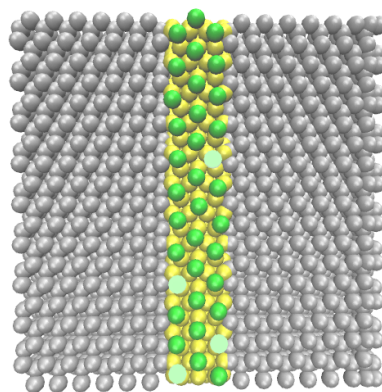
Figure 6.10: Simulation of bisferrocenes mixed with thiols above an Au substrate. Yellow is Au, green is S, black are the atoms of the hydrocarbon chains (belonging both bisferrocenes and thiols), red is N, blue are the atoms of all carbazoles (except N) and ferrocenes.



(a) initial configuration



(b) final configuration - for each bisferrocene only Fe, N and S atoms are shown



(c) final configuration - only S atoms are shown and those of the bisferrocenes are highlighted

Figure 6.11: Simulation of bisferrocenes mixed with thiols above an Au wire with the only top surface exposed. Yellow is Au, silver-grey is Si, green is S, black are the atoms of the hydrocarbon chains (belonging both bisferrocenes and thiols), red is N, blue are the atoms of all carbazoles (except N) and ferrocenes.

Conclusions

In this thesis, molecular dynamics has been used to simulate nanofabrication processes. The formation of a SAM of hexanethiols above an Au(111) surface has been simulated and results agree with experimental ones. Since we are interested in Au(111) surface, a simulations to obtain it has been carried out. Thus, an Au deposition above a Si substrate has been simulated, with and without interposing a Cu thin film between the two materials. As expected, the obtained Au layer is not completely flat and the surface is not of the type (111) everywhere. Interfaces between materials have been quantitatively analyzed with respect to the temperature. Then, the SAM formation has been simulated again above this non-ideal gold surface, obtaining, also in this case, a full coverage of the surface, but the arrangement of the thiols is not perfectly regular as in the case of the ideal gold surface.

The simulation of the formation of an Au layer can be useful in the future whenever you want to complicate a study including the effects of the defects of a non-ideal surface.

Finally MD simulations with bisferrocene molecules has been performed. Unlike thiols, bisferrocenes seem to organize themselves on the surface quite casually, moreover, some tend to lie down on the surface. Several trials have been performed in order to obtain bisferrocenes arranged in line. When bisferrocenes are deposited above a 1 nm wide Au wire with two Si walls on the sides, it has been observed that they arrange themselves quite in line. However, the orientation is not the one hoped, bisferrocenes tend to lie down and are attracted to silicon walls because the latter are very close to the wire. When bisferrocenes are simulated mixed with thiols, it has been seen that, even if they are organized randomly, they stand well up because the surrounding space, where the bisferrocene bind the surface, is occupied by thiols. Bisferrocenes without their hydrocarbon chain has been simulated above a SAM modeling a reaction between N in the carbazole and the tailgroup of the thiols. Probably, this reaction is not trivial to achieve in practice, but anyway, the simulation is useful to understand how bisferrocenes can arrange themselves with respect to each other. The used force field for bisferrocenes has been arranged in this work using parameters found in literature, others obtained with a method conceived in this thesis described in chapter 3 and making approximations. In the future this force field could be improved a lot, also because many parameters have been fixed. Since all the obtained results of a MD simulation depend on the force field, the improvement of the latter is the key to obtain results that match reality. Hence, obtaining also experimental results is essential to validate the simulations and, when MD simulations agree with experimental ones, the simulation model could explain the problem.

In addition, a next step could be taking into account the partial charges of the atoms to consider also the Coulomb contribution in the force field.

Appendix A

Definition of a Molecular Structure

In chemistry the position of an atom in a molecule can be defined using the internal coordinates instead of the usual Cartesian ones. The internal coordinates are more complicated, however, they greatly simplify the calculation of the force field of a molecule. Then, the conformation of a molecule is given in a structure called Z-matrix in which the position of each atom is assigned using the internal coordinates.

In the text below the concepts of internal coordinates and Z-matrix are described.

A.1 Internal Coordinates

Internal coordinates fix the position of an atom with three conditions. Each condition is relative to atoms already present in the system.

To give an example, consider figure A.1 and assume that the position of atoms P_1 , P_2 and P_3 is already fixed and we want to define the position of atom P_4 using internal coordinates.

The first condition is the distance between P_4 and an atom already present in the system, in our case P_3 was chosen (figure A.1(a)).

The second condition is the angle between P_4 , P_3 and any other atom already present in the system, in this case, P_2 was chosen. Note that the central vertex of the angle is P_3 which is the atom respect to the distance condition is given (figure A.1(b)). The considered angle between the three points is always the convex one.

The third condition is an other angle between two semiplanes called dihedral or torsional angle (figure A.1(c)). We have to consider two semiplanes, both of which originate from the straight line running through P_2 and P_3 (the two points used in the previous conditions), the former contains P_4 and the latter contains any other atom already present in the system, in our example the only choice is P_1 but there may be other atoms to use. The angle between these two semiplanes is the dihedral or torsional angle. Note that if the dihedral angle is 0° or 180° the four atoms lie on the same plane.

Unlike the angle in the second condition, which is considered always positive,

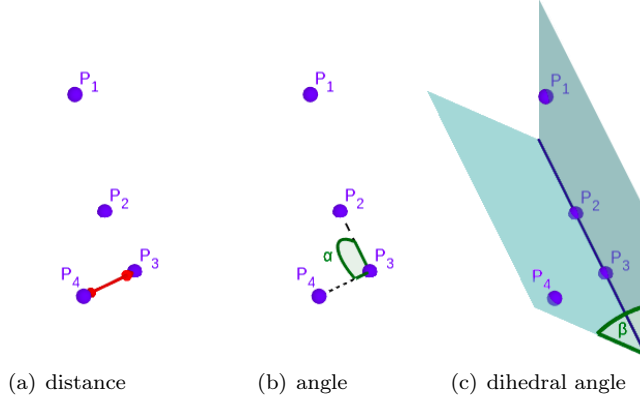


Figure A.1: Internal coordinates.

the dihedral angle is an oriented angle so it can be positive or negative. Its absolute value is that of the convex angle between the two semiplanes. Establish the sign is not trivial as in the case of a planar angle because a clockwise or anti-clockwise rotation cannot be defined in the 3D space since it depends from the spatial observation point. However, the sign of the dihedral is simply to calculate because it is that of the scalar

$$\overrightarrow{P_1P_2} \cdot (\overrightarrow{P_2P_3} \times \overrightarrow{P_3P_4}) \quad (\text{A.1})$$

where \cdot and \times denote respectively the scalar and the vectorial product and

$$\overrightarrow{P_1P_2} = \vec{P}_2 - \vec{P}_1 = (P_{2x} - P_{1x}, P_{2y} - P_{1y}, P_{2z} - P_{1z}) \quad (\text{A.2})$$

$$\overrightarrow{P_2P_3} = \vec{P}_3 - \vec{P}_2 = (P_{3x} - P_{2x}, P_{3y} - P_{2y}, P_{3z} - P_{2z}) \quad (\text{A.3})$$

$$\overrightarrow{P_3P_4} = \vec{P}_4 - \vec{P}_3 = (P_{4x} - P_{3x}, P_{4y} - P_{3y}, P_{4z} - P_{3z}) \quad (\text{A.4})$$

If the dihedral angle is 0° or 180° then equation A.1 returns 0.

In the following, a recipe to compute the dihedral angle directly with the right sign is given:

- compute the vectors $\vec{a}_1 = \overrightarrow{P_1P_2} \times \overrightarrow{P_2P_3}$ and $\vec{a}_2 = \overrightarrow{P_2P_3} \times \overrightarrow{P_3P_4}$;
- compute the versors $\hat{n}_1 = \frac{\vec{a}_1}{\|\vec{a}_1\|}$ and $\hat{n}_2 = \frac{\vec{a}_2}{\|\vec{a}_2\|}$ where $\|\cdot\|$ denotes the 2-norm of the vector;
- compute the versor $\hat{m} = \hat{n}_1 \times \frac{\overrightarrow{P_2P_3}}{\|\overrightarrow{P_2P_3}\|}$;
- compute the scalars $x = \hat{n}_1 \cdot \hat{n}_2$ and $y = \hat{m} \cdot \hat{n}_2$;
- the dihedral angle in radians with the right sign is given by $\beta = -\arctan 2(y, x)$

where

$$\arctan 2(y, x) = \begin{cases} \arctan\left(\frac{y}{x}\right) & x > 0 \\ \arctan\left(\frac{y}{x}\right) + \pi & x < 0 \ \& \ y \geq 0 \\ \arctan\left(\frac{y}{x}\right) - \pi & x < 0 \ \& \ y < 0 \\ \frac{\pi}{2} & x = 0 \ \& \ y > 0 \\ -\frac{\pi}{2} & x = 0 \ \& \ y < 0 \\ \text{not defined} & x = 0 \ \& \ y = 0 \end{cases} \quad (\text{A.5})$$

The dihedral angle must be an oriented angle otherwise the position of the atom P_4 could not be determined uniquely. This is why with the first condition all possible points are those on a sphere centered on P_3 with radius equal to the distance between P_3 and P_4 . With the second condition the possible points become those on a curve drawn on this sphere. The third condition must fix a single point on this curve. If the dihedral is without sign, an angle of 30° for instance, will be the same of an angle equal to $-30^\circ = 330^\circ$, and therefore, there will be two possible points that will satisfy all three conditions. To eliminate this ambiguity, we have to distinguish between the two angles (30° and -30° in our example) introducing the sign in the dihedral angle.

A.2 Z-matrix

The Z-matrix is a structure in which the position of each atom of a molecule is assigned using the internal coordinates.

Below there is the Z-matrix in the format accepted by the software ORCA of a 1-Butanethiol molecule (shown in figure A.2) as example.

```

1      H
2      S   1          1.308
3      C   2   1      1.817   100.2
4      H   3   2   1    1.106   110.5    67.1
5      H   3   2   1    1.108   104.8   -179.2
6      C   3   2   1    1.517   114.7   -57.9
7      H   6   3   2    1.109   110.1    61.0
8      H   6   3   2    1.109   110.2   -55.2
9      C   6   3   2    1.521   111.1   -177.2
10     H   9   6   3    1.108   109.9    58.1
11     H   9   6   3    1.108   110.0   -57.6
12     C   9   6   3    1.512   111.3   -179.8
13     H  12   9   6    1.097   111.2   180.0
14     H  12   9   6    1.098   111.7    60.0
15     H  12   9   6    1.098   111.6   -60.1
```

The first line tell us that there is a hydrogen atom and its ID number is 1. The second line tell us that there is a sulphur atom with ID number 2 placed at a distance 1.308 Å from atom 1. The third line tell us that there is a carbon atom with ID number 3 placed at a distance of 1.817 Å from atom 2 and the angle formed by atoms 1–2–3 is equal to 100.2°. From the fourth line onwards all internal coordinates are used to define the atoms position. For example the fourth line tell us that there is a hydrogen atom with ID number 4 placed at a distance of 1.106 Å from atom 3, the angle formed by atoms 2–3–4 is equal

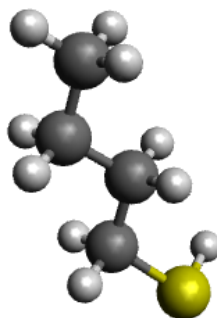


Figure A.2: 1-Butanethiol or butane-1-thiol molecule ($\text{C}_4\text{H}_{10}\text{S}$). Dark grey is carbon (C), light grey is hydrogen (H) and yellow is sulphur (S).

to 110.5° and the dihedral angle formed by atoms $1-2-3-4$ is equal to 67.1° . The fifth line tell us that there is a hydrogen atom with ID number 5 placed at a distance of 1.108 \AA from atom 3, the angle formed by atoms $2-3-5$ is equal to 104.8° and the dihedral angle formed by atoms $1-2-3-5$ is equal to -179.2° .

Actually the first column of the Z-matrix, that of ID numbers, does not appear because it corresponds to the line number of the Z-matrix itself, in this example it has been included for clarity only.

In the Z-matrix, the position of the first three atoms is not completely fixed but only their relative positions are fixed. This is why the Z-matrix fixes the geometry of a molecule, but not the position of the molecule in the space. The molecule can translate and rotate leaving the Z-matrix unchanged.

The atoms in the Z-matrix can be defined in any order, moreover, the three reference atoms in each line (from the fourth onwards) are completely arbitrary, this means that there are many different Z-matrices that can be define the same molecule structure.

From our the example, it is simple to note that if N is the number of the atoms in the molecule, if $N \geq 3$, then $N - 1$ distance conditions, $N - 2$ angle conditions and $N - 3$ dihedral angle conditions are needed to fix the geometry of the molecule. Thus, if $N \geq 3$, the total number of conditions to fix the geometry of the molecule is $3N - 6$. If $N = 2$ only one condition is needed (the distance between the two atoms) and if $N = 1$ no conditions are needed.

Bibliography

- [1] International Roadmap for Devices and Systems (IRDSTM) **2020** Edition.
- [2] Lent C. S., Tougaw P. D., Porod W. and Bernstein G. H. *Quantum cellular automata*. Nanotechnology 4, 49, (**1993**).
- [3] Timler J. and Lent C. S. *Power gain and dissipation in quantum-dot cellular automata*. J. Appl. Phys. 91, 2, 823, (**2001**).
- [4] Tougaw P. D. and Lent C. S. *Logical devices implemented using quantum cellular automata*. J. Appl. Phys. 75, 1818, (**1994**).
- [5] Lent C. S., Tougaw P. D. and Porod W. *Quantum Cellular Automata: The Physics of Computing with Arrays of Quantum Dot Molecules*. Proceedings Workshop on Physics and Computation. PhysComp '94, 5, (**1994**).
- [6] Lent C. S. and Tougaw P. D. *A Device Architecture for Computing with Quantum Dots*. Proc. IEEE 85, 4, 541, (**1997**).
- [7] Jayalakshmi R. and Amutha R. *A Theoretical Study on the Implementation of Quantum Dot Cellular Automata*. 4th International Conference on Advances in Electrical, Electronics, Information, Communication and Bio-Informatics (AEEICB-18), (**2018**).
- [8] Ardesi Y. *Energy Analysis and Bistability Study of Molecular FCN*. Master Thesis, Politecnico di Torino, (**2017**).
- [9] Arima V., Iurlo M., Zoli L., Kumar S., Piacenza M., Della Sala F., Martino F., Maruccio G., Rinaldi R., Paolucci F., Marcaccio M., Cozzi P. G. and Bramanti A. P. *Toward quantum-dot cellular automata units: thiolated-carbazole linked bisferrocenes*. Nanoscale 4, 813, (**2012**).
- [10] Ardesi Y., Wang R., Turvani G., Piccinini G. and Graziano M. *SCERPA: A Self-Consistent Algorithm for the Evaluation of the Information Propagation in Molecular Field-Coupled Nanocomputing*. IEEE Trans. Comput.-Aided Des. Integr. Circuits Syst 39, 10, 2749, (**2020**).
- [11] Ardesi Y., Turvani G., Graziano M. and Piccinini G. *SCERPA Simulation of Clocked Molecular Field-Coupling Nanocomputing*. IEEE Transactions on Very Large Scale Integration (VLSI) Systems 29, 3, 558, (**2021**).
- [12] Roccatano D. *Introduzione alla dinamica molecolare*.
- [13] Hedman F. *Algorithms for Molecular Dynamics Simulations*. (**2006**).

-
- [14] Verlet L. *Computer "Experiments" on Classical Fluids. I. Thermodynamical Properties of Lennard-Jones Molecules**. Phys. Rev. 159, 98, (1967).
- [15] https://lammps.sandia.gov/doc/compute_pressure.html
- [16] <https://lammps.sandia.gov/doc/Manual.html>
- [17] Nosé S. *A molecular dynamics method for simulations in the canonical ensemble*. Mol. Phys. 100, 191, (1983).
- [18] Koch W. and Holthausen M. C. *A Chemist's Guide to Density Functional Theory*. Second Edition, (2001).
- [19] Parr R. G. and Yang W. *Density-Functional Theory of Atoms and Molecules*. University of North Carolina, (1989).
- [20] Watcharinyanon S. *Structure of Self-Assembled Monolayers on Gold Studied by NEXAFS and Photoelectron Spectroscopy*. Dissertation, Karlstad University Studies, (2008).
- [21] Love J. C., Estroff L. A., Kriebel J. K., Nuzzo R. G. and Whitesides G. M. *Self-Assembled Monolayers of Thiolates on Metals as a Form of Nanotechnology*. Chem. Rev. 105, 1103, (2005).
- [22] Matthiesen J. E., Jose D., Sorensen C. M. and Klabunde K. J. *Loss of Hydrogen upon Exposure of Thiol to Gold Clusters at Low Temperature*. J. Am. Chem. Soc. 134, 9376, (2012).
- [23] Järvi T. T., van Duin A. C. T., Nordlund K. and Goddard W. A. III. *Development of Interatomic ReaxFF for Au-S-C-H Systems*. J. Phys. Chem. 115, 10315, (2011).
- [24] Xu S., Crucion-Dupeyrat S. J. N., Garno J. C., Liu G.-Y., Jennings G. K., Yong T.-H. and Laibinis P. E. *In situ studies of thiol self-assembly on gold from solution using atomic force microscopy*. J. Chem. Phys. 108, 5002, (1998).
- [25] Kim H., Saha J. K., Zhang Z., Jang Ji., Matin M. A. and Jang Jo. *Molecular Dynamics Study on the Self-Assembled Monolayer Grown from a Droplet of Alkanethiol*. J. Phys. Chem. C 118, 11149, (2014).
- [26] Hautman J., Klein M. L. *Simulation of a monolayer of alkyl thiol chains*. J. Chem. Phys. 91, 4994, (1989).
- [27] Ryckaert J.-P., Bellemans A. *Molecular Dynamics of Liquid Alkanes*. J. Chem. Soc. Faraday Discuss. 66, 95, (1978).
- [28] Saha J. K., Ahn Y., Kim H., Schatz G. C. and Jang J. *Small Size Limit to Self-Assembled Monolayer Formation on Gold(111)*. J. Phys. Chem. C 115, 13193, (2011).
- [29] Zhao X., Leng Y. and Cummings P. T. *Self-Assembly of 1,4-Benzenedithiolate/Tetrahydrofuran on a Gold Surface: A Monte Carlo Simulation Study*. Langmuir 22, 4116, (2006).

-
- [30] Silva A., Pedersen K., Diekhöner L., Morgen P. and Li Z. *Ordered Au(111) layers on Si(111)*. J. Vac. Sci. Technol A 25, 908, (2007).
- [31] Zhang J., Liu C., Shu Y. and Fan J. *Growth and properties of Cu thin film deposited on Si(001) substrate: A molecular dynamics simulation study*. Applied Surface Science 261, 690, (2012).
- [32] Fan J., Boyd I. D. and Shelton C. *Monte Carlo modeling of electron beam physical vapor deposition of yttrium*. J. Vac. Sci. Technol A 18, 2937, (2000).
- [33] Foiles S. M., Baskes M. I. and Daw M. S. *Embedded-atom-method functions for the fcc metals Cu, Ag, Au, Ni, Pd, Pt, and their alloys*. Phys. Rev. B 33, 7983, (1986).
- [34] Tersoff J. *Modeling solid-state chemistry: Interatomic potentials for multi-component systems*. Phys. Rev. B 39, 5566, (1989).
- [35] Ryu S. and Cai W. *A gold-silicon potential fitted to the binary phase diagram*. J. Phys.: Condens. Matter 22 055401, (2010).
- [36] Canongia Lopes J. N., Cabral do Couto P. and Minas da Piedade M. E. *An All-Atom Force Field for Metallocenes*. J. Phys. Chem. A 110, 13850, (2006).
- [37] Jorgensen W. L. and Tirado-Rives J. *The OPLS Potential Functions for Proteins. Energy Minimizations for Crystals of Cyclic Peptides and Crambin*. J. Am. Chem. Soc. 110, 6, 1657, (1988).
- [38] Maghfiroh C. Y., Arkundato A., Misto and Maulina W. *Parameters (σ , ϵ) of Lennard-Jones for Fe, Ni, Pb for Potential and Cr based on Melting Point Values Using the Molecular Dynamics Method of the Lammmps Program*. J. Phys.: Conf. Ser. 1491, (2020).
- [39] Inui N. and Iwasaki S. *Interaction Energy between Graphene and a Silicon Substrate Using Pairwise Summation of the Lennard-Jones Potential*. e-J. Surf. Sci. Nanotech. 15, 40, (2017).
- [40] Munaò G., Correa A., Pizzirusso A. and Milano G. *On the calculation of potential of mean force between atomistic nanoparticles*. (2018).